International
Progress Report

IPR-02-13

Äspö Hard Rock Laboratory

TRUE Block Scale

Updating of the structural-hydraulic model and compilation of scoping data set

Jan Hermansson
Sven Follin
Golder Assosiates AB

Per Nilsson
VBB VIAK

Göran Nyberg
GEOSIGMA AB

Andrs Winberg
Conterra AB

December 1996

Svensk Kärnbränslehantering AB
Swedish Nuclear Fuel
and Waste Management Co
Box 5864
SE-102 40 Stockholm Sweden
Tel +46 8 459 84 00
Fax +46 8 661 57 19

Äspö Hard Rock
Laboratory

Report no.
IPR-02-13

No.
F56K

Author
Hermansson, Follin,
Nilsson, Nyberg, Winberg

Date
1996-12-01

Checked by

Date

Approved
Christer Svemar

Date
2002-04-12

Äspö Hard Rock Laboratory

TRUE Block Scale

Updating of the structural-hydraulic model and compilation of scoping data set

Jan Hermansson
Sven Follin
Golder Assosiates AB

Per Nilsson
VBB VIAK

Göran Nyberg
GEOSIGMA AB

Andrs Winberg
Conterra AB

December 1996

Keywords: TRUE, block scale, scoping, hydraulic, connecyivity, borehole structural, target, drawdown

This report concerns a study which was conducted for SKB. The conclusions and viewpoints presented in the report are those of the author(s) and do not necessarily coincide with those of the client.

TABLE OF CONTENTS

TABLE OF CONTENTS

1 INTRODUCTION 1

1.2 OBJECTIVES 2

1.3 DISPOSITION OF THE REPORT 2

1.3 COORDINATE SYSTEM AND LOCAL NORTH 2

2 BACKGROUND DATA FOR MODEL UPDATE 3

2.1 BOREHOLE 2511A 3

2.2 BOREHOLE KA2598A 4

2.3 BOREHOLE KC0045F 4

2.4 BOREHOLE KA2162B 5

2.5 BOREHOLE KAS02 5

2.6 BOREHOLE KAS05 5

2.7 TUNNEL AND SHAFT SECTIONS 6

3 UPDATING OF THE STRUCTURAL MODEL 7

3.1 EXISTING CONCEPTUAL STRUCTURAL MODELS 7

3.2 STRUCTURAL MODEL UPDATE 7

4 ASSESSMENT OF HYDRAULIC CONNECTIVITY 10

4.1 DRAWDOWN EVENTS AND THEIR INTERPRETATION 10

4.2 CONNECTIVITY ANALYSIS 11
4.2.1 Hydraulic connectivity in the south west corner of the HRL 11
4.2.2 Hydraulic connectivity in the north east corner of the HRL 12
4.2.3 Hydraulic connectivity in the central part of the HRL 13

5 HYDRAULIC HEAD 14

6 SUMMARY DESCRIPTION OF TARGET VOLUME MODEL 15

6.1 LITHOLOGY 15

6.2 FRACTURE ZONES 15

6.3 ROCK MASS PROPERTIES 17
6.3.1 Fracture network properties 17
6.3.2 Material properties of rock mass domains 17

7 CONCLUSIONS 18

8 REFERENCES 19

TABLES

Table 2-1 Results from flow and pressure build-up tests in borehole KA2511A.
Table 2-2 Summary of anomalies in borehole KA2511A (from Olsson et. al., 1994)
Table 2-3 Summary of anomalies in borehole KA2598A (from Olsson et al., 1994)
Table 2-4 Summary of anomalies in borehole KC0045F (from Olsson et al., 1994)
Table 2-5 Pressure responses in neighboring boreholes and flow into the borehole during drilling of KA2162B (from Forsmark et al. 1994)
Table 2-6 Correlation between inflow into the borehole, geological core mapping and radar reflectors in borehole KA2162B (from Carlsten et al. 1994)
Table 2-7 Identified hydraulic conductors in KAS05
Table 4-1. Pressure response matrix for drilling disturbances.
Table 4-2. Pressure response matrix for an extract of interference tests performed in boreholes in the NE part of the HRL (Winberg et al. 1996a)
Table 4-3. Pressure responses in boreholes during the drilling of the TBM tunnel.
Table 5-1 Evaluated hydraulic head from borehole sections in the vicinity of the target volume.
Table 6-1 Location of hydraulic conductors (Rhén et al. 1996)
Table 6-2 Deterministic hydraulic structures to be used for groundwater flow modelling (Rhén et al. 1996)
Table 6-3 Interpreted hydrological properties of hydraulic conductors (Rhén et al 1996)
Table 6-4 Transmissivity of hydraulic conductors (Rhén et al 1996).
Table 6-5 Identified hydraulic structures within the target volume.
Table 6-6 Äspö Tunnel Fracture Orientation Sets (after Dershowitz et al.,1996)
Table 6-7 Compilation of fracture size statistics.
Table 6-8 Hydraulic conductivity of rock mass domains. Test scale 100 m.
Table 6-9 Hydraulic conductivity of rock mass domains. Test scale 3 m.

FIGURES

Figure 1-1 Location of the target volume.
Figure 2-1 Petrocore log of core from borehole KA2511A
Figure 2-2 Radar and seismic reflectors observed in borehole KA2511A.
Figure 2-3 Fracture orientations in KA2511A, vertical depth 335-400 m.
Figure 2-4 Fracture orientations in KA2511A, vertical depth 400-450 m.
Figure 2-5 Transmissivity distribution in KA2511A from inflow measurements during drilling.
Figure 2-6 Transmissivity distribution in KA2511A from 3 m packer tests.

Figure 2-7 Petrocore log of core from borehole KA2598A
Figure 2-8 Radar and seismic reflectors observed in borehole KA2598A.
Figure 2-9 Petrocore log of core from borehole KC0045F.
Figure 2-10 Radar and seismic reflectors observed in borehole KC0045F.
Figure 2-11 Petrocore log of core from borehole KA2162B.
Figure 2-12 Overview of geological documentation, L=1500 1650 m.
Figure 2-13 Overview of geological documentation, L=1617.1-1762.6 m.
Figure 2-14 Overview of geological documentation, L=1762.1-1910.8 m.
Figure 2-15 Overview of geological documentation, L=2206.6-2383.6 m.
Figure 2-16 Overview of geological documentation, L=2383.6-2526.8 m.
Figure 2-17 Overview of geological documentation, L=2526.8-2722.0 m.
Figure 2-18 Overview of geological documentation, L=2722.0-2867.1 m.
Figure 2-19 Overview of geological documentation, L=3191-3350 m.
Figure 2-20 Overview of geological documentation, L=3350-3500 m.
Figure 2-21 Overview of geological documentation, L=3500-3600 m.
Figure 2-22 Geological mapping of elevator shaft, z=-200 to -440 m.
Figure 2-23 Location of water-bearing structures in the Äspö HRL tunnel.
Figure 3-1 Structural model of Äspö HRL (Rhén & Stanfors 1996).
Figure 3-2 Updated structural model at Z=-400 masl.
Figure 4-1 A heterogeneous fracture plane intersected by two vertical boreholes.
Figure 4-2 Pressure responses in borehole KA1061A during drilling of KA2511A.
Figure 4-3 Pressure responses in borehole KA3010A during drilling of KA2511A.
Figure 4-4 Pressure responses in borehole KA2050A during drilling of KA3010A.
Figure 4-5 Pressure responses in borehole KA2050A during drilling of KA3067A.
Figure 4-6 Pressure responses in borehole KA2162A during drilling of KA3067A.
Figure 4-7 Pressure responses in borehole KA2048A during drilling of KA3110A.
Figure 4-8 Pressure responses in borehole KA2050A during drilling of KA3110A.
Figure 4-9 Pressure responses in borehole KA2162B during drilling of initial parts of the TBM pilot borehole KA3191F.
Figure 4-10 Hydraulic connectivity model interpreted from responses recorded during drilling of KA3191F.
Figure 4-11 Pressure responses in borehole KA2161B during drilling of the TBM.
Figure 4-12 Pressure responses in borehole KA2511A during drilling of the TBM.
Figure 4-13 Pressure responses in borehole KA1751A during drilling of the TBM.
Figure 4-14 Pressure responses in borehole KA1754A during drilling of the TBM.
Figure 6-1 Lithology of the Äspö HRL .
Figure 6-2 Drawdown observed during drilling of TBM pilot borehole KA3191F
Figure 6-3 Connectivity inferred for the target volume

APPENDIX A1 COORDINATES FOR BOREHOLES AND TUNNEL SECTIONS

APPENDIX A2 IDENTIFIED HYDRAULIC STRUCTURES

1 INTRODUCTION

During 1996 the TRUE project will initiate detailed planning and execution of a first characterization phase for the TRUE Block Scale experiment. This initial characterization serves the purpose of finding a suitable location for the experiment. The general objectives of the TRUE Block Scale experiment can be summarized as follows (Bäckblom and Olsson 1994);

- to test numerical models and their predictive capability of radionuclide transport in a fracture network over distances 10-100 m,

- to test and evaluate scaling relationships using data from block, detailed and laboratory scales

The establishment of the experiment in the HRL is dependent not only on suitable geology and hydraulic behavior but also on the availability of locations within the HRL. Several other experiments such as the REX and TRUE-1 experiments already occupy parts of the rock volume in the vicinity to the access ramp. Further, sites for a demonstration repository and a prototype repository are in the process of being established. Also, the experimental setup of the TRUE Block Scale Experiment is not yet decided and may require certain access limitations, i.e. availability of entering the rock volume with new tunnel drifts or shafts. These limits together with the geometry of large zones intersecting the HRL constrains the location to a volume bounded by the following coordinates (Eastings, Northings); (1800,7100), (2200,7100), (2200,7450), (1800,7450) between levels (Masl) z = -350 to z = -450, Figure 1-1. In the following denoted the target volume for the TRUE Blockscale experiment.

A set of desired experimental conditions for the TRUE Block Scale Experiment have been defined (Winberg 1996). The most important ones are;

- Location outside tunnel spiral
- Size of experimental block 100x100x100m
- Location away from major fracture zones (i.e. EW-1 and NE-1)
- Access from multiple locations (vertically) in the laboratory
- No adverse hydraulic interference from other activities in the laboratory
- Transmissivity range of fractures making up the studied fracture network; T = $5 \cdot 10^{-8}$ - $5 \cdot 10^{-7}$ m^2/s
- Small gradient ($I < 0.05$)
- Flow velocities such that diffusion can be a measurable process

These desired experimental conditions should be condidered as guidelines, rather than absolute limitations, i.e. the selected site should qualify to as many limits as possible.

A prerequisite for updating of the conceptual model is the developed framework of major fracture zones as presented by Rhen & Stanfors (1996). However, the degree of detail in the current structural-hydraulic model has to

be increased in order to provide the necessary basis for the site selection within the target volume. Also, for selection of coming experiments in the HRL, there exists a need for enhanced detail of the conceptual model over the z = -400 m level.

1.2 OBJECTIVES

The objectives with this study is two-folded; the primary goal is to provide relevant data for scoping calculations of the TRUE Block Scale experiment and secondary to support future experimental localization and designs. To provide this, the following phases have been completed;

- compilation of available geological and hydrogeological information within the designated experimental volume
- evalution and updating of the existing structural model over the level z=-400 Masl level in the laboratory

The process of updating the conceptual structural-hydraulic model (Rhén et al 1996), is focused primarily on the designated experimental volume. However, to increase the degree of detail of minor waterbearing structures and their material properties throughout the HRL, a first stage update is produced over the section z = -400 Masl. The complexity of comprehending the large amount of available data enforces us to simplify this first stage interpretation.

1.3 DISPOSITION OF THE REPORT

The main result in this report is presented in chapter 5 as quantitative tables with structural and hydraulic data for zones and rock mass. The complete report presents the process of updating as follows;

- Chapter 2 describes the boreholes and tunnel sections which penetrate the target volume and form the basis for the structural-hydraulic model update
- Chapter 3 discusses the updating of the structural model.
- Chapter 4 presents the assessment of hydraulic connectivity providing plausible conductive pathways through the target volume.
- Chapter 5 presents hydraulic head data from selected boreholes penetrating the target volume.
- Chapter 6 summarizes quantitative data for zones and rock mass in the structural-hydraulic model.
- Chapter 7 presents a discussion regarding uncertainties and proposals for future work.

1.3 COORDINATE SYSTEM AND LOCAL NORTH

In this report the coordinate system used is the Äspö local coordinate system ($X_{äspö}$) where Magnetic north ($N_{Magnetic}$) deviates from Äspö local north by a clockwise 12 degrees rotation. All orientation measurements presented in

Appendix A are relative to local $N_{Äspö}$. In Figures and tables with orientation relative to $N_{magnetic}$, extracted from existing reports, this is noted.

2 BACKGROUND DATA FOR MODEL UPDATE

Relevant data has been compiled to provide input to the updating of the structural-hydraulic model. The data are of geological and hydrogeological type and is collected from boreholes, drillcores and tunnels. This chapter presents compiled data with emphasis on the target volume, although more boreholes and tunnel sections have been reviewed in the construction of the model. Integrated presentations are given of results of performed investigations in the identified tunnel sections and boreholes in the following sections. The main results in Chapter 2 are summarized in Chapter 3 and Appendix A2.

A prerequisite for updating of the conceptual model is that the developed framework of major fracture zones, remains as presented by Rhen & Stanfors (1996).

The following parts of the tunnel system intersect the target volume;

Tunnel A (access ramp) L = 1502.5 - 1848.4 m, L = 2300.7 - 2814.0 m.
Tunnel T (TBM) L = 75.0 - 408.4 m. (3266.3 - 3599.7 m)
Tunnel F (pump pit tunnel) L = 15.0 - 75.0 m.
Tunnel H (elevator shaft) Z = -200 - -470 m.

The following core drilled boreholes intersect, or are close, to the target volume; KAS02, KAS05, KA3191F, KA2162B, KC0045F, KA2511A and KA2598A. These holes have been analyzed in a number of different projects and their structural and hydraulic results are compiled below. There are also a large number of percussion drilled bore holes of which drilling and hydraulic testing results have been utilized in the interpretation. These holes are listed in chapter 3.

Tunnel centerline and borehole coordinates are compiled and presented in Appendix A1.

2.1 BOREHOLE 2511A

This borehole was drilled as a part of a program for an experimental site selection reported by Olsson et al. (1994).

The lithology is dominated by Äspö diorite (90%) and intersected by fine-grained granite (8.5%) and greenstone (1.5%). The core log from KA2511A is shown in Figure 2-1. There are three to four sections of increased fracturing confirmed by radar and/or seismics. Figure 2-2 show identified radar and seismic reflectors respectively. The fracture orientation is generally trending NNW with an additional subhorizontal set as shown in Figures 2-3 and 2-4. A

few distinct conductive structures are identified in KA2511A with transmissivities in the range of $T = 10^{-5} - 10^{-4}$ m^2/s as shown in Figure 2-5. Pressure build-up tests and 3 m packer tests yield a geometric mean transmissivity $T = 2.1 \cdot 10^{-7}$ m^2/s in the tested sections in the borehole. Table 2-1 and Figure 2-6, respectively, presents the results of the 3 m packer tests in the test sections.

Table 2-2 summarizes anomalies identified in borehole KA2511A. Three locations along KA2511A can be correlated to both fracturing, seismics, radar and inflow. Two more inflows are located in fine-grained granite. Appendix A2 presents evaluated transmissivity for the five most pronounced conductive structures in KA2511A.

2.2 BOREHOLE KA2598A

This borehole was drilled as a part of a program for an experimental site selection reported by Olsson et al. (1994).

The litology along the borehole is dominated by Småland granite (73%), Äspö diorite 15% and a larger fine-grained granite at L = 2.4 - 47.8 m (12%). In Figure 2-7, corelogging shows a section of crushed rock in a greenstone in the fine-grained granite at L = 62 m. Radar and seismic indications along the borehole are illustrated in Figure 2-8 but do not correlate well. Two radar and one seismic indication, shown in Table 2-3, correlate both with increased fracturing or crushed rock and water inflow. At the two largest inflows, 13 and 18 m, no structural evidences are found. However, the inflows occur in a section of fine-grained granite with low observable fracture frequency, indicating that the fine-grained granite is highly conductive.

2.3 BOREHOLE KC0045F

This borehole was drilled as a part of a program for an experimental site selection reported by Olsson et al. (1994).

The lithology in this hole is dominated by Äspö diorite (60%) and has an unusually large content of fine-grained granite (33%). A hypothesis is that borehole KC0045F intersects a flat lying body of fine-grained granite with large subhorizontal extent. The fracture frequency, visible in the core log in Figure 2-9, is high throughout the fine-grained granite and in the lithological contacts. Radar and seismic observations, in Figure 2-10, indicate larger structures at L = 136, 140-160, 198-207, 230-240 and 260-265 m. A summary of indications in KC0045F is presented in Table 2-4.

Seven conductive structures, NNW trending, have been identified mostly by both hydraulic, structural and geophysical measurements. Appendix A2 lists the locations, known hydraulic responses and evaluated transmissivity for each

of these structures. However, the estimation of material properties may be affected by packer leakage in all sections (Olsson et al., 1994).

2.4 BOREHOLE KA2162B

The drilling and hydraulic testing in KA2162B is reported by Carlsten et al (1994) and Forsmark et al (1994).

The lithology is dominated by Småland granite (60%) where the central part intersects a 80 m wide fine-grained granite (28%). Fracture frequency, Figure 2-11, is high in the fine-grained granite, average RQD ~30, with crushed rock at lithological contacts at L = 170 and 255 m. Table 2-5 presents the pressure response observations and flow into the borehole during the drilling. There are at least three major inflow points at L = 49-53, 121 and 165-174 m. A correlation between radar, inflow and structures, Table 2-6 show a large number of structures intersecting this hole. Most of them are steep NNW trending structures. The material properties and responses from pressure build-up tests of these zones are included in Appendix A2.

2.5 BOREHOLE KAS02

The drilling and hydraulic testing in this borehole is reported by Stanfors (1988) and Rhén (1988).

The lithology in KAS02 between 300 and 500 m depth is equal amount of diorite and Äspö granite and a few sections of fine-grained granite (14%). There is increased fracturing at 315 and 370 m with radar indications at both levels. The subvertical zone interpreted to intersect KAS02 at 315 m is zone NE-2. Spinner measurements for section 309 to 318 show a transmissivity of $1.4 \cdot 10^{-5}$ m^2/s. No data is available for borehole section 370 m.

2.6 BOREHOLE KAS05

The drilling and hydraulic testing in this borehole is reported by Nilsson (1989).

The lithology in KAS05 between depth -300 to -500 masl is dominated by Äspö diorite (~80%) with few fine-grained granites. Fracture orientation is mostly subhorizontal according to Nilsson (1989). The borehole intersects a major zone at L = 310 - 337 m which may be interpreted as zone NE-2. The identified hydraulic conductors are shown in Table 2-7.

2.7 TUNNEL AND SHAFT SECTIONS

Stanfors and Rhén (1993, 1994, 1995) presented the geological compilation of tunnel and shaft data.

Compiled geological information of tunnel sections L = 1502.5 - 1848.4 m to L = 2300.7 - 2814.0 m are shown in Figures 2-12 to 2-18. Documented observations from both the TBM tunnel and the elevator shaft, below -200 masl, are shown in Figures 2-19 to 2-22. Fracture orientations are given for each tunnel leg.

In the updating process, only waterbearing fractures intersecting 75% or more of the tunnel perimeter are considered. The compilation has been focused on minor faults and zones, thus excluding the major zones. Mazurek et al (1995) compiled information of waterbearing faults and fault systems throughout the HRL. Tunnel structures included in the updating process generally follow their compilation. Figure 2-23 shows the location and spatial distribution of waterbearing faults.

3 UPDATING OF THE STRUCTURAL MODEL

To increase the degree of detail in the existing structural model, information of faults and minor zones acting as hydraulic conductors are compiled and presented in a conceptual structural model. The primary goal for the updating process has been to increase the degree of detail in the TRUE Block Scale target volume. However, an updated structural model has been produced over the whole HRL at level z = -400 masl. A summary of identified hydraulic structures is listed in Appendix A2.

3.1 EXISTING CONCEPTUAL STRUCTURAL MODELS

Previously, a number of different conceptual structural-hydraulic models have been published. Some of these models have been produced within specific experiments at certain localities in the HRL, others has concentrated on specific structures or zones. Stanfors & Rhén (1992 - 1996) produced and updated a site scale structural model throughout the construction phase, Figure 3-1. Winberg et al. (1996) developed several detailed structural models over specific locations along the access ramp describing minor zones and single waterbearing faults. Hermanson (1995) showed the 3D spatial variability of large waterbearing fault in the HRL.

In order to assess minor waterbearing structures a review of previously published structural and hydraulic models has been made. Where applicable, minor structures have been extracted and included in the new model, or reanalyzed with respect to its structural characteristics. However, the major zones intersecting the HRL form the framework of the updated structural model, i.e. major zones are implemented in the new model as is. The updated model only intends to increase degree of detail, not to change the foundations of the general structural model.

3.2 STRUCTURAL MODEL UPDATE

Fractures have been continuously mapped during the construction of the HRL. Most fractures tend to be non-water conducting and only approximately 10% of all mapped fractures in the tunnel are mapped to be waterbearing.

Looking at the waterbearing fracture population, only a few crosscut the whole or most of the tunnel. It is assumed that this population is true waterbearing structures extending beyond the tunnel perimeter. This assumption and this population is supported by Mazurek et al.(1996) in their selective mapping of hydraulically important minor zones and major faults along the access ramp. Most of these faults are steeply dipping or vertical with a major trend towards NW-NNW.

Note that waterbearing faults along the tunnel occur on different levels, between -230 to -470 masl, in the HRL. This implies that a true structural model needs to be in 3D rather than a 2D planar map. But the fact that these faults are mostly very steep suggest that it may be possible to visualize a structural map in one single plane. However, the major structures dip around 75° to 85° degrees which means that a lateral shift in zone intersection at depth change with as much as 50 m per 100 m elevation difference may be expected. The intersection of dipping structures is a 3D problem and can not be satisfactorily analyzed in 2D. Nevertheless, for purposes of easy understanding of the major structural trends, the interpreted possible structural-hydraulic pathways are presented in a map *in plano* at the -400 m level.

In the updating process, all cored boreholes, many percussion boreholes and selected tunnel sections in the HRL or in its vicinity have been considered, although the updating has been focused on the target volume. Following a similar approach as outlined in Chapter 2, information has been compiled from the following boreholes:

Core drilled boreholes (surface)	Core drilled boreholes (tunnel)
KAS 02	KA1751A
KAS 04	KA1754A
KAS 05	KA1755A
KAS 06	KA2048A
KAS 07	KA2162B
KAS 08	KC0045F
KAS 12	KA2511A
KAS 16	KA2512A
Percussion boreholes	KA2598A
HA1684B	KA2858A
HA1704B	KA2868A
HA1749A	KA3005A
HA1852A	KA3010A
HA1896A	KA3067A
HA1960A	KA3110A
HA2074A	KA3191F
HA2074B	KA3385A
HD0025A	
SA2025B	

In these boreholes, a systematical review has been performed of structural and hydraulic anomalies. Previously executed tests have been compiled into one table describing the characteristics of faults and minor structures and the evidence of their existence. Appendix A2 summarizes all structural and hydraulic evidence for the identified structures. The indications are listed by borehole, i.e. structures in a borehole are tabulated with listings of known hydraulic, geophysical or geological indications. Where interpreted, a specific zone notation has been assigned to a given structure.

The location of each hydraulic structure has been added to the structural model, and based on individual locations and orientations, interpretation of possible hydraulic pathways is suggested. Figure 3-2 show the updated structural model with interpretations of possible hydraulic pathways in the HRL on -400 masl. As most of the indications in both boreholes and tunnel are subvertical, it is possible to integrate information from many different levels in the HRL. However, the hydraulic pathways also works in 3D which makes the impression of Figure 3-2 somewhat misleading.

The structural information from boreholes and the tunnel is most often not enough to define a single structure. It is important to know that geological structures rarely occur as perfectly planar features. Faults commonly connect to each other through stepping with splay fractures forming the steps. The faults also show a wide variety of complexity along the strike. Observations in the tunnel has shown that a planar single fault observed in the tunnel may well transform into a complex fault system with lenses of good rock (Mazurek et al., 1995). Possible connectivity in the structural model is therefore illustrated as bands of possibly higher probability of having waterbearing structures.

Fault stepping may exist, with faults partly overlapping each other, and connected with each other by splay fractures and thus forming a hydraulic pathway trending 20° to 30° away from a linear projection of the fault. If fault stepping exists in a large scale, the number of possible pathways of connectivity increases dramatically. However, with no other evidence the first assumption is connectivity is highest parallel to strike rather than 20°-30° offset.

The framework of major zones constrain the projected extension of possible hydraulic pathways as they in most cases act as hydraulic boundaries. Zone NE-2 is different as it is a central zone intersecting the whole HRL. This zone is variable in width and are reported to be a m wide dry mylonite at several tunnel intersections as well as being characterized as faulted and highly conductive at others. It is one of the few structures with a NE trend and may therefore play an important role in connectivity through the HRL.

The numerous NNW trending faults in the central part of the HRL indicate the presence of the zones NNW-1 and NNW-2 c.f. Figure 3-2. The NNW trend seem to be persistent with a more or less regular interval westwards. The poorly defined zone NNW-5 is assumed to intersect KA2598A and KA2511A but is doubtful to be visible in the pit tunnel (F-tunnel) or the TBM.

The north western part of the HRL has a slight tendency of offspring structures parallel to EW-1 or NE-2 whereas the easterly part seem to have a more definite NW trend, sustained by zones NNW-4, NW-2 and NW-3.

4 ASSESSMENT OF HYDRAULIC CONNECTIVITY

Hydraulic connectivity is assessed through various hydraulic tests and activities performed in the HRL. Pressure changes caused by activities such as drilling and blasting and pump tests are regularly monitored by the Hydraulic Monitoring System, HMS. In addition portable loggers are frequently used in specific tests. In this chapter sources to analyzed pressure changes are discussed. By reviewing the pressure history of undertaken drilling and testing activities, the connectivity between borehole sections is examined. The result is presented as connectivity matrices.

4.1 DRAWDOWN EVENTS AND THEIR INTERPRETATION

The following types of possible "pressure sources" have been examined:

- tunnel excavation
- borehole drilling
- pump testing
- injection testing
- water sampling (opening valve)

The origin of pressure changes may be difficult to assess as different sources may be active simultaneously. That is, pressure changes are additive (through superposition). To increase the probability of understanding the proper connectivity a large number of different pressure change events are used in the analysis.

The problem of superposition is not the only factor that may hinder a correct interpretation of whether there exits a response between any two points. One important factor is the distance between the "pressure source" and the "receiver point" of observation. That is, the larger the distance the smaller the response and vice versa (all other factors kept constant). Other important factors are the magnitude and duration of the pressure change and any heterogeneity and/or anisotropy in the hydraulic properties (permeability and compressibility).

For a homogeneous medium the principle of reciprocity says that the test response between any two points A and B is identical regardless of which point that is acting as the source point. That is, the pressure changes at B while pumping at A are the same as the pressure changes at A while pumping at B. The principle of reciprocity is valid to all flow systems. However, in heterogeneous media, such as fracture zones, it may be difficult to validate in the field for practical reasons. For example, the hydraulic testing conducted in the SELECT programme of interference tests (Winberg et al., 1996a) shows evidence where testing at "point A" gives a response at "point B" but the reciprocity is not found when the test is reversed. This fact can in most cases be be explained by the fact that the source strength (pump rate) is not equal

due to difference in transmissivity in the test sections in question and the limited duration of the tests.

Figure 4-1 shows a simple hypothetical situation which illustrates the difficulty to validate the principle of reciprocity. The figure shows a heterogeneous horizontal fracture plane intersected by two vertical boreholes, A and B. Borehole A is located in the centre of a region with low transmissivity whereas B is closer to the surrounding region where the transmissivity is much higher. The evolution in time of the response at point B while pumping at point A will be quite different from the evolution of the response at A while pumping at B (if the discharge rate is kept constant valued between the two pumping tests). While pumping at point B the region with a high transmissivity will interact at a different time and unless the discharge rate at B is increased, practically no pressure changes will be recorded at point A.

4.2 CONNECTIVITY ANALYSIS

The connectivity has been assessed through pressure monitoring during hydraulic tests or other activities in the HRL. The main objective has been to describe the general site scale pattern of connectivity. Available data are presented in three parts of the HRL: the south west corner, north east corner and the central part of the HRL . A matrix of connectivity, based on pressure disturbance from drilling, is shown in Table 4-1. Selected interference test results in the north east corner around the TRUE-1 site are presented in Table 4-2. Finally the more complex connectivity pattern in the central part of the HRL is illustrated through responses to the excavation process of the TBM tunnel, Table 4-3.

In Chapter 6, c.f. Figure 6-3, a summary of the inferred connectivity in the HRL is presented.

4.2.1 Hydraulic connectivity in the south west corner of the HRL

Zone NE-1 forms the southern hydraulic boundary in this area. Drilling of KA2511A revealed responses in KA1061A and KA1131B, c. f. Figures 4-2 and 4-3, which are located in zone NE-1 (Olsson et al., 1994). This implies connectivity between one or more structures intersecting KA2511A and NE-1. There are also pressure disturbances in SA1684B, SA1861B, Ka1751A, KA1754A and SA2338A. One possibility to explain this connection is a north easterly connector. There are three possible pathways according to the structural model; connectivity through either EW-1 or through NE-2. EW-1 is reported to be locally conductive ($T = 1.2 \cdot 10^{-5}$ m^2/s) (Rhén 1996). NE-2 intersects the south west corner, and is reported as a comparatively tight structure, $T = 1.2 \cdot 10^{-7}$ m^2/s, (Rhén 1996). Both zones seem possible as connectors.

Fracture zone NNW-5 intersects KA2511A at 53 m and KA2598A at 75 m (Stanfors 1994). Evaluated pump tests show a transmissivity of NNW-5 between $3.6 \cdot 10^{-5}$ to $1.2 \cdot 10^{-6}$ m^2/s (Olsson et al., 1994). To the west of NNW-5 there are two more minor zones intersecting KA2511A. These structures also connect to NE-1, KA1751, KA1754A and SA2338A and has a transmissivity range between T $=10^{-5}$ to 10^{-6} m^2/s (Olsson et al., 1994).

In summary the south western part of the HRL appears dominated by NNW trending hydraulic conductors, comparatively isolated from each other. Although structurally a minor zone, NNW-5 and its sub parallel sister structures further west dominates the hydraulic connectivity together with either EW-1 or NE-2, or both, acting as E-W connectors.

4.2.2 Hydraulic connectivity in the north east corner of the HRL

The drilling of KA3010 caused pressure drops in the order of 40 kPa in all three sections of KA2050A, c.f. Figure 4-4. The intersected structures are interpreted as Zones NW-2 or NW-3 (Winberg 1996b). Pressure responses in the order of 80 kPa where observed during drilling of KA3067A in all sections in KA2050A , c. f. Figure 4-5. It is notable that the East-West connectivity is limited as no pressure perturbations are recorded in the otherwise highly conductive borehole KA2162B, c.f. Figure 4-6.

Drilling of KA3110A caused rapid drawdowns in test sections KA2048A:P5, (interpreted to contain NNW-4) and all three sections in KA2050A (interpreted to contain NW-2 and NW-3), c.f. Figures 4-7 and 4-8 (Winberg 1996b). The response in KA2050A is not as pronounced as the response in NNW-4 (KA2048A:5P).

Table 4-2 presents results from an extensive program of interference tests in the north eastern part of the HRL. There is reported connectivity between boreholes KA3010A, KA3068A, KA3105A and KA3110A implying NW connectivity (Winberg 1996a). However, there is also connectivity with KA2858A, KA2862A, HA1960A, KA2162B (section P3 and P4), SA2880 and SA3045. One possible pattern of connectivity is a NW-2 intersection with NNW-4 north of the spiral. NNW trending faults connected to the zone NW-2 intersect KA2162B and NNW-4, thus forming a plausible pathway of connectivity. There is also a possibility that NE-2 acts as a north easterly connector, intersecting both NW-2 and NNW-4.

The general picture of hydraulic connectivity in the north easterly part of the HRL is dominated by the three zones, NW-2 and NW-3 and NNW-4 all of which intersect this rock volume. The zones are possibly interconnected with each other either by splay faults from NW-2 (Winberg, 1996b), or by intersection of the zones to the east of the tunnel, or to the north of the tunnel. There seem to be very little connectivity to the western part of the HRL although NE-2 may work as a east-westerly conductor.

4.2.3 Hydraulic connectivity in the central part of the HRL

Investigations of the central part of the HRL show a more complex picture of connectivity. A fairly large number of waterbearing structures intersect the central part of the TBM tunnel and tunnel legs E-F, F-G and J-K. Surface investigations predicted three NNW trending zones through the spiral. The waterbearing faults in the indicated sections are interpreted as swarms rather than zones, but may well be hydraulic connectors. Boreholes KA2162B, KA3191F and KC0045A intersect this volume with almost an orthogonal angle to the dominating fracture network. KA2162B intersects a splay structure to NNW-4 at L=49-53 m which induces responses in HA1960A, SA1861B and SA1680A. Again the same responses are found at intersection L = 121 m. The latter is interpreted as part of the NNW-2 zone, although connected to NNW-4.

The drilling of the TBM pilot hole KA3191F caused responses in all four sections of KA2162B, Figure 4-9, in the order of 40 kPa. There were also responses of varying quality in KAS16:P2, SA2240B, KAS05:P3, KAS05:P2, KAS02:P3, SA2663B and SA2734A. Figure 4-10 illustrates the complex connectivity pattern when drilling through one structure in KA3191F, based on the possible pathways in the structural model.

The drilling of the TBM tunnel imposed drawdowns in large volumes of the HRL and especially in the neighboring borehole KA2162B. Drawdowns were identified in borehole KA2162B, all sections, at TBM length L = 249 m. Figures 4-11 to 4-14 and Table 4-2 summarize pressure responses in KA2162B, KA1751A, KA1754A and KA2511A dueto the TBM drilling. At TBM length L=299 m there was a pressure drop in all sections in KA2511A. This is explained by a NE trending fault system through the TBM and pit pump tunnel at L = 380 m intersecting NNW-5 and its sister structures NNW-5b and NNW-5c.

Advancing with the TBM up to 350 m, KA1751A, KA1754A, KA2511A, and KA2162B are affected by the pressure disturbance. There is good connectivity in the NNW trending faults west and south of the elevator shaft, with responses in KA2162B.

In summary the connectivity in the central (and southern) part is governed by NNW to NW trending structures. NE-2 may affect the connectivity in an east-west direction, although the NE trending fault system through the TBM and pit pump tunnel may do it equally well. However, in the central part of the HRL a body of fine-grained granite found in both KC0045A and KA2162B, interpreted as a possible gently dipping sheet, may act as connector between NNW trending zones.

5 HYDRAULIC HEAD

Low hydraulic gradient is one criteria set up for selection of target volume for TRUE Block scale experiment, and can be assessed from hydraulic head measurements in sectioned-off boreholes. Hydraulic head has been calculated for HMS monitored boreholes below tunnel section L = 2000 m.

Hydraulic head for each monitored borehole section is calculated according to Rhén (1993) as follows:

$HH=K1+K2\times MV$

HH = hydraulic head (masl)
MV = pressure measured by pressure tranducer

$$K1 = \frac{\rho_s g(Z_{tr} - Z_{mid}) - P_0}{\rho_0 g + Z_{mid}}$$

ρ_s = density in tube between pressure transducer and section center
g = 9.81 m/s^2
Z_{tr} = level of pressure transducer (masl)
Z_{mid} = level of section centre (masl)
P_0 = normal atmospheric pressure (Pa)
ρ_0 = density of fresh water (kg/m^3)

$K2 = 1000/(\rho_0 \times g)$

The density ρ_s has been estimated trough calculations of measured or estimated values of the electrical conductivity. Values of the electrical conductivity of Äspö water is collected from Nilsson (1995) and from Nilsson (pers. comm. 1996). In the cases of missing measurements, electrical conductivity from adjacent borehole sections have been used. The density ρ_0 has been given values according to Rhén (1993). Values of Z_{mid} have been extracted from SICADA in june 1996. Values for Z_{tr} is collected at the time of installation of the pressure transducers. Table 5-1 presents the calculated head for each monitored borehole section.

6 SUMMARY DESCRIPTION OF TARGET VOLUME MODEL

This chapter summarizes the structural-hydraulic model update. Below follows short concise descriptions and graphics of lithology, key features and quantitative tables of major fracture zones, minor fracture zones and rock mass properties.

6.1 LITHOLOGY

The lithology of the rock mass in the target volume, as shown in Figure 6-1, is dominated by Äspö diorite and intersected by dikes, strongly foliated and deformed fine-grained granite. There exists a penetrative planar foliation in the diorite, steeply dipping towards 80° NNW and locally disturbed by ductile shear or intruded fine-grained granite. The NW part of the block intersects a larger body of fine-grained granite which is highly conductive. Also, the central part of the HRL hosts a large body of fine-grained granite, interpreted to be subhorizontal. A hypothesis is that this body may be an important connector between steep NNW trending structures.

6.2 FRACTURE ZONES

The major fracture zones in the vicinity of the HRL are provided as defined by Stanfors & Rhén (1996). Table 6-1 describes the location and orientation of the major zones, here approximated to planes. Assumed extension of each zone and its interaction with other major structures is provided in Table 6-2. Interpreted hydraulic properties are presented in Table 6-3 with width estimations from borehole intersections. Table 6-4 provides transmissivity based on results from hydraulic tests and interpreted intersections of the Äspö HRL tunnel and boreholes (see also Table 6-3).

Evaluated minor fracture zones and waterbearing faults in boreholes and tunnels in the HRL are provided in Appendix A2. Identified hydraulic structures within the target volume are compiled in Table 6-5. Where possible notations are made of intercepts of identified zones.

Structurally EW-1 and NE-2 are the largest zones within the target volume. However the main trend of waterbearing faults is NW to NNW. Indications of connectivity show that NW to NNW trending structures are the main conductors (see Chapter 4) and Figure 6-2. This figure illustrates the drawdown ellipse during drilling through water conductors in KA3191F and is a representation of the general trend of connectivity in the HRL. E-W structures are reported comparatively tight (Rhén 1996), except for the southern flank of EW-1. There are a few more hydraulic indications of E-W connectivity which is attributed to the fracture network and possible interconnection between single faults. Further, the subhorizontal body of fine-grained granite is a possible connector between NW trending zones.

Although E-W connectivity exists, based on the hydraulic information from pump tests and drilling activities it appears that the SW part of the HRL is hydraulically separated from the NE part. However, the testing period of most hydraulic tests is too short to achieve steady state conditions. The understanding of tests is therefore local and does not fully reveal connectivity over longer distances.

The main identified hydraulic structures within the target volume are NNW-5c, NNW-5b, NNW-5, NNW-1, NNW-2, EW-1 and NE-2, c. f. Figure 6-3. There are more indications of hydraulic connectivity, as suggested in Figure 6-3, although not properly defined due to lack of information. Note that Figure 6-3 illustrates connectivity (blue stroked lines), as indications of most plausible pathways based on the structural model. Some lines of connectivity lack quantitative data on material properties but are inferred by responses from pump tests in boreholes in the vicinity and from waterbearing faults in the tunnel.

Identified zones not covered by table 6-1 to 6-4 is shortly described below:

- The vertical minor zone NNW-1b intersects the tunnel at L =1700 m and the TBM at L = 3355 m and has an evaluated transmissivity T = $0.6 \cdot 10^{-5}$ to $2.9 \cdot 10^{-5}$ m^2/s (Forsmark et al., 1994). The extent of this zone is poorly known. Its width is estimated to be at least 2 m (Mazurek et al., 1995).

- The vertical structures NNW-5b and NNW-5c are interpreted from intersections with KA2511A. NNW-5b may also intersect the end of the TBM, c.f. Figure 6-3.

The evaluated transmissivity of NNW5b and NNW-5c is T = $2.4 \cdot 10^{-5}$ m^2/s respectively (Olsson et al., 1994). The extents of these zones are poorly known and are only documented in KA2511A as intersecting waterbearing faults.

6.3 ROCK MASS PROPERTIES

Rock mass properties are divided into fracture network properties describing fracture specific information, and hydraulic properties for rock mass units in the HRL.

6.3.1 Fracture network properties

Quantification of the fracture network of Äspö has been attempted by several authors (Dershowitz et al 1996, Follin et al 1996, Hermanson 1996, La Pointe et al 1996, Mazurek et al 1995, Poteri 1996, Uschida 1994). Dershowitz et al (1996) also incorporated borehole information from the TRUE-1 site with results from earlier investigations of the fracture network in estimating fracture network properties such as orientation, size, intensity, and spatial model.

Waterbearing fracture orientation statistics for tunnel data, presented in Table 6-6 is based on 2D and 3D trace map data from the tunnel. Three sets are defined in the fracture network, with dominance of NW trending structures. There is also a subhorizontal fracture set. This data, from the whole HRL is consistent with data from the TBM tunnel.

Fracture size is estimated through intersection statistics with the tunnel. Dershowitz et al (1996) show that depending on the methology of mapping the results can vary, c. f. Table 6-7. However, studies by La Pointe (1995), Hermanson (1996), Follin et al., (1996) and Dershowitz et al., (1996) all show a logarithmically distributed waterbearing fracture population with arithmetic mean size of 6 m a standard deviation of 2 to 3 m.

Indications from the TRUE-1 site show that the rock mass has an intensity of conductive fractures (with transmissivity greater than 10^{-9} m^2/s) of between 0.8 to 1.3 m^{-1} for the conductive fracture intensity range of 3 to 8 m^{-1} which provides the best fit to spinner log results. Dershowitz reports an evaluated $\log_{10}$ mean transmissivity of -9.3 for the fracture network.

The storativity and transport aperture for fracture planes was estimated as a first approximation using the relationship derived for the LPT2 experiment (Uchida et al., 1994), i.e. $S = 0.001\ T^{1/2}$ and $e = 0.5\ T^{1/2}$.

6.3.2 Material properties of rock mass domains

The hydraulic conductivity of the rock mass is presented in Table 6-8 from a compilation of data from boreholes intersecting the Äspö Island. The test scale is 100 m and results are presented in 100 m sections. Results of hydraulic conductivity of the rock mass from 3 m tests in boreholes intersecting the HRL (KAS02, KAS05-08) are presented in Table 6-9.

7 CONCLUSIONS

The major hydraulic connectors in the HRL at -400 masl are NW to NNW trending zones. The connectivity in E-W direction exist but is not dominating. There are indications of low connectivity between the SW corner of the HRL and NE corner. However, connectivity is not only sustained through fracture zones. The fracture network contain waterbearing faults that may interconnect through splay fractures and thus acting at hydraulic connectors to larger NW trending zones. A large body of fine grained granite, in the central part of the HRL may also affect the E-W connectivity.

An important constraint to production of this report is the limited time available for the updating process. The updating of the structural-hydraulic model involves extensive literature surveys as the accumulated data at Äspö HRL is huge. Interpretations of structures and their hydraulic properties also change by the evolution of the HRL, making earlier work in part misleading. The large amount of pump tests, their interpretation and the assignment of the results to geological structures involve allow possibilities of error.

A thorough connectivity analysis of the fracture network at the Äspö HRL must be made in three dimensions using a computer based visualization tool. Regarding the available information on hydraulic responses, great concern must be put on quality assurance. The subjective expressions about observed hydraulic responses that are frequently used in the reporting must be revised and evaluated with regard to time, distance and heterogeneity in material properties. It is emphazised that there exists a need to assign analytical values to the often used qualifiers "great, large, good, weak, small, poor, none".

8 REFERENCES

Carlsten S., Ramquist G., Stanfors R., 1994. Supplementary investigations of fracture zones in the tunnel, core mapping data and radar measurement. Compilation of technical notes.

Carlsten S., Stanfors R., Askling P., Annertz C., 1995. Comparison between borehole radar data and geological parameters from tunnel mapping. SKB PR 25-95-22.

Dershowitz, W. Thomas, A., Busse, R., 1996. Discrete fracture analysis in support of the Äspö Tracer Retention Understanding Experiment (TRUE-1). SKB ICR 96-05.

Follin S., Hermansson J., 1996, Discrete fracture network modeling of the TBM tunnel rock mass, Äspö HRL. SKB AR D-97-001.

Forsmark T., Stenberg L., 1994. Supplementary investigations of fracture zones in the tunnel. Hydrogeology. Compilation of technical notes. SKB PR 25-94-06.

Hermansson J., 1996. Visualization of the fracture network in rock blocks along the Äspö HRL tunnel using a DFN model approach. SKB PR HRL-96-08.

La Pointe P. et al. 1995. Estimation of effective block scale conductivity's based on discrete network analyses using data from the Äspö site. SKB TR 95-15.

Nilsson L., 1989. Hydraulik tests at Äspö, KAS05-KAS08, HAS13-HAS17, evaluation. SKB PR 25-89-20.

Mazurek, M. Bossart, P. 1995. Classification and characterization of water-conducting features at Äspö. Results of phase I investigations. SKB PR 25-95-21.

Munier R., 1995, Studies of Geological structures at Äspö. SKB PR 25-95-21.

Olsson O., Stanfors R., Ramquist G., Rhén I., 1994. Localization of experimental sites and layout of turn 2- results of investigations. SKB PR 25-94-14.

Olsson O., 1994. . Localization of experimental sites and layout of turn 2 - results from core mapping, radar and hydraulic investigations. Compilation of technical notes. SKB PR 25-94-15.

Poteri A., 1996. Analysis of bedrock fracturing at Äspö. SKB ICR 96-01.

Rhén I., Forsmark T., Danielsson P., Piezometric levels, evaluation of the data from section 1475-2265. SKB PR 25-93-13.

Rhén I., Stanfors R., Wikberg P., Forsmark T., 1995. Comparative study between the cored test borehole KA3191F and the first 200 m extension of the TBM tunnel. SKB PR 25-95-09.

Rhen I., Stanfors R., 1995. Supplementary investigations of fracture zones in Äspö tunnel. SKB PR 25-95-20.

Rhén I., 1995, Documentation of tunnel and shaft data, tunnel section 2874 - 3600 m, hoist and ventilation shafts 0 - 450 m. SKB PR 25-95-28.

Rhén I., (ed), Gustafsson G., Stanfors R., Wikberg P., (in prep) Äpö HRL-Geoscientific evaluation 1997/5. Models based on site characterization 1986-1995. SKB TR 97-06.

Stanfors R., et al. 1993. Geological-structural and rock mechanical evaluation of data from tunnel section 1475 - 2265 m. SKB PR 25-93-10.

Stanfors R., et al. 1994. Geological-structural and rock mechanical evaluation of data from tunnel section 2265-2874 m. SKB PR 25-93-19.

Stanfors R., Rhén I., Forsmark T., Wikberg P., 1994. Evaluation of the fracture zone EW-1, based on the cored boreholes KA1755A, KA1751A, KA1754A and KAS04. SKB PR 25-94-39.

Uchida, M., Doe, T. Dershowitz, W., Wallmann, P., Sawada, A., 1994.Discrete-fracture modeling of the Äspö LPT-2, large scale pumping and tracer test. International cooperation report ICR 93-09.

Winberg A., Andersson P., Hermansson J., Stenberg L., 1996a. Results of the SELECT project, investigation program for selection of experimental sites for the operational phase. SKB PR HRL-96-01

Winberg A.(ed), , 1996b. Descriptive structural-hydraulic models on block and detailed scales. Äspö Task Force Task 4A (SKB TRUE project team, PNC/Golder team, USDOE/LBNL team). SKB International cooperation report ICR 96-04.

TABLES

Table 2-1 Results from flow and pressure build-up tests in KA2511A (from Olsson et al., 1994)

Section (m)	Flowrate Q (m^3/s)	Spec. capacity Q/dh (m^2/s)	Trans-missivity (drawdown) (m^2/s)	Trans-missivity (1/Q) (m^2/s)
172 - 175	$3.58 \cdot 10^{-7}$	$6.5 \cdot 10^{-9}$	$3.3 \cdot 10^{-7}$	-
175 - 178	$1.37 \cdot 10^{-6}$	$7.0 \cdot 10^{-9}$	$1.9 \cdot 10^{-7}$*	-
178 - 181	$7.39 \cdot 10^{-6}$	$3.8 \cdot 10^{-8}$	$9.9 \cdot 10^{-8}$	$7.6 \cdot 10^{-8}$
181 - 184	0	$1.0 \cdot 10^{-12}$	$1.0 \cdot 10^{-11}$	-
184 - 187	$8.33 \cdot 10^{-8}$	$4.9 \cdot 10^{-9}$	$1.5 \cdot 10^{-6}$	-
187 - 190	$1.33 \cdot 10^{-7}$	$3.3 \cdot 10^{-9}$	$1.6 \cdot 10^{-7}$**	-
190 - 193	$1.08 \cdot 10^{-7}$	$1.1 \cdot 10^{-8}$	$6.0 \cdot 10^{-7}$	-
193 - 196	$1.58 \cdot 10^{-7}$	$2.9 \cdot 10^{-9}$	$1.5 \cdot 10^{-7}$	-
196 - 199	$2.50 \cdot 10^{-7}$	$2.0 \cdot 10^{-8}$	$3.5 \cdot 10^{-7}$	-
199 - 202	$1.83 \cdot 10^{-7}$	$3.1 \cdot 10^{-9}$	$3.4 \cdot 10^{-6}$*	-
202 - 205	$1.61 \cdot 10^{-7}$	$1.1 \cdot 10^{-7}$	$7.4 \cdot 10^{-7}$	-
205 - 208	$1.00 \cdot 10^{-7}$	$1.6 \cdot 10^{-9}$	$9.2 \cdot 10^{-8}$	-
208 - 211	$2.33 \cdot 10^{-7}$	$1.5 \cdot 10^{-8}$	$1.8 \cdot 10^{-7}$	-
211 - 214	$3.33 \cdot 10^{-8}$	$1.1 \cdot 10^{-9}$	$7.3 \cdot 10^{-8}$	-
214 - 217	$1.67 \cdot 10^{-8}$	$7.6 \cdot 10^{-9}$	$2.9 \cdot 10^{-7}$**	-
217 - 220	$1.67 \cdot 10^{-8}$	$3.8 \cdot 10^{-10}$	$1.8 \cdot 10^{-8}$	-
220 - 223	$9.14 \cdot 10^{-6}$	$2.9 \cdot 10^{-8}$	$3.9 \cdot 10^{-7}$***	$2.4 \cdot 10^{-7}$
223 - 226	$2.93 \cdot 10^{-4}$	$1.1 \cdot 10^{-6}$	$2.3 \cdot 10^{-5}$*	-
226 - 229	$1.68 \cdot 10^{-4}$	$5.8 \cdot 10^{-7}$	$1.7 \cdot 10^{-5}$***	$1.0 \cdot 10^{-6}$
229 - 232	$4.33 \cdot 10^{-5}$	$1.4 \cdot 10^{-7}$	$2.7 \cdot 10^{-6}$***	$3.5 \cdot 10^{-7}$
232 - 235	$3.06 \cdot 10^{-5}$	$9.9 \cdot 10^{-8}$	$9.3 \cdot 10^{-7}$	$7.1 \cdot 10^{-7}$
235 - 238	$8.23 \cdot 10^{-6}$	$2.6 \cdot 10^{-8}$	$7.0 \cdot 10^{-7}$***	$3.8 \cdot 10^{-7}$
238 - 241	$4.36 \cdot 10^{-5}$	$1.4 \cdot 10^{-7}$	$3.7 \cdot 10^{-6}$***	$4.6 \cdot 10^{-6}$
241 - 244	$1.67 \cdot 10^{-8}$	$8.4 \cdot 10^{-11}$*	$1.1 \cdot 10^{-8}$**	-
244 - 247	$1.67 \cdot 10^{-8}$	$8.4 \cdot 10^{-11}$*	$1.1 \cdot 10^{-8}$**	-

Table 2-2 Summary of anomalies in borehole KA2511A (from Olsson et al., 1994)

Borehole length (m)	Radar indication Magn.	Dip/strike	Seismic indication Magn.	Dip/Strike	Water inflow (l/min)	Geological indication in core
25	-				30	21-23 m. Fine-grained granite
40			2	22/346		No indication (RQD = 90)
54	1	11/169	3 (51 m)	24/332	36 (53 m)	53-57 m. Fine-grained granite
58	3	76/164				Crush < 1 m. Increased fracturing
78	1	6/105	2 (83 m)	82/4		No indication
87			3	87/2		No indication
94	1	75/155				Crush < 1 m
106	1	78/153	3	27/334	24 (100 m)	103-106 m. Crush < 1 m. Increased fracturing. Fine-grained granite
121	2	71/248				122 m. Crush c 1 m
136	1	11/169	2 (132 m)	88/206		131-134 m. Fine-grained granite. Normal fracturing
150	-					149-151 m. Crush. Äspö diorite
153	-		2 (159 m)	70/164		153 m. Crush < 1 m.
185-190	-					Oxidation
199	2	68/112				198-200 m. Oxidation
214	-				24	Contact Fine-grained granite - Äspö diorite
231	2	64/264				No indication
241	1	85/111			20 (242 m)	240-243 m. Crush < 1 m
251-254	-		3 (253 m)	12/168		Greenstone. Crush 3-5 m
259	U	69/340				Crush 1 m
268	U	29/281				No indication
276-278	-		3 (275 m)	88/44		Crush < 1 m
293	1	80/265				Crush c 1 m

Table 2-3 Summary of anomalies in borehole KA2598A (from Olsson et al., 1994)

Borehole length (m)	Radar indication Magn.	Dip/strike	Seismic indication Magn.	Dip/Strike	Water inflow (l/min)	Geological indication in core
13	-				10	No indication. (RQD = 90)
18	-				12	No indication. (RQD = 90)
45	2	87/251	3 (36 m)	79/94	4 (38 m)	Alteration
			2 (40 m)	86/222		
			3 (41 m)	22/34		
50			3 (50 m)	21/62	1	Crush < 1 m
			2 (52 m)	75/106		
74	2	84/346			3	Greenstone contact. Crush 1-2 m
88			3	18/28		No indication (RQD = 100)
94					2	Oxidation
103			2	16/52		No indication (RQD = 100)
113	2	84/173				Contact f.-gr. granite - Sm. granite
136	1	55/058				Sm. granite (RQD = 75). Alteration
159	-		2 (157 m)	71/198		Crush < 1 m
			3 (165 m)	83/214		
179	1	9/319				No indication. Sm. granite. (RQD = 90)
210	2	9/258	3 (198 m)	7/222		No indication. (RQD = 80)
217	-					Crush < 1 m
226	1	37/054				Increased fracturing. Alteration
282	1	86/358				No indication. (RQD = 90-100)

Table 2-4 Summary of anomalies in borehole KC0045F (from Olsson et al., 1994)

Borehole Length (m)	Radar indication Magn.	Dip/strike	Seismic indication Magn.	Dip/Strike	Water inflow (l/min)	Geological indication in core
20	-					Crush < 1 m
32	-				15	Crush 1 m
45	2	68/321			21 (58 m)	45-60 m. Several crush c 1 m
67-72	-				24	Crush < 1 m. Increased fracturing
85	-				12	Increased fracturing
95	3	70/312			18 (94 m)	90-103 m. Increased fracturing. Several crush < 1 m
103	3	69/311			210 (99-105 m)	
119	2	12/118			145 (112-117 m)	110-115 m. Increased fracturing
127	-				18	No indications
130	2	73/288				
132	2	59/356				
136	2	61/105	2 (135 m)	85/16	18 (132-136 m)	Crush < 1 m. Increased fracturing
140-160	-		2 (144 m)	31/162	67 (142-149 m)	Several crush < 1 m. Increased fracturing. Contacts f.-gr granite - Sm. granite
172	U	20/274				Crush c 2 m
181-184	1	35/131, 88/295				Pegmatite
191	1	86/292			43 (196 m)	Increased fracturing
200	1	60/220	3 (200 m)	79/144		198-207 m. Crush 1-2 m
207	U	54/128				
215-217	-		2 (217 m)	87/342	101	No indication. RQD = 90
222			3 (221 m)	79/24	12 (223 m)	No indication. RQD = 90
231-234	1	82/300				
		85/205	1 (236 m)	76/354	582 (232-238 m)	230-240 m. Crush < 1 m. Contact greenstone - Äspö diorite. Alteration
237	2	80/137				Crush < 1 m. Alteration
246	-				250	No indication. RQD = 80-90
253	-					Crush < 1 m
262/266	1	86/292	2 (258 m)	87/326	1060 (261-267m)	260-265 m. Crush > 1 m
		75/134	2 (259 m)	3/226		
273	-				60 (273-275 m)	Increased fracturing.
286	2	79/208			138	Crush < 1 m
298	2	70/229				No indication. RQD = 80-90

Table 2-5 Pressure responses in neighboring boreholes and flow into the borehole, during drilling of KA2162B (from Forsmark et al., 1994)

A = SA1680B D = SA1861B
B = SA1713B E = HA1960A
C = SA1731B F = SA1997A

Depth of borehole (m)	Estimated waterflow during the drilling or from spinner surveys (l/min)	Pressure responses in borehole (m)			
		Δp>2.0	2.0>Δp>0.5	0.5>Δp>0	Δp=0
49 -53	375	A,D,E	F		B,C
85-91	50		A?,F		B,C,D,E
98	28				A,B,C,D,E,F
121	222	A	D	E,F	B,C
126-129	150		A?		B,C,D,E,F
158	26		A?		B,C,D,E,F
165-174	324	A,D	F,E		B,C
180-184	109*	D	E,F		A,B,C
194	81*		D	A?	F
203-207	20*		AD		F
224-225	52*				A,D,F
237-238	30*	D			A,F
252-257	4*				A,D,F
270-271	35*				

Table 2-6 Correlation between inflow into the borehole , geological core mapping and radar reflectors in borehole KA2162B (from Carlsten et al., 1994)

Inflow of water during drilling		Core mapping		Radar reflectors		
Depth (m)	Accumulated inflow (l/min)	Depth (m)	Character	Depth (m)	Dip/Strike (degrees)	Magnitude
		13.8- 14.2	Fractured, grey-red finegrained granite			
		15.6- 16.6	Fractured, grey-red finegrained granite			
		17.1- 17.3	Fractured			
		28.8- 29.2	Fractured, tectonized			
		34.7- 34.9	Fractured			
		35.2- 35.3	Fractured			
49	21	46.1- 46.2	Fractured			
50	300					
53	375			52	73/302	1
		60.4- 60.5	Crushed	62	76/139	1
		64.0- 65.5	Fractured	70	88/213	1
	Injection					
85	17	84.5- 85.5	Pegmatite	82	58/44	1
91	50					
		94.5- 95.0	Fractured			
98	78					
		104.5-104.8	Fractured			
		106.3-108.8	Fractured, red finegrained granite	111	88/232	1
		113.3-113.6	Fractured	112	72/306	1
		116.4-116.6	Fractured, red tectonized granite			
121	300	119.6-120.0	"	118	58/304	1
				122	79/306	3
	Injection					
126	42	125.0-126.4	Fractured, red finegrained granite			
128	60	128.3-130.4	"	129	68/128	2
129	150					
		136.8-137.5	Fractured, red finegrained granite			
		137.8-138.4	"			
140	120	139.7-140.0	Crushed, red finegrained granite			
		144.4-144.8	Fractured, red finegrained granite			
149	144	146.3-147.0	"	149	30/286	3
		151.5-152.0	"			
158	176	152.3-163.2	"			
		163.2-163.9	Crushed, "			
165	210	163.9-179.0	Fractured,"	165	14/310	2
169	228			171	87/306	2
173	425					
174	500					
	Injection					
181	96	179.7-190.8	Fractured, tect.	182	48/277	1
				186	76/126	1
				190	77/128	1
		191.2-191.8	Breccia, fractured			
		193.3-193.4	Breccia, fractured			
195	200	193.4-198.0	Fractured, red tect. finegrained granite	198	48/276	3

Table 2-7 Identified hydraulic conductors in KAS05 and their interpreted transmissivity (from Nilsson, 1989)

Conductor	Hydraulic conductive zone (m)	Max hydraulic conductivity (m)	Transmissivity $T(m^2/s)$
KAS 05-A	229-232		$7.7 \cdot 10^{-6}$
-B_a	274-286	283-286	$4.5 \cdot 10^{-6}$
-B_b	295-301		$9.3 \cdot 10^{-6}$
-C	310-337	319-325	$2.7 \cdot 10^{-5}$
-D	361-382	364-367	$1.1 \cdot 10^{-5}$
-E	427-445	442-445	$3.0 \cdot 10^{-5}$
-F	466-481	466-469	$7.2 \cdot 10^{-6}$

Table 4-1. Pressure response matrix for drilling disturbances.

PRESSURE RESPONSE MATRIX									
	HMS monitored boreholes								
Drilling boreholes	KA1061A	KA1131B	KA1751A	KA1754A	KA1755A	KA2048A	KA2050A	KA2162A	KA2511A
KA2511A	1	1	x	x	x	x	x	x	
KA2598A	0	0	x	x	x	x	x	x	x
KA2858A	x	x	0	x	x	x	x	x	0
KA2862A	x	x	0	x	x	x	x	x	0
KA3005A	0	0	0	0	0	x	x	0	0
KA3010A	0	0	0	0	0	x	1	0	0
KA3067A	0	0	0	0	0	0	1	0	1
KA3110A	0	0	0	0	0	1	1	0	0
KA3191F	-	-	-	-	-	-	-	1	-
TBM	0	0	1	1	0	x	0	1	1
1 = good response 0=no or weak response									
- = no registration in HMS x = no data ???? = response of unknown origin									

Table 4-2. Pressure response matrix for an extract of interference tests performed in boreholes in the NE part of the HRL (Winberg et al. 1996a)

PRESSURE RESPONSE MATRIX							
	Interference tests within the SELECT project						
Boreholes	KA3005A	KA3010A	KA3067A	KA3068A	KA3105A	KA3110A	Figures
KA2858A	0	1	1	1	0	1	4-13
KA2862A	0	1	1	1	0	1	4-14
KA3005A		1	1	1	0	1	4-15
KA3010A	0		1	1	1	1	4-16
KA3067A	0	1		1	0	1	4-17
KA3105A	0	1	1	1		1	4-18
KA3110A	0	1	0	0	1		4-19
1 = good response 0=no or weak response							
- = no registration in HMS x = no data ???? = response of unknown origin							

Table 4-3. Pressure responses in boreholes during the drilling of the TBM tunnel.

Responses during the TBM drilling					
Date	950816	950825	950901	950902	950907
TBM length	249	299	331	no drilling	350
Responses in boreholes	KA1751A KA1754A KA2162A KA2511A	KA2511A	KA1751A KA1754A KA2511A	KA2511A	KA1751A KA1754A KA2162A KA2511A

Table 5-1 Evaluated hydraulic head from borehole sections in the vicinity of the target volume.

#	Idcode	secup	seclow	from-Date	BHlen mid	P (kPa)	H (masl)
1	KA2048B	149.5	184.45	941212	166.975	2368.5	-57.88
2	KA2048B	100	148.5	941212	124.250	1972.2	-98.34
3	KA2048B	50.5	99	941212	74.750	2100.4	-85.33
4	KA2048B	5	49.5	941212	27.250	2365.1	-58.39
	HA1960A	4	32	910101	18.000	2429.2	-51.90
1	KA2050A	155	211.57	940414	183.285	2657.4	-27.63
2	KA2050A	102	154	940414	128.000	2600.1	-33.79
3	KA2050A	6	101	940414	53.500	2584.9	-35.73
1	KA2162B	201.5	288.1	940415	244.800	2257.4	-68.84
2	KA2162B	143	200.5	940415	171.750	2278.2	-66.86
3	KA2162B	80.5	142	940415	111.250	2316.2	-63.10
4	KA2162B	40	79.5	940415	59.750	2438.0	-50.78
1	KA2511A	171	293	940504	232.000	3143.6	-23.23
2	KA2511A	81	170	940504	125.500	3105.2	-27.69
3	KA2511A	31	80	940504	55.500	3070.0	-31.61
4	KA2511A	6	30	940504	18.000	3050.5	-33.77
1	KA2858A	41.77	59.7	950701	50.735	Not measured	
2	KA2858A	39.77	40.77	950701	40.270	3602.5	-42.27
3	KA2858A	6.02	38.77	950701	22.395	Not measured	
1	KA2862A	15.02	15.98	950704	15.500	2900.0	-113.95
2	KA2862A	5.52	14.02	950704	9.770	Not measured	
1	KA3005A	46.43	58.11	950704	52.270	3560.5	-46.31
1	KA3005A	0	58.11	951101	29.055	Not relevant	
1	KA3005A	51.03	58.11	951207	54.570	Not relevant	
2	KA3005A	44.43	45.43	950704	44.930	3600.9	-42.19
2	KA3005A	46.78	50.03	951207	48.405	Not relevant	
3	KA3005A	38.93	43.43	950704	41.180	3609.0	-41.37
3	KA3005A	44.78	45.78	951207	45.280	Not relevant	
4	KA3005A	36.93	37.93	950704	37.430	3614.3	-40.83
4	KA3005A	39.03	43.78	951207	41.405	Not relevant	
5	KA3005A	6.53	35.93	950704	21.230	Not measured	
5	KA3005A	6.53	38.03	951207	22.280	Not relevant	
1	KA3010A	16.06	60.66	950720	38.360	3702.9	-31.79
2	KA3010A	8.56	15.06	950720	11.810	3692.0	-32.92
1	KA3067A	34.55	40.05	950228	37.300	3851.5	-30.69
2	KA3067A	30.55	33.55	950228	32.050	3845.9	-31.26
3	KA3067A	28.05	29.55	950228	28.800	3842.9	-31.57
4	KA3067A	6.55	27.05	950228	16.800	3830.7	-32.82
1	KA3105A	53.01	68.95	950301	60.980	3800.8	-35.78
2	KA3105A	25.51	52.01	950301	38.760	3671.5	-48.97
3	KA3105A	22.51	24.51	950301	23.510	3682.4	-47.87
4	KA3105A	17.01	19.51	950301	18.260	3688.3	-47.27
5	KA3105A	6.51	16.01	950301	11.260	3667.2	-49.46
1	KA3110A	20.05	28.63	950223	24.340	3643.0	-51.89
2	KA3110A	6.55	19.05	950223	12.800	3611.4	-55.15
1	KXTT1	17	28.76	950707	22.880	3613.9	-40.83
2	KXTT1	15	16	950707	15.500	3607.1	-41.56

Table 5-1 Evaluated hydraulic head from borehole sections in the vicinity of the target volume (continued).

#	Idcode	secup	seclow	from-Date	BHlen mid	P (kPa)	H (masl)
3	KXTT1	8.5	10.5	950707	9.500	3507.6	-51.74
3	KXTT1	7.5	11.5	951207	9.500	Not relevant	
4	KXTT1	3	7.5	950707	5.250	3494.1	-53.14
4	KXTT1	3	6.5	951207	4.750	Not relevant	
1	KXTT2	14.3	18.3	950708	16.300	3604.4	-41.83
1	KXTT2	16.55	18.3	951207	17.425	Not relevant	
2	KXTT2	11.3	13.3	950708	12.300	3498.6	-52.64
2	KXTT2	14.55	15.55	951207	15.050	Not relevant	
3	KXTT2	8.8	10.3	950708	9.550	3475.7	-54.99
3	KXTT2	11.55	13.55	951207	12.550	Not relevant	
4	KXTT2	3.05	7.8	950708	5.425	3481.1	-54.46
4	KXTT2	7.55	10.55	951207	9.050	Not relevant	
5	KXTT2	3.05	6.55	951207	4.800	Not relevant	
1	KXTT3	15.42	17.43	950708	16.425	3610.1	-41.27
2	KXTT3	10.92	14.42	950708	12.670	3595.0	-42.83
2	KXTT3	12.42	14.42	951207	13.420	Not relevant	
3	KXTT3	8.92	9.92	950708	9.420	3522.2	-50.26
3	KXTT3	8.92	11.42	951207	10.170	Not relevant	
4	KXTT3	3.17	7.92	950708	5.545	3498.2	-52.73
1	KXTT4	24.42	49.31	950718	36.865	3657.2	-36.37
2	KXTT4	14.92	23.42	950718	19.170	3601.6	-42.13
3	KXTT4	11.42	13.92	950718	12.670	3606.8	-41.62
3	KXTT4	11.92	13.92	951207	12.920	Not relevant	
4	KXTT4	8.42	10.42	950718	9.420	3515.1	-50.99
4	KXTT4	8.42	10.92	951207	9.670	Not relevant	
5	KXTT4	3.17	7.42	950718	5.295	3482.5	-54.33

Table 6-1 Location of hydraulic conductors. The hydraulic conductors are in this table approximated to planes. Assumed extension of each plane is discussed in Table A5-5.Coordinates for zones are given in the local Äspö-system. w = waterbearing structure. p = predicted structure */Wikberg et al, 1991/*. r = revised structure */Stanfors et al, 1994/*. n= new structure.

Zone		X-coordinate (m)	Y-coordinate (m)	Z (masl)
$EW\text{-}1_r$	88°SE	7482.0	1811.5	0
		7698.3	2197.1	0
		7575.4	2000.0	-327.4
$EW\text{-}1_r$	78°SE	7433.6	1838.7	0
		7649.8	2224.3	0
		7500.0	2110.9	-369.5
$EW\text{-}3_r$	79°S	7093.0	2047.7	0
		7143.1	2289.2	0
		7010.0	2166.5	-542.2
$EW\text{-}7_r$	81°SE	6418.9	2023.7	0
		6504.7	2343.8	0
		6428.2	2200.0	-231.8
$NE\text{-}1_r$	70°NW	6807.6	1967.2	0
		7005.9	2350.7	0
		7135.2	2054.6	-689.1
$NE\text{-}1_r$	75°NW	6807.6	1967.2	0
		7005.9	2350.7	0
		7081.0	2082.6	-708.4
$NE\text{-}2_r$	77°SE	7038.5	1829.9	0
		7540.7	2194.8	0
		7250.0	2083.3	-349.4
$NE\text{-}3_r$	80°NW	6495.5	1984.3	0
		6650.7	2253.1	0
		6610.0	2094.7	-233.2
$NE\text{-}3_r$	70°NW	6499.7	1983.1	0
		6654.9	2251.9	0
		6650.0	2076.0	-221.9
$NE\text{-}4_r$	71°SE	6443.0	2016.6	0
		6569.3	2300.2	0
		6440.0	2197.9	-224.5
$NE\text{-}4_r$	78°SE	6448.8	2010.3	0
		6596.9	2283.1	0
		6480.0	2169.6	-232.2
$NW\text{-}1_{wp}$	30°NE	7882.0	1257.6	0
		7510.3	1600.0	0
		7934.5	1790.0	-246.6
$NNW\text{-}1_{wp}$	(vertical)	7538.9	2039.4	
		7151.9	2218.6	

Table 6-1 continued

Zone		X-coordinate (m)	Y-coordinate (m)	Z (masl)
NNW-2_{wr}	(vertical)	7484.1	2134.6	
		7106.1	2300.2	
NNW-3_{wp}	(vertical)	7025.4	2143.6	
		6812.9	2136.9	
NNW-4_{wr}	85°NE	7391.8	2275.3	0
		7184.0	2301.7	0
		7300.0	2325.5	-436.7
NNW-5_{wp}	(vertical)	7394.1	1962.8	
		6421.1	2020.8	
NNW-6_{wp}	(vertical)	7058.1	2298.7	
		6529.1	2373.7	
NNW-7_{wn}	85°NE	7492.2	1967.6	0
		7129.2	2135.7	0
		7299.3	2074.7	-185
NNW-8_{wn}	(vertical)	8060	1540	-300
		7570	2030	-300
		8060	1540	-700
		7570	2030	-700

Table 6-2 **Deterministic hydraulic structures to be used for groundwater flow modelling. If the extension is not known of a zone at deeper levels and/or outside Äspö the zone is assumed to terminate at the model boundaries or at zones outside Äspö, if nothing else is said in the comments of the extension on the zone.**

Zone	Comments on extension of the zone
EW-$1N_r$	This conductor explains some of the hydraulic responses in the upper part of KAS04 during some of the interference tests . The conductor is assumed to be in contact with NNW-8. Possibly there are several conductors causing the connectivity between KAS03 and KAS04 but so far it has not been possible to resolve these. The rockmass between EW-1N and EW-1S is partly low conductive perpendicular to these conductor.
EW-$1S_r$	This conductor explains some of the hydraulic responses in the E-W direction that was seen during the construction of the Äspö HRL. The conductors NNW-1, NNW-2 and NNW-4 are assumed to be in contact with EW-1S.
EW-3_r	The conductor is assumed to intersect NE-2 and NE-1.
EW-7_r	The conductor is assumed to penetrat into and terminate at NE-4 to the west.
NE-1_r	In *Table A2-4* two dips are given which more or less gives the boundaries of the conductor at approximately Z = 180 m. The direction may be approximated with the average values of X, Y and Z for NE-1, 70°NW and NE-1, 75°NW.

Table 6-2 Contnued

$NE\text{-}2_r$	The conductor is assumed to intersect EW-3 and all NNW structures but terminate at EW-1, 78°SE and EW-3.
$NE\text{-}3_r$	In *Table A2-4* two dips are given which more or less gives the boundaries of the conductor at approximately Z= -140 m. The direction may be approximated with the average values of X, Y and Z for NE-3, 80°NW and NE-3, 70°NW.
$NE\text{-}4_r$	In *Table A2-4* two dips are given which more or less gives the boundaries of the conductor at approximately Z = 110 m. The direction may be approximated with the average values of X, Y and Z for NE-4, 71°SE and NE-4, 78°SE.
$NW\text{-}1_{wp}$	The conductor is assumed to terminate to the south at EW-1N, 88°SE. This zone explains some of the hydraulic responses during some of the interference tests performed in KAS03. Possibly there are several conductors causing the connectivity between KAS03 and the percussion boreholes west of KAS03, but so far it has not been possible to resolve these. The conductor should be considered as possible.
$NNW\text{-}1_{wp}$	The conductor is assumed to terminate at EW-3 and EW-1S, 78°SE.
$NNW\text{-}2_{wr}$	The conductor is assumed to intersect EW-3 and terminates at NE-1 and EW-1S, 78°SE. The zone is in good contact with NE-1.
$NNW\text{-}3_{wp}$	The horizontal extension is assumed to limited by the coordinates given in *Table* A2-4. The extension towards the depth is badly known. The conductor should be considered as possible.
$NNW\text{-}4_{wr}$	The conductor intersects EW-3 and NE-2 and terminate at NE-1 and EW-1, 78°SE. The zone is in good contact with $NE\text{-}1_r$.
$NNW\text{-}5_{wp}$	The conductor intersect EW-3, NE-1, NE-2 and NE-3. The horizontal extension is limited to the north by the coordinates in *Table A2-4* and to the south the conductor terminates at NE-4. The conductor should be considered as possible.
$NNW\text{-}6_{wp}$	The conductor is assumed to intersect NE-1, NE-3 and NE-4 and terminate at NE-1 and EW-7. The conductor should be considered as possible.
$NNW\text{-}7_{wn}$	The conductor is considered possible and is assumed to terminate at EW-3 and EW-1S, 78°SE. The conductor is assumed to intersect the elevator shaft at level -185 m.
$NNW\text{-}8_{wn}$	New conductor not shown on figures.This conductor explains some of the hydraulic responses during some of the interference testsin KAS03. The conductor is considered possible and terminates at EW-1N, 88°SE and about 600 m to the North of EW-1N . The conductor intersects or is close to KAS03. Possibly there are several conductors causing the connectivity between KAS03 and KAS04 but so far it has not been possible to resolve these. The extension is assumed to be approximatly within the coordinates given in Table A2-4.

Note : Table A2-4 referenced in Table 6-2 corresponds to Table 6-1

Table 6-3 Interpreted hydrological properties of hydraulic conductors. Width estimated from mapping in the tunnel and interpreted intersections with boreholes. The value given should be concidered as an approximative value. Transmissivity = T, Storativity = S, Flow porosity = n_e. Uncertain values or based on professional judgement within parenthesis.

Zone	Width (m)	T (m^2/s) $x \cdot 10^{-5}$	S (-) $x \cdot 10^{-5}$	n_e (%)	Comments
$EW\text{-}1N_r$	(30)	*	-	-	
$EW\text{-}1S_r$	(30)	*	-	-	
$EW\text{-}3_r$	15	*	-		Z = 0 to -300 m. There are tests in KAS06 and in the tunnel that indicate values approximately as the given. There are geological indications that the core of the zone should be low conductive, at least partly. The transmissivity given is therefore assumed to represent the outer part of the zone.
$EW\text{-}3_r$	(15)	0.05	-	-	Z < -300 m. Injection tests in KAS07 indicate low transsmissivity where EW-3 is interpreted to intersect KAS07.
$EW\text{-}7_r$	(10)	*	-	-	
$NE\text{-}1_r$	30	*	2.6	0.7	Evaluation of a simple tracer test gave a range (depending on the concept for the flowfield) of flow porosity of 0.06 % - 2.2 %. The evaluation of spread of the grout around the tunnel gave a range of flow porosity of 0.07 % - 1 %. */Rhén and Stanfors, 1993/.*
$NE\text{-}2_r$	5	*	-	-	The zone is possibly more transmissive at levels higher than Z -250 m.
$NE\text{-}3_r$	50	*	-	-	
$NE\text{-}4_r$	40	*	-	-	
$NW\text{-}1_{wp}$	(10)	*	-	-	
$NNW\text{-}1_{wp}$	(20)	*	0.5	-	
$NNW\text{-}2_{wp}$	(20)	*	0.2	0.34	Evaluation of LPT2 gave a range (depending on the concept for the flowfield) of the flow porosity of 0.02 % - 0.1 %. */Rhén et al,. 1992/.*
$NNW\text{-}3_{wp}$	(20)	2	-	-	
$NNW\text{-}4_{wr}$	10	*	-	-	
$NNW\text{-}5_{wp}$	(20)	*	-	-	
$NNW\text{-}6_{wp}$	(20)	(1.4)	-	-	
$NNW\text{-}7_{wn}$	(20)	*	-	-	
$NNW\text{-}8_{wn}$	(20)	*	-	-	

Table 6-4 Transmissivity of hydraulic conductors based on results from hydraulic tests and interpreted intersections of the Äspö HRL tunnel and boreholes.Äspö area.

Zone (-)	Sample size (-)	Mean (m^2/s)	Median (m^2/s)	s (Log10 T) (-)	Conf.lim.(97.5 %) (m^2/s)	Conf.lim.(2.5 %) (m^2/s)	Mean + st.dev (m^2/s)	Mean - st.dev (m^2/s)
EW-1N	4	5.2E-07	1.5E-06	1.60	1.8E-04	1.5E-09	2.1E-05	1.3E-08
EW-1S	4	1.2E-05	2.2E-05	1.17	8.8E-04	1.7E-07	1.8E-04	8.1E-07
EW-3	4	1.7E-05	2.4E-05	0.54	1.2E-04	2.4E-06	5.9E-05	5.0E-06
EW-7	3	1.5E-05	6.8E-05	1.27	2.1E-02	1.0E-08	2.7E-04	7.8E-07
NE-1	16	2.2E-04	3.0E-04	0.51	4.2E-04	1.2E-04	7.2E-04	6.9E-05
NE-2	12	1.2E-07	4.1E-07	2.14	2.8E-06	5.3E-09	1.7E-05	8.8E-10
NE-3	9	3.2E-04	2.9E-04	0.46	7.2E-04	1.4E-04	9.2E-04	1.1E-04
NE-4	8	3.1E-05	3.0E-05	0.79	1.4E-04	6.8E-06	1.9E-04	5.0E-06
NNW-1	7	8.6E-06	1.1E-05	0.82	4.9E-05	1.5E-06	5.6E-05	1.3E-06
NNW-2	4	2.4E-05	5.6E-05	1.06	4.4E-03	1.3E-07	2.7E-04	2.1E-06
NNW-4	8	6.5E-05	1.5E-04	1.50	1.2E-03	3.6E-06	2.1E-03	2.1E-06
NNW-5	3	4.0E-06	2.0E-06	0.84	4.9E-04	3.3E-08	2.8E-05	5.9E-07
NNW-7	5	7.5E-06	4.8E-06	0.87	8.9E-05	6.3E-07	5.5E-05	1.0E-06
NNW-8	3	8.4E-06	1.0E-05	0.13	1.8E-05	4.1E-06	1.1E-05	6.3E-06
NW-1	3	4.1E-07	1.7E-07	1.08	2.0E-04	8.4E-10	5.0E-06	3.4E-08

Table 6-5 Identified hydraulic structures within the target volume.
Where possible structures have been assined a specific zone notation.

Waterbearing structure	Zone ID	Borehole ID	Section (m)	Orientation	T	Q	Q/p	Diffusivity	Storativity
Z1700	NNW-1B	Tunnel section	1700.0	N70W	2.9E-5 - 0.6E-5				
Z2162A	NNW-4	KA2162A	49-53	NNW-NW	5.8E-05	4.6E-03	2.6E-05	31.0	1.9E-06
Z2162D	NNW-2	KA2162A	121.0	306/79	3.3E-05			20.2 - 3.7	
Z2162G	NNW-1	KA2162A	165-174	306/74	7.8E-05			9.2 - 3.2	
Z3191A	NNW-2	KA3191F	4.9	265/79	5.2E-06				
Z3191B		KA3191F	14.5	29/29	2.4E-06				
Z3191C		KA3191F	47.0	200/55	6.6E-07				
Z3191D		KA3191F	77.0	114/77	3.9E-07				
Z3191E		KA3191F	89.5-98.0	114/77	3.9E-07				
Z3191F	NNW-1	KA3191F	123.6-124.1	35/70	1.3E-05				
Z3191G		KA3191F	195.0	?	2.0E-07				
Z3191H		KA3191F	202.5	?	7.2E-07				
Z2511A		KA2511A	25.0	?	3.0E-05	4.2E-03	1.3E-06		
Z2511B	NNW-5	KA2511A	52.8	164/76	3.6E-05				
Z2511C	NNW-5b	KA2511A	100.1	153/78	2.4E-05				
Z2511D	NNW-5c	KA2511A	214.0	?	2.4E-05				
Z2511E		KA2511A	242.0	111/85	4.6E-06				
Z2598A		KA2598A	12.7	?	4.0E-06				
Z2598B		KA2598A	18.5	?	4.8E-06				
Z2598C		KA2598A	37.4-39.4		1.6E-06				
Z2598D		KA2598A	49.8-52.4		4.0E-07				
Z2598E	NNW-5	KA2598A	73.5-75.5	346/84	1.2E-06				
Z2598F		KA2598A	92.5-96.5	346/84	8.0E-07				
Z0045A	NNW-2	KC0045F	101.9-104.8	311/69	8.0E-06				
Z0045B		KC0045F	112.1-113.6	?	6.1E-6 - 9.9E-6				
Z0045C		KC0045F	235.2-245.9	137/80	6.3E-6 - 6.5E-6				
Z0045D	NNW-1	KC0045F	264.2-266.7	134/75	1.9E-5 -5.9E-5				
Z0045E		KC0045F	272.4-275.4	?	7E-6 - 3.5E-5				
Z0045F		KC0045F	285.2-286.2	208/79	2.1E-5 - 7.6E-5				
Z0045G		KC0045F	305.2	108/86	1.1E-05				

Table 6-6 Äspö Tunnel Fracture Orientation Sets (after Dershowitz et al.,1996)

Set	Mean Pole (Trend,Plunge)	Fisher Dispersion κ	Percent of Fractures
Based on original SICADA database			
1	(203.2, 2.6)	9.15	48.1%
2	(290.4, 8.5)	7.13	33.1%
3	(312.5, 85.1)	7.31	18.8%
Based on Viak (1995) data			
1	(232.2, 71.1)	12.9	26.7%
2	(231.7, 0.6)	7.13	33.1%
3	(312.5, 85.1)	7.31	18.8%

Table 6-7 Compilation of fracture size statistics

Evidence	Geological or Conductive Features	Trace Length or Radius	Mean, Std. Dev.
GEOTAB (Viak, 1995)	Conductive, Tunnel	Trace Length	Mean =3.67 m, Std. Dev. = 2.04 m
Mazurek et al (1995)	Conductive, Tunnel	Trace Length	Mean = 1.33 m Std. Dev. = 1.17 m
Borehole Intersection Simulation	Conductive, Borehole	Radius	Mean = 2 to 3 m Std. Dev. = 2-3 m
La Pointe et al. (1995)	Conductive Tunnel	Radius	Mean = 6 Std. Dev. =2
Uchida et al. (1994)	Geological Surface	Radius	Mean = 13.7, Std. Dev. = 12.7
Tunnel Intersection Simulation	Conductive Tunnel	Radius	Mean = <1 to 2.25 m

Table 6-8 . Hydraulic conductivity of rock mass domains. Äspö island. Testscale 100 m. Zonation.

Upper level	Lower level	Sample size	Mean	Median	s (Log10 K)	Conf.lim.(97.5 %)	Conf.lim.(2.5 %)	Mean + st.dev	Mean - st.dev
0	-200	22	2.8E-08	2.6E-08	1.09	8.4E-08	9.1E-09	3.4E-07	2.2E-09
-200	-400	12	7.9E-08	9.1E-08	0.58	1.8E-07	3.4E-08	3.0E-07	2.1E-08
-400	-600	2	1.0E-07	1.0E-07	0.24	1.6E-05	6.4E-10	1.7E-07	5.7E-08
-600	-1000	1	1.6E-08	1.6E-08	0.00	ET	ET	1.6E-08	1.6E-08
0	-1000	37	4.1E-08	5.8E-08	0.92	8.3E-08	2.0E-08	3.4E-07	4.9E-09

Table 6-9 Hydraulic conductivity of rock mass domains . Site scale area. Testscale 3 m. Zonation. KAS02, 05-08-"rock".

Upper level	Lower level	Sample size	Mean	Median	s (Log10 K)	Conf.lim.(97.5 %)	Conf.lim.(2.5 %)	Mean + st.dev	Mean - st.dev
0	-100	20	1.3E-09	5.0E-10	1.74	8.2E-09	1.9E-10	7.0E-08	2.3E-11
-100	-200	155	3.2E-10	1.2E-10	1.58	5.7E-10	1.8E-10	1.2E-08	8.5E-12
-200	-300	185	3.7E-10	8.8E-11	1.67	6.4E-10	2.1E-10	1.7E-08	7.8E-12
-300	-400	160	3.8E-10	1.0E-10	1.78	7.1E-10	2.0E-10	2.3E-08	6.2E-12
-400	-500	132	4.9E-10	1.2E-10	1.80	1.0E-09	2.4E-10	3.1E-08	7.8E-12
-500	-600	43	5.9E-11	6.1E-11	0.95	1.2E-10	3.0E-11	5.3E-10	6.6E-12
-600	-700	34	3.4E-10	1.8E-10	1.02	7.9E-10	1.5E-10	3.6E-09	3.3E-11
-700	-800	30	1.2E-10	1.5E-10	0.53	1.9E-10	7.8E-11	4.1E-10	3.6E-11
0	-800	759	3.4E-10	1.1E-10	1.63	4.4E-10	2.6E-10	1.4E-08	7.9E-12

APPENDIX A1 COORDINATES FOR BOREHOLES AND TUNNEL SECTIONS

These coordinates are extracted from the SKB SICADA database in August 1996.

IDCODE	NT_SEQ_	LOCAL_X	LOCAL_Y	Z	LENGTH
KA2162B	0	7225.04	2296.4	-289.87	0
KA2162B	1	7225.15	2293.51	-290.66	3
KA2162B	2	7225.26	2290.61	-291.45	6
KA2162B	3	7225.38	2287.72	-292.24	9
KA2162B	4	7225.5	2284.83	-293.03	12
KA2162B	5	7225.63	2281.94	-293.83	15
KA2162B	6	7225.76	2279.06	-294.63	18
KA2162B	7	7225.89	2276.17	-295.43	21
KA2162B	8	7226.02	2273.28	-296.23	24
KA2162B	9	7226.16	2270.39	-297.03	27
KA2162B	10	7226.31	2267.5	-297.83	30
KA2162B	11	7226.46	2264.62	-298.63	33
KA2162B	12	7226.61	2261.73	-299.43	36
KA2162B	13	7226.76	2258.84	-300.23	39
KA2162B	14	7226.91	2255.95	-301.02	42
KA2162B	15	7227.06	2253.06	-301.82	45
KA2162B	16	7227.21	2250.17	-302.61	48
KA2162B	17	7227.37	2247.28	-303.4	51
KA2162B	18	7227.53	2244.39	-304.19	54
KA2162B	19	7227.68	2241.5	-304.98	57
KA2162B	20	7227.85	2238.61	-305.77	60
KA2162B	21	7228.01	2235.73	-306.56	63
KA2162B	22	7228.18	2232.84	-307.36	66
KA2162B	23	7228.35	2229.95	-308.15	69
KA2162B	24	7228.53	2227.06	-308.94	72
KA2162B	25	7228.71	2224.17	-309.73	75
KA2162B	26	7228.89	2221.28	-310.51	78
KA2162B	27	7229.08	2218.39	-311.3	81
KA2162B	28	7229.26	2215.5	-312.08	84
KA2162B	29	7229.45	2212.61	-312.86	87
KA2162B	30	7229.64	2209.72	-313.64	90
KA2162B	31	7229.83	2206.83	-314.42	93
KA2162B	32	7230.02	2203.94	-315.21	96
KA2162B	33	7230.21	2201.05	-315.99	99
KA2162B	34	7230.41	2198.16	-316.77	102
KA2162B	35	7230.6	2195.27	-317.55	105
KA2162B	36	7230.8	2192.38	-318.34	108
KA2162B	37	7231	2189.49	-319.12	111
KA2162B	38	7231.2	2186.61	-319.91	114
KA2162B	39	7231.4	2183.72	-320.7	117
KA2162B	40	7231.61	2180.83	-321.48	120
KA2162B	41	7231.82	2177.94	-322.27	123
KA2162B	42	7232.03	2175.06	-323.06	126
KA2162B	43	7232.24	2172.17	-323.84	129
KA2162B	44	7232.46	2169.28	-324.63	132
KA2162B	45	7232.68	2166.39	-325.41	135
KA2162B	46	7232.9	2163.5	-326.19	138
KA2162B	47	7233.12	2160.62	-326.97	141
KA2162B	48	7233.34	2157.73	-327.74	144
KA2162B	49	7233.57	2154.84	-328.52	147
KA2162B	50	7233.8	2151.95	-329.29	150
KA2162B	51	7234.02	2149.06	-330.06	153

KA2162B	52	7234.26	2146.17	-330.83	156
KA2162B	53	7234.49	2143.28	-331.6	159
KA2162B	54	7234.72	2140.39	-332.37	162
KA2162B	55	7234.96	2137.5	-333.14	165
KA2162B	56	7235.21	2134.61	-333.91	168
KA2162B	57	7235.45	2131.72	-334.68	171
KA2162B	58	7235.7	2128.83	-335.45	174
KA2162B	59	7235.96	2125.94	-336.22	177
KA2162B	60	7236.21	2123.05	-336.99	180
KA2162B	61	7236.47	2120.16	-337.76	183
KA2162B	62	7236.73	2117.27	-338.52	186
KA2162B	63	7236.98	2114.39	-339.29	189
KA2162B	64	7237.24	2111.5	-340.05	192
KA2162B	65	7237.5	2108.61	-340.82	195
KA2162B	66	7237.77	2105.72	-341.58	198
KA2162B	67	7238.03	2102.83	-342.34	201
KA2162B	68	7238.3	2099.94	-343.1	204
KA2162B	69	7238.57	2097.05	-343.85	207
KA2162B	70	7238.83	2094.16	-344.61	210
KA2162B	71	7239.11	2091.26	-345.36	213
KA2162B	72	7239.38	2088.37	-346.11	216
KA2162B	73	7239.67	2085.48	-346.86	219
KA2162B	74	7239.95	2082.59	-347.61	222
KA2162B	75	7240.23	2079.7	-348.36	225
KA2162B	76	7240.52	2076.81	-349.1	228
KA2162B	77	7240.8	2073.91	-349.85	231
KA2162B	78	7241.1	2071.02	-350.59	234
KA2162B	79	7241.39	2068.13	-351.33	237
KA2162B	80	7241.68	2065.24	-352.06	240
KA2162B	81	7241.98	2062.34	-352.8	243
KA2162B	82	7242.28	2059.45	-353.53	246
KA2162B	83	7242.58	2056.56	-354.26	249
KA2162B	84	7242.89	2053.66	-354.99	252
KA2162B	85	7243.19	2050.77	-355.72	255
KA2162B	86	7243.5	2047.87	-356.45	258
KA2162B	87	7243.81	2044.98	-357.17	261
KA2162B	88	7244.13	2042.08	-357.89	264
KA2162B	89	7244.44	2039.19	-358.62	267
KA2162B	90	7244.76	2036.29	-359.34	270
KA2162B	91	7245.08	2033.4	-360.05	273
KA2162B	92	7245.4	2030.5	-360.77	276
KA2162B	93	7245.73	2027.61	-361.48	279
KA2162B	94	7246.06	2024.71	-362.2	282
KA2162B	95	7246.39	2021.82	-362.91	285
KA2162B	96	7246.72	2018.92	-363.62	288
KA2162B	97	7246.73	2018.82	-363.64	288.1
KA2511A	0	7212.38	2020.9	-335.2	0
KA2511A	1	7210.95	2018.85	-336.86	3
KA2511A	2	7209.52	2016.81	-338.53	6
KA2511A	3	7208.09	2014.76	-340.2	9
KA2511A	4	7206.66	2012.72	-341.86	12
KA2511A	5	7205.23	2010.67	-343.53	15
KA2511A	6	7203.8	2008.63	-345.2	18

KA2511A	7	7202.37	2006.59	-346.87	21
KA2511A	8	7200.94	2004.55	-348.54	24
KA2511A	9	7199.51	2002.51	-350.21	27
KA2511A	10	7198.08	2000.47	-351.88	30
KA2511A	11	7196.66	1998.43	-353.55	33
KA2511A	12	7195.23	1996.39	-355.23	36
KA2511A	13	7193.8	1994.35	-356.9	39
KA2511A	14	7192.38	1992.31	-358.57	42
KA2511A	15	7190.95	1990.26	-360.24	45
KA2511A	16	7189.53	1988.22	-361.92	48
KA2511A	17	7188.11	1986.17	-363.59	51
KA2511A	18	7186.69	1984.13	-365.26	54
KA2511A	19	7185.27	1982.08	-366.94	57
KA2511A	20	7183.85	1980.04	-368.61	60
KA2511A	21	7182.43	1977.99	-370.28	63
KA2511A	22	7181.02	1975.94	-371.96	66
KA2511A	23	7179.6	1973.89	-373.63	69
KA2511A	24	7178.19	1971.85	-375.31	72
KA2511A	25	7176.78	1969.8	-376.98	75
KA2511A	26	7175.36	1967.75	-378.66	78
KA2511A	27	7173.95	1965.7	-380.33	81
KA2511A	28	7172.53	1963.65	-382.01	84
KA2511A	29	7171.12	1961.61	-383.68	87
KA2511A	30	7169.7	1959.56	-385.35	90
KA2511A	31	7168.29	1957.5	-387.02	93
KA2511A	32	7166.87	1955.45	-388.69	96
KA2511A	33	7165.46	1953.4	-390.36	99
KA2511A	34	7164.04	1951.35	-392.03	102
KA2511A	35	7162.62	1949.3	-393.7	105
KA2511A	36	7161.2	1947.25	-395.37	108
KA2511A	37	7159.79	1945.2	-397.04	111
KA2511A	38	7158.37	1943.15	-398.7	114
KA2511A	39	7156.95	1941.09	-400.37	117
KA2511A	40	7155.53	1939.04	-402.04	120
KA2511A	41	7154.11	1936.99	-403.71	123
KA2511A	42	7152.69	1934.94	-405.38	126
KA2511A	43	7151.27	1932.89	-407.04	129
KA2511A	44	7149.85	1930.84	-408.71	132
KA2511A	45	7148.44	1928.79	-410.38	135
KA2511A	46	7147.02	1926.74	-412.04	138
KA2511A	47	7145.6	1924.68	-413.71	141
KA2511A	48	7144.19	1922.63	-415.38	144
KA2511A	49	7142.77	1920.57	-417.04	147
KA2511A	50	7141.35	1918.52	-418.7	150
KA2511A	51	7139.94	1916.46	-420.37	153
KA2511A	52	7138.52	1914.4	-422.03	156
KA2511A	53	7137.11	1912.34	-423.69	159
KA2511A	54	7135.7	1910.28	-425.35	162
KA2511A	55	7134.29	1908.22	-427.01	165
KA2511A	56	7132.88	1906.16	-428.67	168
KA2511A	57	7131.46	1904.1	-430.33	171
KA2511A	58	7130.05	1902.03	-432	174
KA2511A	59	7128.64	1899.97	-433.66	177

KA2511A	60	7127.23	1897.91	-435.32	180
KA2511A	61	7125.82	1895.85	-436.98	183
KA2511A	62	7124.41	1893.79	-438.64	186
KA2511A	63	7123	1891.72	-440.3	189
KA2511A	64	7121.59	1889.66	-441.96	192
KA2511A	65	7120.18	1887.6	-443.62	195
KA2511A	66	7118.77	1885.53	-445.28	198
KA2511A	67	7117.37	1883.46	-446.94	201
KA2511A	68	7115.96	1881.4	-448.6	204
KA2511A	69	7114.55	1879.34	-450.26	207
KA2511A	70	7113.14	1877.27	-451.91	210
KA2511A	71	7111.73	1875.21	-453.57	213
KA2511A	72	7110.32	1873.15	-455.23	216
KA2511A	73	7108.91	1871.08	-456.89	219
KA2511A	74	7107.51	1869.02	-458.55	222
KA2511A	75	7106.1	1866.95	-460.22	225
KA2511A	76	7104.69	1864.89	-461.88	228
KA2511A	77	7103.28	1862.83	-463.54	231
KA2511A	78	7101.87	1860.77	-465.21	234
KA2511A	79	7100.46	1858.71	-466.87	237
KA2511A	80	7099.05	1856.65	-468.54	240
KA2511A	81	7097.64	1854.59	-470.2	243
KA2511A	82	7096.23	1852.53	-471.86	246
KA2511A	83	7094.82	1850.47	-473.53	249
KA2511A	84	7093.42	1848.41	-475.19	252
KA2511A	85	7092.01	1846.35	-476.86	255
KA2511A	86	7090.6	1844.29	-478.52	258
KA2511A	87	7089.2	1842.22	-480.18	261
KA2511A	88	7087.8	1840.15	-481.84	264
KA2511A	89	7086.39	1838.08	-483.51	267
KA2511A	90	7084.99	1836.02	-485.17	270
KA2511A	91	7083.59	1833.95	-486.83	273
KA2511A	92	7082.19	1831.89	-488.49	276
KA2511A	93	7080.78	1829.82	-490.1	279
KA2511A	94	7079.38	1827.76	-491.82	282
KA2511A	95	7077.97	1825.69	-493.4	285
KA2511A	96	7076.57	1823.63	-495.1	288
KA2511A	97	7075.16	1821.57	-496.8	291
KA2511A	98	7074.22	1820.2	-497.9	293
KA3385A	0	7250.95	2085.59	-446.01	0
KA3385A	1	7248.13	2086.56	-446.26	3
KA3385A	2	7245.3	2087.53	-446.52	6
KA3385A	3	7242.47	2088.5	-446.77	9
KA3385A	4	7239.64	2089.47	-447.02	12
KA3385A	5	7236.81	2090.44	-447.28	15
KA3385A	6	7233.99	2091.4	-447.53	18
KA3385A	7	7231.16	2092.38	-447.79	21
KA3385A	8	7228.33	2093.35	-448.05	24
KA3385A	9	7225.51	2094.32	-448.3	27
KA3385A	10	7219.86	2096.28	-448.82	33
KA3385A	11	7218.75	2096.66	-448.92	34.18
KAS02	1	7261.99	2125.22	7.68	0
KAS02	2	7262.37	2124.94	2.7	5

KAS02	3	7262.46	2124.89	1.71	6
KAS02	4	7262.53	2124.84	0.71	7
KAS02	5	7262.61	2124.79	-0.28	8
KAS02	6	7262.69	2124.75	-1.28	9
KAS02	7	7262.77	2124.7	-2.28	10
KAS02	8	7262.85	2124.65	-3.27	11
KAS02	9	7262.93	2124.6	-4.27	12
KAS02	10	7263.01	2124.56	-5.26	13
KAS02	11	7263.09	2124.52	-6.26	14
KAS02	12	7263.17	2124.48	-7.25	15
KAS02	13	7263.25	2124.43	-8.25	16
KAS02	14	7263.32	2124.39	-9.25	17
KAS02	15	7263.4	2124.35	-10.24	18
KAS02	16	7263.47	2124.31	-11.24	19
KAS02	17	7263.54	2124.28	-12.24	20
KAS02	18	7263.62	2124.25	-13.23	21
KAS02	19	7263.7	2124.22	-14.23	22
KAS02	20	7263.78	2124.19	-15.23	23
KAS02	21	7263.86	2124.16	-16.22	24
KAS02	22	7263.94	2124.12	-17.22	25
KAS02	23	7264.01	2124.09	-18.21	26
KAS02	24	7264.08	2124.05	-19.21	27
KAS02	25	7264.16	2124.01	-20.21	28
KAS02	26	7264.23	2123.97	-21.2	29
KAS02	27	7264.3	2123.93	-22.2	30
KAS02	28	7264.37	2123.9	-23.2	31
KAS02	29	7264.45	2123.87	-24.2	32
KAS02	30	7264.52	2123.84	-25.19	33
KAS02	31	7264.59	2123.81	-26.19	34
KAS02	32	7264.67	2123.78	-27.19	35
KAS02	33	7264.74	2123.74	-28.18	36
KAS02	34	7264.81	2123.7	-29.18	37
KAS02	35	7264.88	2123.67	-30.18	38
KAS02	36	7264.96	2123.65	-31.17	39
KAS02	37	7265.03	2123.62	-32.17	40
KAS02	38	7265.1	2123.59	-33.17	41
KAS02	39	7265.18	2123.56	-34.16	42
KAS02	40	7265.26	2123.53	-35.16	43
KAS02	41	7265.33	2123.5	-36.16	44
KAS02	42	7265.41	2123.47	-37.15	45
KAS02	43	7265.48	2123.43	-38.15	46
KAS02	44	7265.56	2123.4	-39.15	47
KAS02	45	7265.63	2123.37	-40.14	48
KAS02	46	7265.7	2123.34	-41.14	49
KAS02	47	7265.77	2123.31	-42.14	50
KAS02	48	7266.5	2122.99	-52.11	60
KAS02	49	7267.22	2122.66	-62.07	70
KAS02	50	7267.97	2122.32	-72.04	80
KAS02	51	7268.73	2121.99	-82.01	90
KAS02	52	7269.48	2121.65	-91.97	100
KAS02	53	7270.25	2121.32	-101.94	110
KAS02	54	7271.02	2120.98	-111.9	120
KAS02	55	7271.78	2120.6	-121.87	130

KAS02	56	7272.54	2120.22	-131.83	140
KAS02	57	7273.31	2119.88	-141.79	150
KAS02	58	7274.09	2119.54	-151.76	160
KAS02	59	7274.87	2119.18	-161.72	170
KAS02	60	7275.62	2118.86	-171.69	180
KAS02	61	7276.38	2118.54	-181.65	190
KAS02	62	7277.16	2118.24	-191.62	200
KAS02	63	7277.94	2117.95	-201.58	210
KAS02	64	7278.69	2117.67	-211.55	220
KAS02	65	7279.45	2117.38	-221.52	230
KAS02	66	7280.22	2117.07	-231.48	240
KAS02	67	7281	2116.76	-241.45	250
KAS02	68	7281.79	2116.49	-251.41	260
KAS02	69	7282.57	2116.18	-261.38	270
KAS02	70	7283.36	2115.87	-271.34	280
KAS02	71	7284.17	2115.59	-281.31	290
KAS02	72	7284.97	2115.35	-291.27	300
KAS02	73	7285.77	2115.13	-301.24	310
KAS02	74	7286.56	2114.9	-311.2	320
KAS02	75	7287.35	2114.65	-321.17	330
KAS02	76	7288.14	2114.38	-331.13	340
KAS02	77	7288.92	2114.09	-341.1	350
KAS02	78	7289.71	2113.82	-351.06	360
KAS02	79	7290.51	2113.55	-361.03	370
KAS02	80	7291.32	2113.29	-370.99	380
KAS02	81	7292.15	2113.02	-380.95	390
KAS02	82	7292.98	2112.75	-390.91	400
KAS02	83	7293.82	2112.5	-400.88	410
KAS02	84	7294.65	2112.25	-410.84	420
KAS02	85	7295.45	2112	-420.8	430
KAS02	86	7296.24	2111.76	-430.77	440
KAS02	87	7297.02	2111.57	-440.74	450
KAS02	88	7297.8	2111.39	-450.7	460
KAS02	89	7298.6	2111.22	-460.67	470
KAS02	90	7299.4	2111.07	-470.64	480
KAS02	91	7300.18	2110.97	-480.61	490
KAS02	92	7300.93	2110.84	-490.58	500
KAS02	93	7301.69	2110.7	-500.55	510
KAS02	94	7302.45	2110.6	-510.52	520
KAS02	95	7303.22	2110.5	-520.49	530
KAS02	96	7304.01	2110.4	-530.46	540
KAS02	97	7304.8	2110.33	-540.43	550
KAS02	98	7305.59	2110.26	-550.39	560
KAS02	99	7306.35	2110.16	-560.36	570
KAS02	100	7307.1	2110.04	-570.34	580
KAS02	101	7307.86	2109.96	-580.31	590
KAS02	102	7308.62	2109.94	-590.28	600
KAS02	103	7309.4	2109.92	-600.25	610
KAS02	104	7310.19	2109.9	-610.22	620
KAS02	105	7310.94	2109.89	-620.19	630
KAS02	106	7311.7	2109.93	-630.16	640
KAS02	107	7312.46	2110	-640.13	650
KAS02	108	7313.2	2110.06	-650.1	660

KAS02	109	7313.96	2110.14	-660.07	670
KAS02	110	7314.77	2110.23	-670.04	680
KAS02	111	7315.65	2110.3	-680	690
KAS02	112	7316.54	2110.37	-689.96	700
KAS02	113	7317.43	2110.47	-699.92	710
KAS02	114	7318.32	2110.57	-709.88	720
KAS02	115	7319.2	2110.66	-719.84	730
KAS02	116	7320.06	2110.76	-729.8	740
KAS02	117	7320.94	2110.87	-739.76	750
KAS02	118	7321.81	2110.99	-749.73	760
KAS02	119	7322.64	2111.09	-759.69	770
KAS02	120	7323.43	2111.2	-769.66	780
KAS02	121	7324.23	2111.32	-779.63	790
KAS02	122	7325.07	2111.44	-789.59	800
KAS02	123	7325.93	2111.6	-799.55	810
KAS02	124	7326.78	2111.8	-809.51	820
KAS02	125	7327.65	2112	-819.47	830
KAS02	126	7328.51	2112.21	-829.43	840
KAS02	127	7329.35	2112.4	-839.4	850
KAS02	128	7330.2	2112.6	-849.36	860
KAS02	129	7331.06	2112.8	-859.32	870
KAS02	130	7331.92	2113.03	-869.28	880
KAS02	131	7332.78	2113.24	-879.24	890
KAS02	132	7333.65	2113.42	-889.2	900
KAS02	133	7334.54	2113.61	-899.16	910
KAS02	134	7335.49	2113.83	-909.11	920
KAS02	135	7335.88	2113.92	-913.13	924.04
KAS05	1	7247.97	2059.61	8.68	0
KAS05	2	7247.2	2060.05	-1.28	10
KAS05	3	7246.33	2060.3	-11.24	20
KAS05	4	7245.43	2060.57	-21.2	30
KAS05	5	7244.53	2060.84	-31.15	40
KAS05	6	7243.63	2061.12	-41.11	50
KAS05	7	7242.69	2061.41	-51.06	60
KAS05	8	7241.73	2061.7	-61.01	70
KAS05	9	7240.78	2062.01	-70.96	80
KAS05	10	7239.83	2062.3	-80.91	90
KAS05	11	7238.87	2062.59	-90.86	100
KAS05	12	7237.9	2062.87	-100.81	110
KAS05	13	7236.94	2063.14	-110.76	120
KAS05	14	7236	2063.39	-120.71	130
KAS05	15	7235.05	2063.64	-130.66	140
KAS05	16	7234.11	2063.87	-140.61	150
KAS05	17	7233.18	2064.09	-150.57	160
KAS05	18	7232.21	2064.33	-160.52	170
KAS05	19	7231.22	2064.59	-170.47	180
KAS05	20	7230.2	2064.87	-180.41	190
KAS05	21	7229.18	2065.17	-190.35	200
KAS05	22	7228.16	2065.48	-200.3	210
KAS05	23	7227.14	2065.8	-210.24	220
KAS05	24	7226.12	2066.12	-220.18	230
KAS05	25	7225.11	2066.45	-230.13	240
KAS05	26	7224.1	2066.79	-240.07	250

KAS05	27	7223.08	2067.14	-250.01	260
KAS05	28	7222.08	2067.47	-259.95	270
KAS05	29	7221.06	2067.8	-269.9	280
KAS05	30	7220.05	2068.11	-279.84	290
KAS05	31	7219.02	2068.42	-289.78	300
KAS05	32	7217.99	2068.73	-299.72	310
KAS05	33	7216.93	2069.04	-309.66	320
KAS05	34	7215.85	2069.37	-319.6	330
KAS05	35	7214.78	2069.69	-329.54	340
KAS05	36	7213.7	2070.01	-339.47	350
KAS05	37	7212.62	2070.34	-349.41	360
KAS05	38	7211.55	2070.68	-359.35	370
KAS05	39	7210.47	2071.02	-369.28	380
KAS05	40	7209.4	2071.36	-379.22	390
KAS05	41	7208.34	2071.71	-389.16	400
KAS05	42	7207.26	2072.06	-399.09	410
KAS05	43	7206.17	2072.4	-409.03	420
KAS05	44	7205.11	2072.73	-418.96	430
KAS05	45	7204.05	2073.05	-428.9	440
KAS05	46	7202.95	2073.38	-438.84	450
KAS05	47	7201.81	2073.72	-448.77	460
KAS05	48	7200.68	2074.06	-458.7	470
KAS05	49	7199.55	2074.42	-468.62	480
KAS05	50	7198.42	2074.79	-478.55	490
KAS05	51	7197.3	2075.15	-488.48	500
KAS05	52	7196.17	2075.52	-498.41	510
KAS05	53	7195.03	2075.88	-508.34	520
KAS05	54	7193.89	2076.23	-518.27	530
KAS05	55	7192.75	2076.59	-528.2	540
KAS05	56	7191.67	2076.94	-537.73	549.6
KC0045F	0	7288.4	2084.11	-341.53	0
KC0045F	1	7288.64	2086.87	-342.69	3
KC0045F	2	7288.88	2089.62	-343.86	6
KC0045F	3	7289.12	2092.37	-345.02	9
KC0045F	4	7289.36	2095.13	-346.19	12
KC0045F	5	7289.6	2097.88	-347.36	15
KC0045F	6	7289.83	2100.63	-348.53	18
KC0045F	7	7290.06	2103.39	-349.69	21
KC0045F	8	7290.29	2106.14	-350.86	24
KC0045F	9	7290.51	2108.9	-352.03	27
KC0045F	10	7290.73	2111.65	-353.2	30
KC0045F	11	7290.95	2114.41	-354.36	33
KC0045F	12	7291.16	2117.16	-355.53	36
KC0045F	13	7291.38	2119.92	-356.69	39
KC0045F	14	7291.58	2122.68	-357.86	42
KC0045F	15	7291.79	2125.43	-359.02	45
KC0045F	16	7291.99	2128.19	-360.18	48
KC0045F	17	7292.18	2130.95	-361.34	51
KC0045F	18	7292.38	2133.71	-362.5	54
KC0045F	19	7292.57	2136.47	-363.66	57
KC0045F	20	7292.77	2139.23	-364.82	60
KC0045F	21	7292.96	2141.99	-365.98	63
KC0045F	22	7293.14	2144.76	-367.13	66

KC0045F	23	7293.32	2147.52	-368.29	69
KC0045F	24	7293.5	2150.28	-369.44	72
KC0045F	25	7293.68	2153.04	-370.6	75
KC0045F	26	7293.85	2155.81	-371.75	78
KC0045F	27	7294.02	2158.57	-372.91	81
KC0045F	28	7294.19	2161.34	-374.06	84
KC0045F	29	7294.36	2164.1	-375.21	87
KC0045F	30	7294.52	2166.87	-376.36	90
KC0045F	31	7294.68	2169.63	-377.52	93
KC0045F	32	7294.84	2172.4	-378.67	96
KC0045F	33	7294.99	2175.16	-379.82	99
KC0045F	34	7295.14	2177.93	-380.96	102
KC0045F	35	7295.29	2180.7	-382.11	105
KC0045F	36	7295.43	2183.47	-383.26	108
KC0045F	37	7295.57	2186.24	-384.41	111
KC0045F	38	7295.71	2189	-385.56	114
KC0045F	39	7295.85	2191.77	-386.71	117
KC0045F	40	7295.99	2194.54	-387.85	120
KC0045F	41	7296.12	2197.31	-389	123
KC0045F	42	7296.25	2200.08	-390.15	126
KC0045F	43	7296.37	2202.85	-391.29	129
KC0045F	44	7296.49	2205.62	-392.44	132
KC0045F	45	7296.61	2208.39	-393.58	135
KC0045F	46	7296.72	2211.16	-394.72	138
KC0045F	47	7296.83	2213.94	-395.86	141
KC0045F	48	7296.94	2216.71	-397	144
KC0045F	49	7297.04	2219.48	-398.14	147
KC0045F	50	7297.14	2222.25	-399.28	150
KC0045F	51	7297.24	2225.03	-400.43	153
KC0045F	52	7297.34	2227.8	-401.57	156
KC0045F	53	7297.43	2230.57	-402.72	159
KC0045F	54	7297.53	2233.34	-403.86	162
KC0045F	55	7297.62	2236.11	-405.01	165
KC0045F	56	7297.7	2238.88	-406.15	168
KC0045F	57	7297.79	2241.65	-407.3	171
KC0045F	58	7297.87	2244.43	-408.44	174
KC0045F	59	7297.95	2247.2	-409.58	177
KC0045F	60	7298.04	2249.97	-410.72	180
KC0045F	61	7298.12	2252.75	-411.86	183
KC0045F	62	7298.19	2255.52	-413	186
KC0045F	63	7298.26	2258.3	-414.14	189
KC0045F	64	7298.34	2261.07	-415.27	192
KC0045F	65	7298.41	2263.85	-416.4	195
KC0045F	66	7298.47	2266.63	-417.53	198
KC0045F	67	7298.54	2269.41	-418.65	201
KC0045F	68	7298.6	2272.19	-419.78	204
KC0045F	69	7298.66	2274.97	-420.9	207
KC0045F	70	7298.72	2277.75	-422.02	210
KC0045F	71	7298.78	2280.54	-423.14	213
KC0045F	72	7298.83	2283.32	-424.26	216
KC0045F	73	7298.88	2286.1	-425.38	219
KC0045F	74	7298.92	2288.89	-426.5	222
KC0045F	75	7298.96	2291.67	-427.61	225

KC0045F	76	7299	2294.46	-428.72	228
KC0045F	77	7299.04	2297.25	-429.82	231
KC0045F	78	7299.08	2300.04	-430.92	234
KC0045F	79	7299.11	2302.83	-432.02	237
KC0045F	80	7299.15	2305.62	-433.12	240
KC0045F	81	7299.18	2308.41	-434.22	243
KC0045F	82	7299.21	2311.21	-435.32	246
KC0045F	83	7299.25	2314	-436.42	249
KC0045F	84	7299.28	2316.79	-437.51	252
KC0045F	85	7299.3	2319.58	-438.61	255
KC0045F	86	7299.33	2322.37	-439.71	258
KC0045F	87	7299.35	2325.16	-440.81	261
KC0045F	88	7299.37	2327.96	-441.91	264
KC0045F	89	7299.39	2330.75	-443	267
KC0045F	90	7299.4	2333.54	-444.1	270
KC0045F	91	7299.41	2336.33	-445.19	273
KC0045F	92	7299.42	2339.13	-446.28	276
KC0045F	93	7299.42	2341.92	-447.37	279
KC0045F	94	7299.42	2344.72	-448.46	282
KC0045F	95	7299.42	2347.51	-449.55	285
KC0045F	96	7299.42	2350.31	-450.64	288
KC0045F	97	7299.41	2353.11	-451.73	291
KC0045F	98	7299.41	2355.9	-452.81	294
KC0045F	99	7299.4	2358.7	-453.89	297
KC0045F	100	7299.39	2361.5	-454.97	300
KC0045F	101	7299.37	2364.3	-456.04	303
KC0045F	102	7299.36	2367.1	-457.12	306
KC0045F	103	7299.34	2369.9	-458.2	309
KC0045F	104	7299.32	2372.7	-459.28	312
KC0045F	105	7299.3	2375.5	-460.37	315
KC0045F	106	7299.28	2378.29	-461.46	318
KC0045F	107	7299.26	2381.09	-462.55	321
KC0045F	108	7299.23	2383.88	-463.64	324
KC0045F	109	7299.2	2386.67	-464.74	327
KC0045F	110	7299.17	2387.41	-465.84	330
KC0045F	111	7299.14	2392.25	-466.94	333
KC0045F	112	7299.11	2395.04	-468.04	336
KC0045F	113	7299.1	2395.69	-468.3	336.7
KA3191F	0	7308.87	2269.78	-417.82	0.00
KA3191F	1	7308.35	2266.85	-418.26	3.00
KA3191F	2	7307.82	2263.93	-418.69	6.00
KA3191F	3	7307.29	2261.01	-419.13	9.00
KA3191F	4	7306.76	2258.09	-419.57	12.00
KA3191F	5	7306.22	2255.18	-420.02	15.00
KA3191F	6	7305.69	2252.26	-420.47	18.00
KA3191F	7	7305.16	2249.34	-420.93	21.00
KA3191F	8	7304.63	2246.42	-421.38	24.00
KA3191F	9	7304.11	2243.51	-421.84	27.00
KA3191F	10	7303.59	2240.59	-422.30	30.00
KA3191F	11	7303.07	2237.67	-422.76	33.00
KA3191F	12	7302.55	2234.75	-423.21	36.00
KA3191F	13	7302.05	2231.83	-423.67	39.00
KA3191F	14	7301.55	2228.90	-424.13	42.00

KA3191F	15	7301.05	2225.98	-424.58	45.00
KA3191F	16	7300.55	2223.06	-425.03	48.00
KA3191F	17	7300.05	2220.13	-425.48	51.00
KA3191F	18	7299.56	2217.21	-425.93	54.00
KA3191F	19	7299.06	2214.28	-426.38	57.00
KA3191F	20	7298.57	2211.36	-426.82	60.00
KA3191F	21	7298.08	2208.43	-427.27	63.00
KA3191F	22	7297.60	2205.50	-427.72	66.00
KA3191F	23	7297.11	2202.58	-428.16	69.00
KA3191F	24	7296.63	2199.65	-428.61	72.00
KA3191F	25	7296.15	2196.72	-429.06	75.00
KA3191F	26	7295.67	2193.80	-429.51	78.00
KA3191F	27	7295.20	2190.87	-429.95	81.00
KA3191F	28	7294.72	2187.94	-430.40	84.00
KA3191F	29	7294.24	2185.01	-430.84	87.00
KA3191F	30	7293.77	2182.08	-431.29	90.00
KA3191F	31	7293.30	2179.15	-431.73	93.00
KA3191F	32	7292.83	2176.22	-432.18	96.00
KA3191F	33	7292.36	2173.30	-432.63	99.00
KA3191F	34	7291.89	2170.37	-433.08	102.00
KA3191F	35	7291.42	2167.44	-433.54	105.00
KA3191F	36	7290.96	2164.51	-433.99	108.00
KA3191F	37	7290.51	2161.58	-434.45	111.00
KA3191F	38	7290.05	2158.65	-434.91	114.00
KA3191F	39	7289.60	2155.72	-435.37	117.00
KA3191F	40	7289.15	2152.79	-435.84	120.00
KA3191F	41	7288.70	2149.86	-436.30	123.00
KA3191F	42	7288.26	2146.93	-436.77	126.00
KA3191F	43	7287.81	2144.00	-437.25	129.00
KA3191F	44	7287.37	2141.07	-437.72	132.00
KA3191F	45	7286.93	2138.15	-438.20	135.00
KA3191F	46	7286.50	2135.22	-438.68	138.00
KA3191F	47	7286.06	2132.29	-439.17	141.00
KA3191F	48	7285.63	2129.36	-439.65	144.00
KA3191F	49	7285.19	2126.43	-440.14	147.00
KA3191F	50	7284.76	2123.50	-440.63	150.00
KA3191F	51	7284.33	2120.57	-441.12	153.00
KA3191F	52	7283.91	2117.65	-441.62	156.00
KA3191F	53	7283.49	2114.72	-442.11	159.00
KA3191F	54	7283.07	2111.79	-442.61	162.00
KA3191F	55	7282.65	2108.86	-443.11	165.00
KA3191F	56	7282.23	2105.93	-443.61	168.00
KA3191F	57	7281.82	2103.00	-444.10	171.00
KA3191F	58	7281.41	2100.07	-444.60	174.00
KA3191F	59	7281.00	2097.14	-445.11	177.00
KA3191F	60	7280.59	2094.21	-445.61	180.00
KA3191F	61	7280.19	2091.29	-446.11	183.00
KA3191F	62	7279.79	2088.36	-446.62	186.00
KA3191F	63	7279.39	2085.43	-447.12	189.00
KA3191F	64	7279.00	2082.49	-447.63	192.00
KA3191F	65	7278.60	2079.57	-448.14	195.00
KA3191F	66	7278.21	2076.63	-448.65	198.00
KA3191F	67	7277.82	2073.70	-449.16	201.00

KA3191F	68	7277.43	2070.77	-449.67	204.00
KA3191F	69	7277.05	2067.84	-450.19	207.00
KA3191F	70	7276.67	2064.91	-450.70	210.00
KA3191F	71	7276.62	2064.52	-450.77	210.40

Type	Section	Northing	Easting	Elevation	Radius	negative radius indicates a left turn
Straight stretch	0.000	5740.711	2158.345	-5.000		
Curve	20.000	5730.410	2175.488	-7.000	-40.000	
Straight stretch	109.381	5769.780	2235.666	-15.9381		
Curve	925.787	6579.547	2131.761	-127.290	10.061	
Straight stretch	930.527	6584.215	2132.274	-127.954		
Curve	980.179	6630.919	2149.130	-134.905	-20.486	
Straight stretch	989.780	6640.378	2150.139	-136.249		
Curve	1497.719	7143.774	2082.356	-207.361	-40.000	
Straight stretch	1513.095	7158.251	2077.461	-209.513		
Curve	1599.107	7232.968	2034.854	-221.555	40.000	
Straight stretch	1635.101	7267.679	2032.479	-225.154		
Curve	1753.466	7377.526	2076.560	-230.903	20.000	
Straight stretch	1771.651	7389.299	2089.596	-240.388		
Curve	1900.361	7424.856	2213.297	-257.447	20.000	
Straight stretch	1921.305	7420.030	2232.706	-259.542		
Curve	2048.243	7331.910	2324.074	-276.353	20.000	
Straight stretch	2069.187	7312.688	2329.600	-278.447		
Curve	2196.125	7189.501	2298.970	-295.259	20.000	
Straight stretch	2217.069	7175.105	2285.086	-297.353		
Curve	2373.135	7131.991	2135.094	-318.243	20.000	
Straight stretch	2394.080	7136.817	2115.684	-320.337		
Curve	2503.092	7212.494	2037.220	-335.119	40.000	
Straight stretch	2550.496	7256.182	2027.865	-339.859		
Curve	2712.932	7406.930	2088.360	-359.408	20.000	
Straight stretch	2731.113	7418.702	2101.392	-361.953		
Curve	2860.060	7454.353	2225.313	-380.006	20.000	
Straight stretch	2874.045	7453.399	2238.981	-381.963		
Curve	3006.879	7399.315	2360.307	-400.560	40.000	
Straight stretch	3108.693	7323.405	2351.060	-414.814		
Curve	3422.400	7268.197	2042.248	-450.022	470.000	
Curve	3453.433	7263.749	2011.541	-449.264	221.235	
Straight stretch	3509.346	7264.381	1955.780	-449.071		
Straight stretch	3599.346	7277.112	1866.685	-447.271		

APPENDIX A2 IDENTIFIED HYDRAULIC STRUCTURES

This appendix describes identified hydraulic structures in the HRL. The header describes the location and properties of the feature as follows:

Waterbearing structure	= ID code for the structure
Zone ID	= zone of which the structure is interpreted as
Borehole ID	= borehole name
Section	= borehole length (tunnel length)
Responses & confirmation	= boreholes confirming hydraulic responses or structural evidence
TD/MI or TD/MI/PR	= Total depth/Measurement interval or Total depth/Measurement interval/Point response
Fracturing	= evidence of fracturing
Radar	= evidence of radar reflector
Seismics	= evidence of seismic reflector
Flow log	= evidence in flow log from spinner or UCM
BUP tests	= evidence from pressure build-up tests
Other tests	= interference tests (INT)
Orientation	= orientation relative to $N_{äspö}$
T	= Transmissivity (m^2/s)
Q	= Hydraulic conductivity (m/s)
Q/s	= Specific capacity (m^2/s)
Diffusivity	= (m^2/s)
Storativity	
Report	= Reference to the source of information

Waterbearing structure	Zone ID	Borehole ID	Section (m)	Responses & confirmation	TD/MI or TD/MI/PR	Fracturing	Radar	Seismics	Flow log	BUP tests	Other tests	Orientation	T	Q	Q/p	Diffusivity	Storativity	Report
Z2048A	NNW-4	KA2048B	28.0	HA1960A	?/3.9-32.0/32	X			X	X		350/90	1.6E-5 - 8.6E-5					PR25-94-06
			39.0	SA2025B		X	X					189/88						PR25-94-01
			(T2020-2140)	HA2074B	?/4.0-20.0/?													
Z2048B	NE-1	KA2048B	166-184			X			X	X		NE	1.6E-04					PR25-94-06
Z1700				HA1684A	?/1.6-25.0/3.5,10.5				X	X		N70W	2.9E-5 - 0.6E-5					PR25-94-06
				HA1714A	?/5.9-25.0/7.5,9.5													
				SA1696A														
Z1730				HA1749A	?/5.8-25.0/23.5				X	X		N60W	2.9E-5 - 1E-5					PR25-94-06
				HA1704B	?/3.9-25.0/17													PR25-94-01
Z1850				HA1852A	?/5.8-25.0//21.5				X	X		N70W	3.9E-5 - 0.9E-5					PR25-94-06
				HA1896B	?/5.8-25.0/12.5,21.5													PR25-94-01
Z2162A	NNW-4	KA2162A	49-53	SA1680B		X			X	X		NNW-NW	5.8E-05	4.6E-03	2.6E-05	31.0	1.9E-06	PR25-94-06
				SA1861B		X												PR25-94-01
				HA1960A	?/3.9-32.0/32	X												
Z2162D	NNW-2	KA2162A	121.0	SA1680B		X	X		X	X		306/79	3.3E-05			20.2 - 3.7		PR25-94-06
				SA1861B		X												PR25-94-01
				HA1960A	?/3.9-32.0/32	X												
Z2162G	NNW-1	KA2162A	165-174	SA1680B		X	X		X	X		306/74	7.8E-05			9.2 - 3.2		PR25-94-06
				SA1861B		X												PR25-94-01
				HA1960A	?/3.9-32.0/32	X												
Z1751A		KA1751A	29.0	KAS04	481/215-287,393-481	X			X	X		?	3.7E-06					PR25-94-06
Z1751B		KA1751A	31-33	KAS04	481/215-287,393-481	X			X	X		?	1.3E-06					PR25-94-01
Z1751C		KA1751A	44.0	KAS04	481/215-287,393-481	X			X	X		?	2.7E-06					
Z1751D		KA1751A	65-66	KAS04	481/215-287,393-481	X			X	X		?	1.4E-06					
Z1754A		KA1754A	50-51	KAS04	481/215-287,393-481	X			X	X			3.0E-07					PR25-94-06
Z1754B		KA1754A	81-84	KAS04	481/215-287,393-481	X			X	X		119/66	2.6E-06					PR25-94-06
				KA1751A	150/65-66													PR25-94-01

Waterbearing structure	Zone ID	Borehole ID	Section (m)	Responses & confirmation	TD/MI or MI/PR	Fracturing	Radar	Seismics	Flow log	BUP tests	Other tests	Orientation	T	Q	Q/p	Diffusivity	Storativity	Report
Z1755E		KA1755A	52.6-57.1	KA1754A	160/81-84	X			X	X		NNW	2.8E-05					PR 25-94-39
				KA1751A	150/65-66													
				KA2598A	?/in the beginning													
Z3191A	NNW-2	KA3191F	4.9	KA2162B:4	288.1/40.0-79.5	X	X		X	X		265/79	5.2E-06					PR 25-95-09
				KA2162B:3	288.1/80.5-142													
				KA2162B:2	288.1/143-200													
				KA2162B:1	288.1/201-288.1													
				KAS06:2	602/391-430													
				KAS16:2	548/390-465													
				KAS12:1	380/330-380													
Z3191B		KA3191F	14.5	SA2834B		X	X		X	X		29/29	2.4E-06					PR 25-95-09
Z3191C		KA3191F	47.0	SA2240B		X	X		X	X		200/55	6.6E-07					PR 25-95-09
				SA2734A														
				SA2834B														
				KAS06:2	602/391-430													
				KA2162B:4	288.1/40.0-79.5													
				KA2162B:3	288.1/80.5-142													
				KA2162B:2	288.1/143-200													
				KA2162B:1	288.1/201-288.1													
				KAS16:2	548/390-465													
Z3191D		KA3191F	77.0			X	X		X	X		114/77	3.9E-07					PR 25-95-09
Z3191D		KA3191F	89.5-98.0	SA2663B		X	X		X	X		114/77	3.9E-07					PR 25-95-09
Z3191F	NNW-1	KA3191F	123.6-124.1	SA2240B		X	X		X	X		35/70	1.3E-05					PR 25-95-09
				KAS12	380/													
				KAS02:3	346-799													
				KAS06:2	602/391-430													
				KA2162B:4	288.1/40.0-79.5													
				KA2162B:3	288.1/80.5-142													
				KA2162B:2	288.1/143-200													
				KA2162B:1	288.1/201-288.1													
				KAS05:2	550/381-439													
				KAS05:3	550/320-380													
Z3191G		KA3191F	195.0	KAS05:2	550/381-439	X	X		X	X		?	2.0E-07					PR 25-95-09
				KAS05:3	550/320-380													
				KA2162B:3	288.1/80.5-142													
				KA2162B:2	288.1/143-200													
				KA2162B:1	288.1/201-288.1													

Waterbearing structure	Zone ID	Borehole ID	Section (m)	Responses & confirmation	TD/MI or MI/PR	Fracturing	Radar	Seismics	Flow log	BUP tests	Other tests	Orientation	T	Q	Q/p	Diffusivity	Storativity	Report
Z3191H		KA3191F	202.5	KAS05:2	550/381-439	X	X		X	X		?	7.2E-07					PR 25-95-09
				KAS05:3	550/320-380													
				KA2162B:3	288.1/80.5-142													
				KA2162B:2	288.1/143-200													
				KA2162B:1	288.1/201-288.1													
Z2511A		KA2511A	25.0			X		X	X	X	3M	?	3.0E-05	4.2E-03	1.3E-06			PR 25-94-15
Z2511B	NNW-5	KA2511A	52.8	SA1684B		X	X	X	X	X	3M	164/76	3.6E-05					PR 25-94-15
				KA1751A	150/65-66													
				KA1754A	160/81-84													
				SA1861B														
				KA2048B	?													
				SA2338A														
Z2511C	NNW-5b	KA2511A	100.1	KA1751A	150/65-66	X	X	X	X	X	3M	153/78	2.4E-05					PR 25-94-15
				KA1754A	160/81-84													
				SA1861B														
				SA2338A														
Z2511D	NNW-5c	KA2511A	214.0	KA1751A	150/65-66	X					3M	?	2.4E-05					PR 25-94-15
				KA1754A	160/81-84													
				SA2338A														
Z2511E		KA2511A	242.0	KA1754A	160/81-84	X	X	X			3M	111/85	4.6E-06					PR 25-94-15
				KA1751A	150/65-66													
				SA2338A														
Z2598A		KA2598A	12.7	KA1754A	160/81-84	X			X	X		?	4.0E-06					PR 25-94-15
				KA1751A	150/65-66													
				SA2338A														
				SA1684B														
				SA1861B														
Z2598B		KA2598A	18.5	KA1754A	160/81-84	X			X	X		?	4.8E-06					PR 25-94-15
				KA1751A	150/65-66													
				SA2338A														
				SA1684B														
				SA1861B														
Z2598C		KA2598A	37.4-39.4	KA1754A	160/81-84				X	X			1.6E-06					PR 25-94-15
				KA1751A	150/65-66													
				SA2338A														
Z2598D		KA2598A	49.8-52.4	SA2338A									4.0E-07					PR 25-94-15

Waterbearing structure	Zone ID	Borehole ID	Section (m)	Responses & confirmation	TD/MI or MI/PR	Fracturing	Radar	Seismics	Flow log	BUP tests	Other tests	Orientation	T	Q	Q/p	Diffusivity	Storativity	Report
Z2598E	NNW-5	KA2598A	73.5-75.5	KA1754A KA1751A SA2338A	160/81-84 150/65-66	X	X	X	X	X		346/84	1.2E-06					PR 25-94-15
Z2598F		KA2598A	92.5-96.5	KA1754A KA1751A SA2338A	160/81-84 150/65-66	X		X	X	X		346/84	8.0E-07					PR 25-94-15
Z0045A	NNW-2	KC0045F	101.9-104.8	KA2162B1-B4 SA1861B KA2048B SA2338A	Packer leakage ? ? 	X	X	X	X	X		311/69	8.0E-06					PR 25-94-15
Z0045B		KC0045F	112.1-113.6	KA2162B1-B4 SA1861B KA2048B SA2338A	Packer leakage ? ? 	X			X	X		?	6.1E-6 - 9.9E-6					PR 25-94-15
Z0045C		KC0045F	235.2-245.9	KA2048B KA2162B1-B4 SA2338A	? Packer leakage ? 	X	X	X	X	X		137/80	6.3E-6 - 6.5E-6					PR 25-94-15
Z0045D	NNW-1	KC0045F	264.2-266.7	KA2048B KA2162B1-B4 SA2338A	? Packer leakage ? 	X	X	X	X	X		134/75	1.9E-5 -5.9E-5					PR 25-94-15
Z0045E		KC0045F	272.4-275.4	KA2048B KA2162B1-B4	? Packer leakage ?	X	X	X	X	X		?	7E-6 - 3.5E-5					PR 25-94-15
Z0045F		KC0045F	285.2-286.2	KA2048B KA2162B1-B4	? Packer leakage ?	X	X	X	X	X		208/79	2.1E-5 - 7.6E-5					PR 25-94-15
Z0045G		KC0045F	305.2	KA2048B KA2162B1-B4	? Packer leakage ?	X	X	X	X	X		108/86	1.1E-05					PR 25-94-15
Z2858A		KA2858A:2	39.77-40.77	NO RESPONSE		X			X	X	INT		1.0E-08					PR HRL-96-01
Z2862A		KA2862A:1	15.02-15.98	NO RESPONSE		X	X		X	X	INT	295/90	4.4E-08					PR HRL-96-01
Z3067A		KA3067A:2	30.55-33.55	KA3010A:1 KA3010A:2 KA3067A:1 KA3067A:3 SA3045A	60.66/16.06-60.66 60.66/8.56-15.06 40.05/34.55-40.05 40.05/28.05-29.55 	X	X		X	X	INT	N65W	4.1E-07					PR HRL-96-01

Waterbearing structure	Zone ID	Borehole ID	Section (m)	Responses & confirmation	TD/MI or MI/PR	Fracturing	Radar	Seismics	Flow log	BUP tests	Other tests	Orientation	T	Q	Q/p	Diffusivity	Storativity	Report
Z3010A	NNW-2	KA3010A:1+2	8.56-60.66	KA2858A:2	59.7/39.77-40.77		X		X	X	INT	131/70	1.8E-5 - 5.5E-5				9E-7-19E-6	PR HRL-96-01
				KA2862A:1	15.98/15.02-15.98													
				KA3005A:1	58.11/46.43-58.11													
				KA3005A:2	58.11/44.43-45.43													
				KA3005A:3	58.11/38.93-43.43													
				KA3005A:4	58.11/36.93-37.93													
				KA3067A:1	40.05/34.55-40.05													
				KA3067A:2	40.05/30.55-33.55													
				KA3067A:3	40.05/28.05-29.55													
				KA3067A:4	40.55/6.55-27.05													
				KA3105A:1	68.95/53.01-68.95													
				KA3105A:2	68.95/25.51-52.01													
				KA3105A:3	68.95/22.51-24.51													
				KA3105A:4	68.95/17.01-19.51													
				KA3110A:1	28.63/20.05-28.63													
				KA3110A:2	28.63/6.55-19.05													
				HA1960A	?/3.9-32.0/32													
				KA2050A:1	211.5/?													
				KA2050A:2	211.5/?													
				KA2050A:3	211.5/?													
				KA2162B:3	288.1/80.5-142													
				KA2162B:4	288.1/40.0-79.5													
				SA2880A														
				SA3045A														
Z3105A		KA3105A:4	17.01-19.51	KA3005A:3	58.11/38.93-43.43	X	X		X	X	INT		3.3E-07					PR HRL-96-01
				KA3010A:2	60.66/8.56-15.06													
				KA3067A:2	40.05/30.55-33.55													
				KA3067A:3	40.05/28.05-29.55													
				KA3067A:4	40.55/6.55-27.05													
				KA3105A:1	68.95/53.01-68.95													
				KA3105A:2	68.95/25.51-52.01													
				KA3105A:3	68.95/22.51-24.51													
				KA3110A:1	28.63/20.05-28.63													
				KA3110A:2	28.63/6.55-19.05													
				HA1960A	?/3.9-32.0/32													
				KA2048B:1	?													
				KA2048B:2	?													
				KA2048B:3	?													
				KA2048B:4	?													
				KA2050A:1	211.5/?													
				KA2050A:2	211.5/?													
				KA2050A:3	211.5/?													
				KA2162B:1	288.1/201-288.1													
				KA2162B:2	288.1/143-200													
				KA2162B:3	288.1/80.5-142													
				KA2162B:4	288.1/40.0-79.5													
				SA3045A														

FIGURES

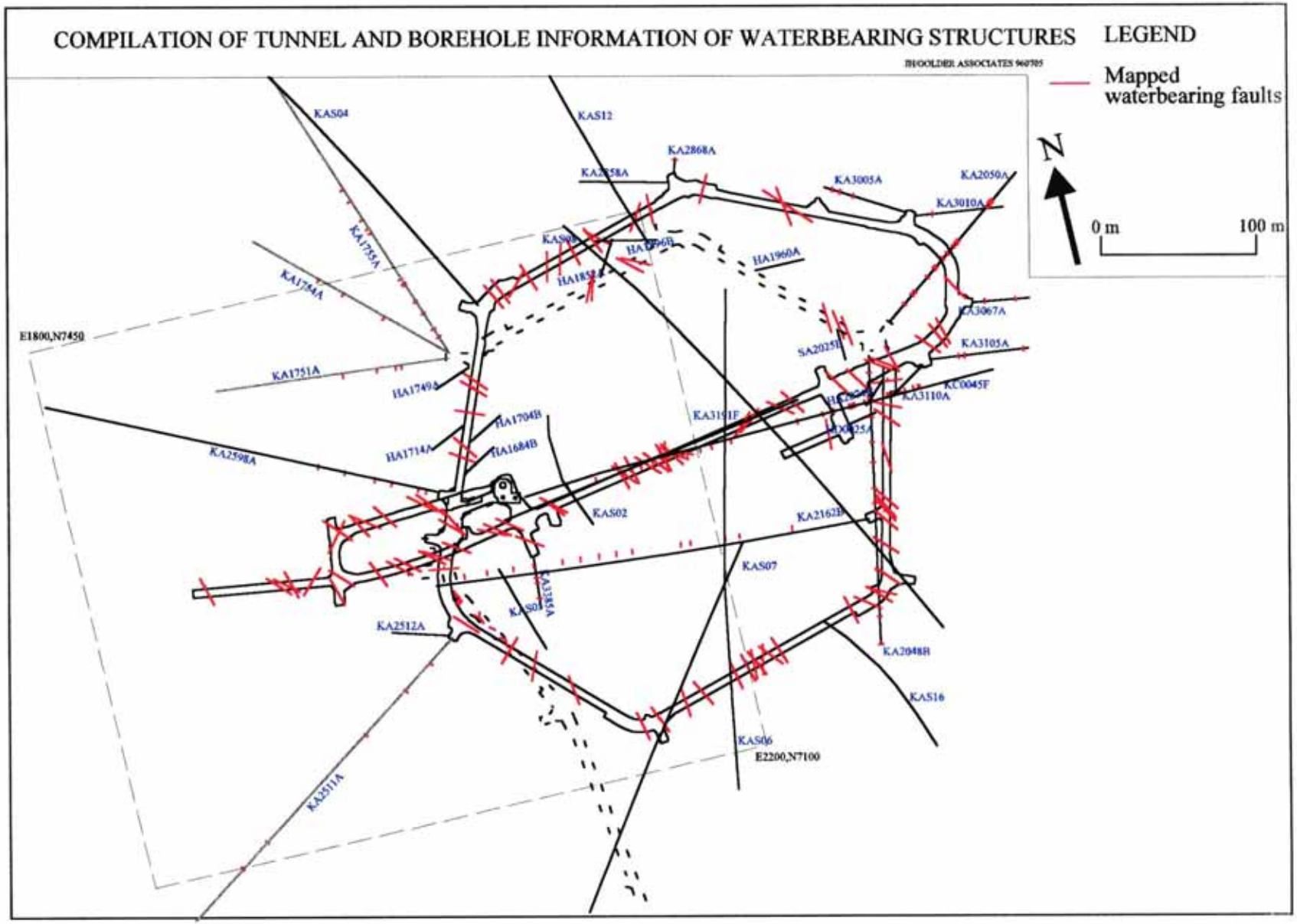

Figure 1-1 Location of the target volume.

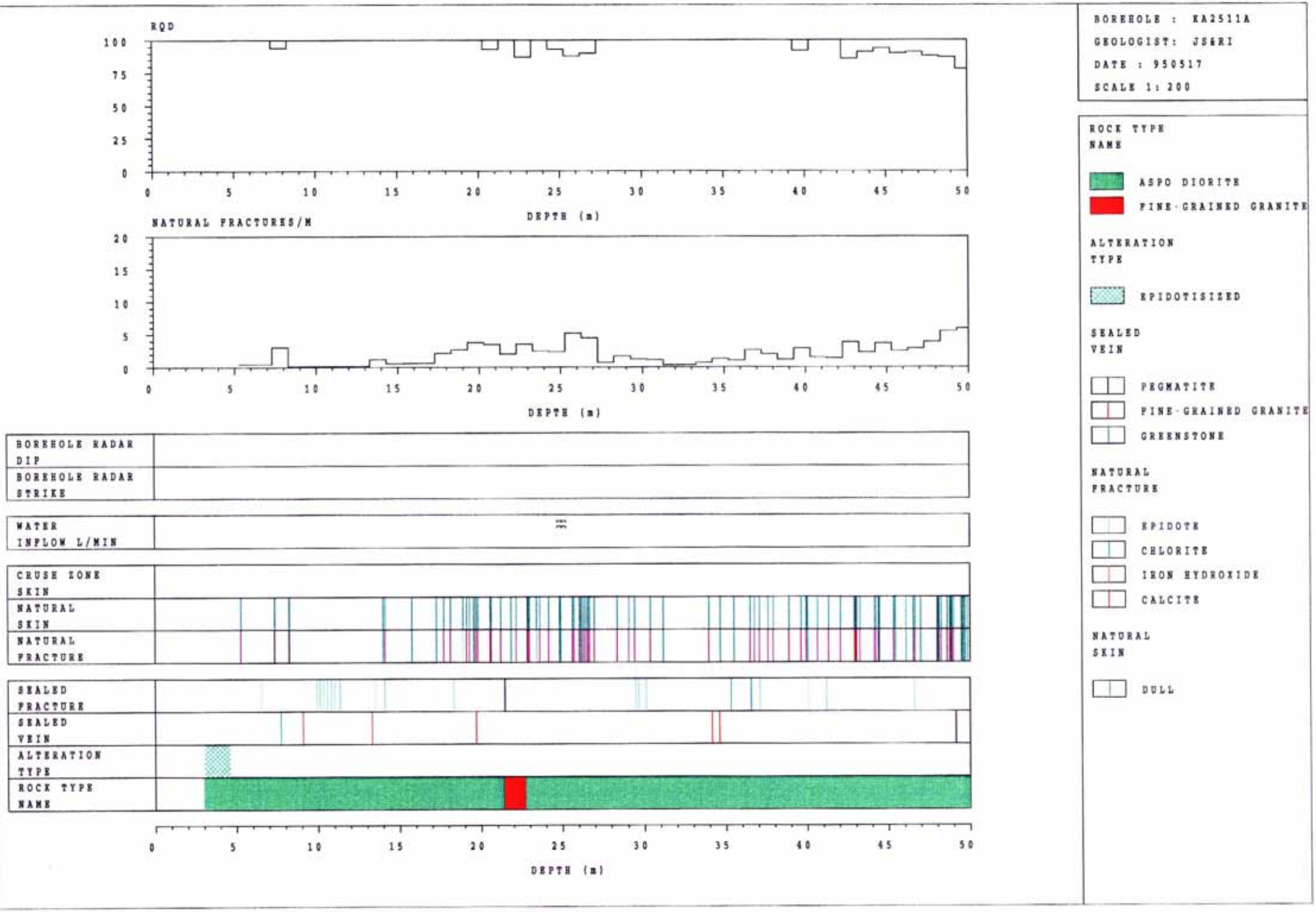

Figure 2-1a Petrocore log of core from borehole KA2511A

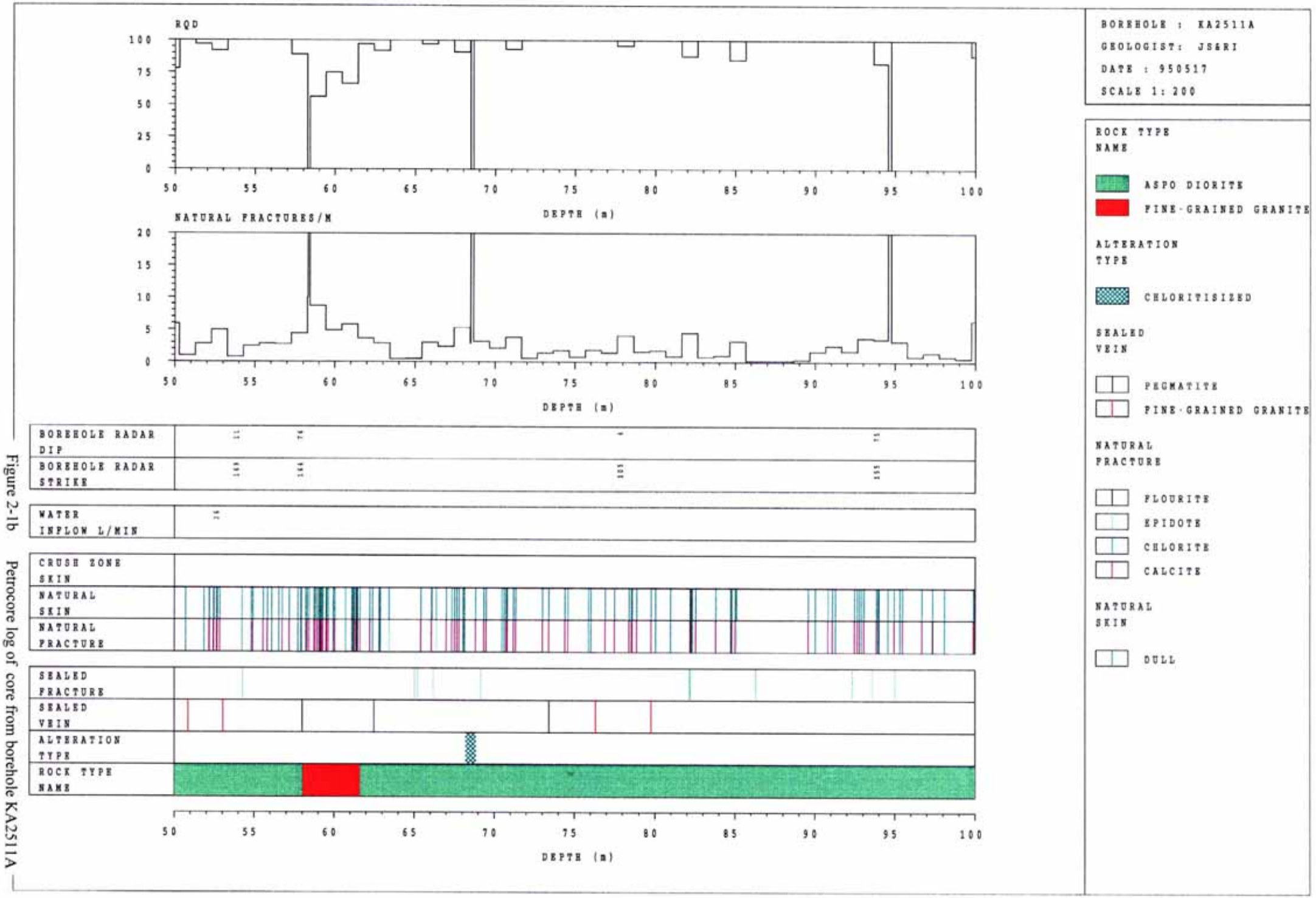

Figure 2-1b Petrocore log of core from borehole KA2511A

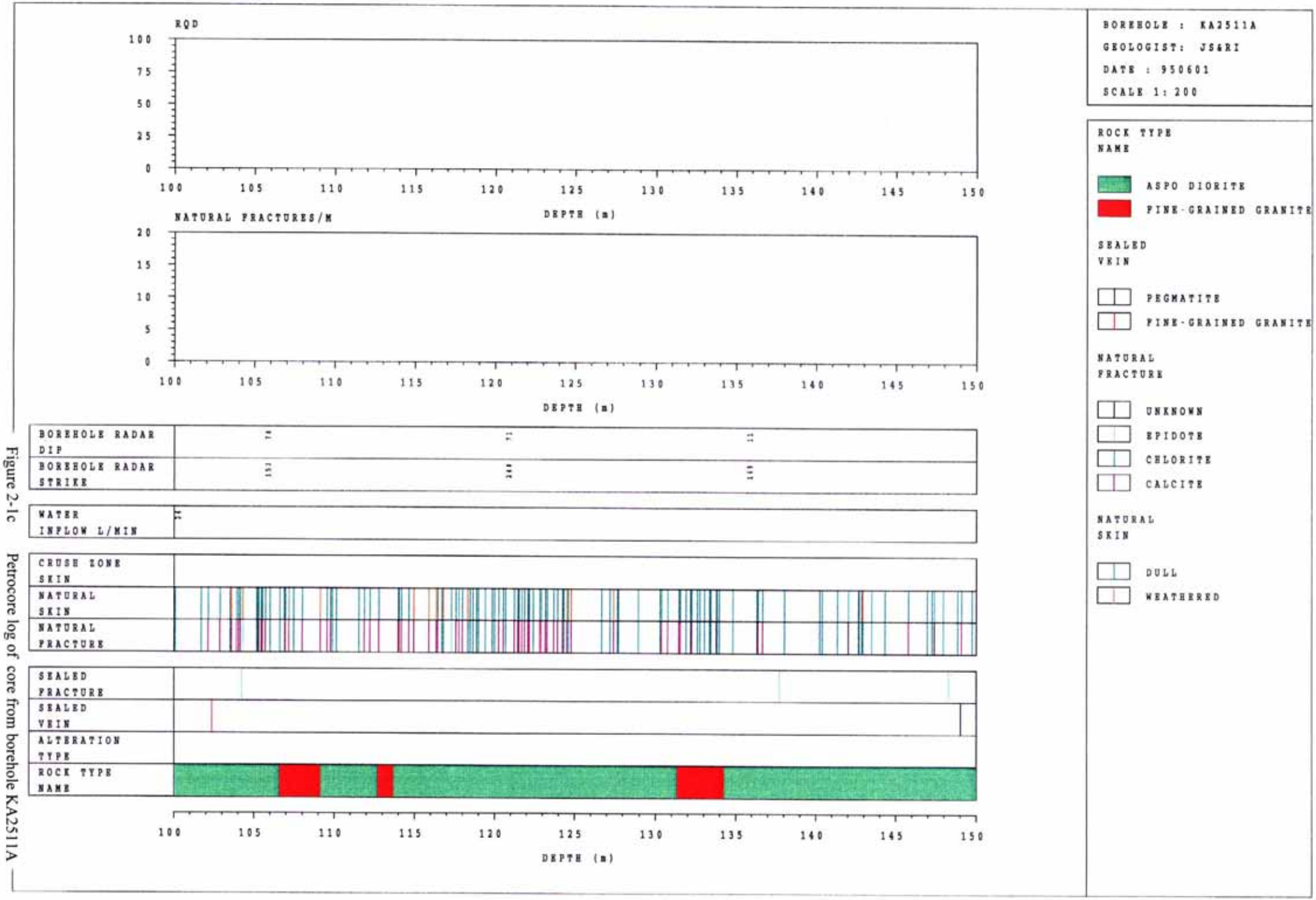

Figure 2-1c Petrocore log of core from borehole KA2511A

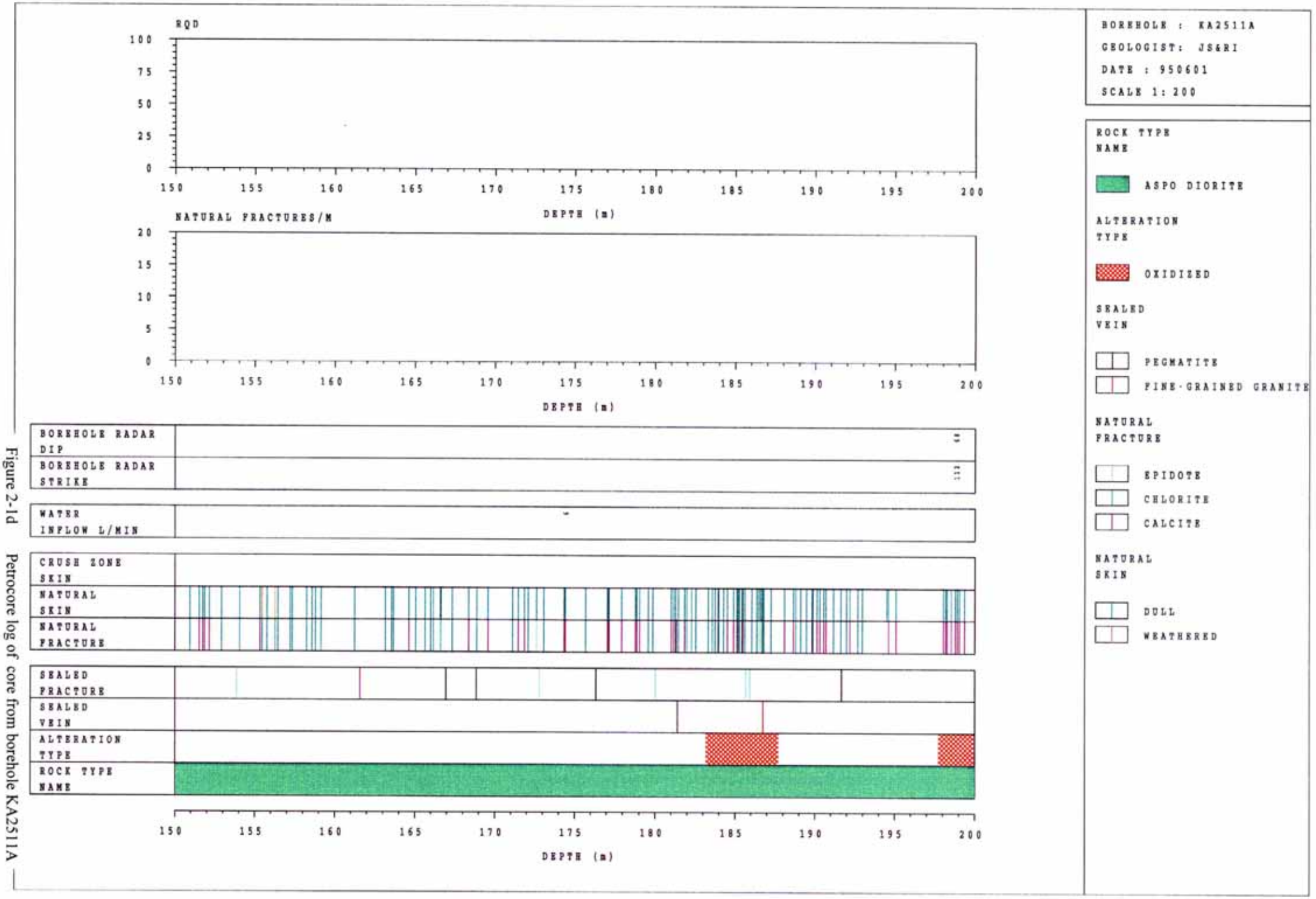

Figure 2-1d Petrocore log of core from borehole KA2511A

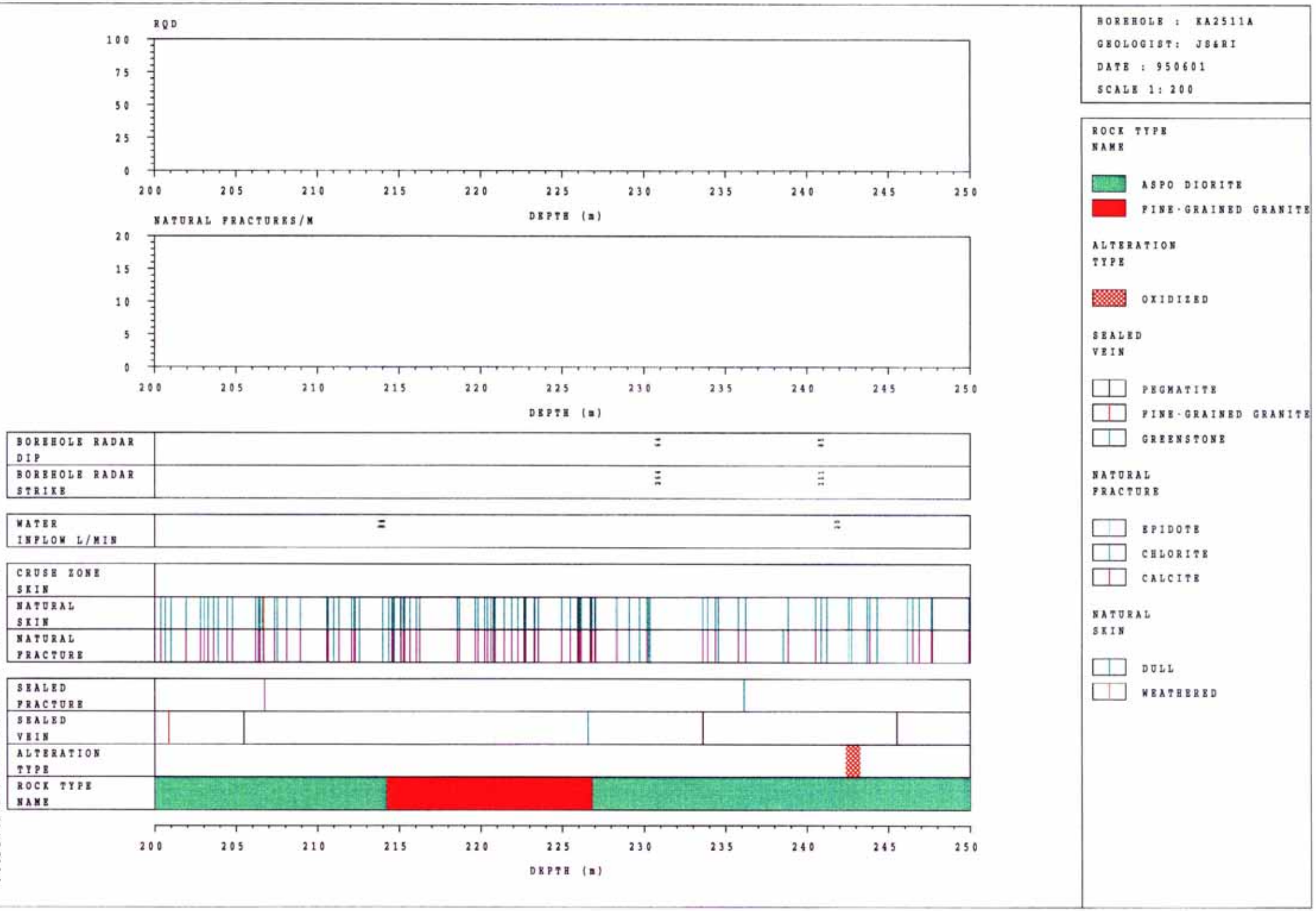

Figure 2-1c Petrocore log of core from borehole KA2511A

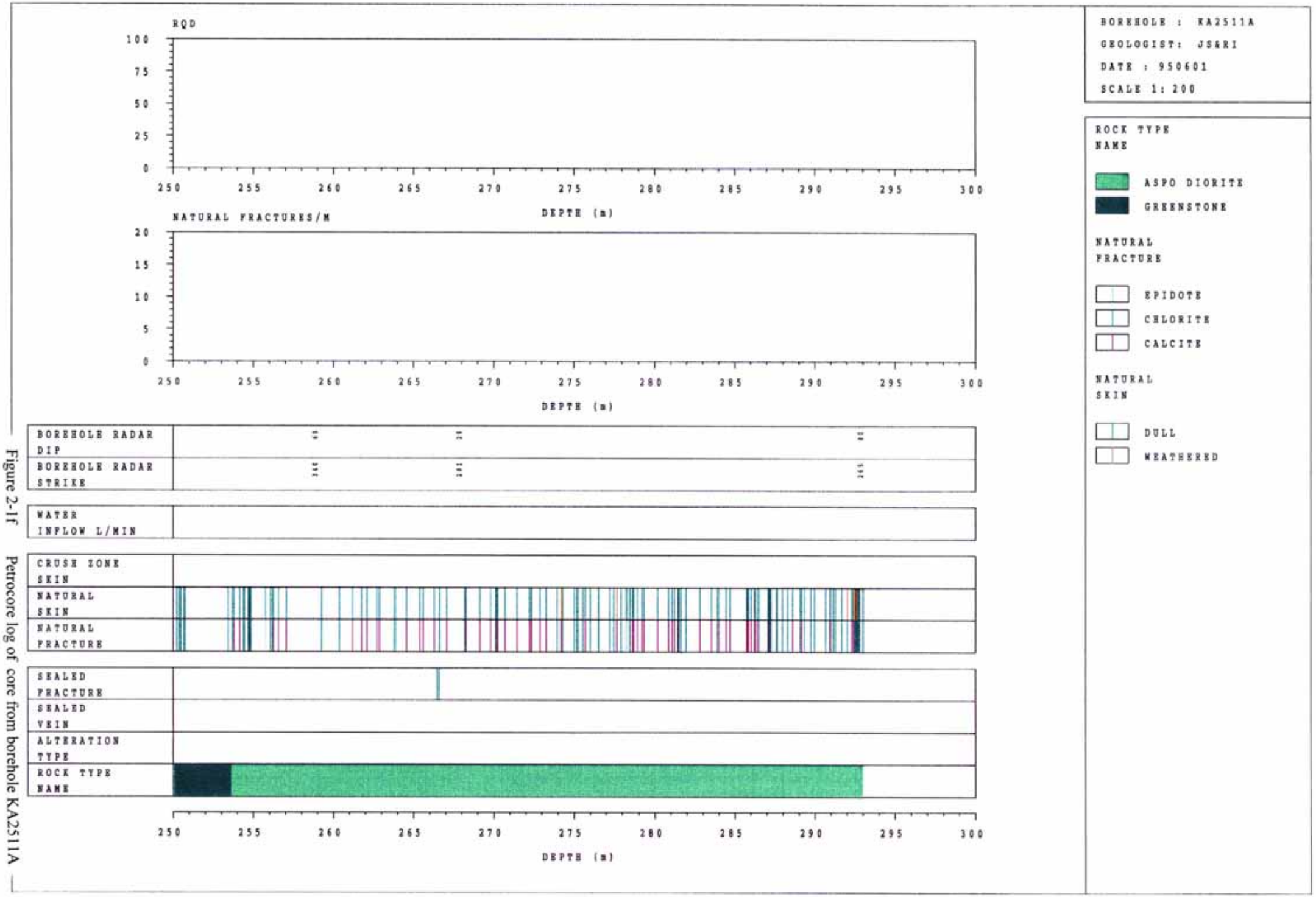

Figure 2-1f Petrocore log of core from borehole KA2511A

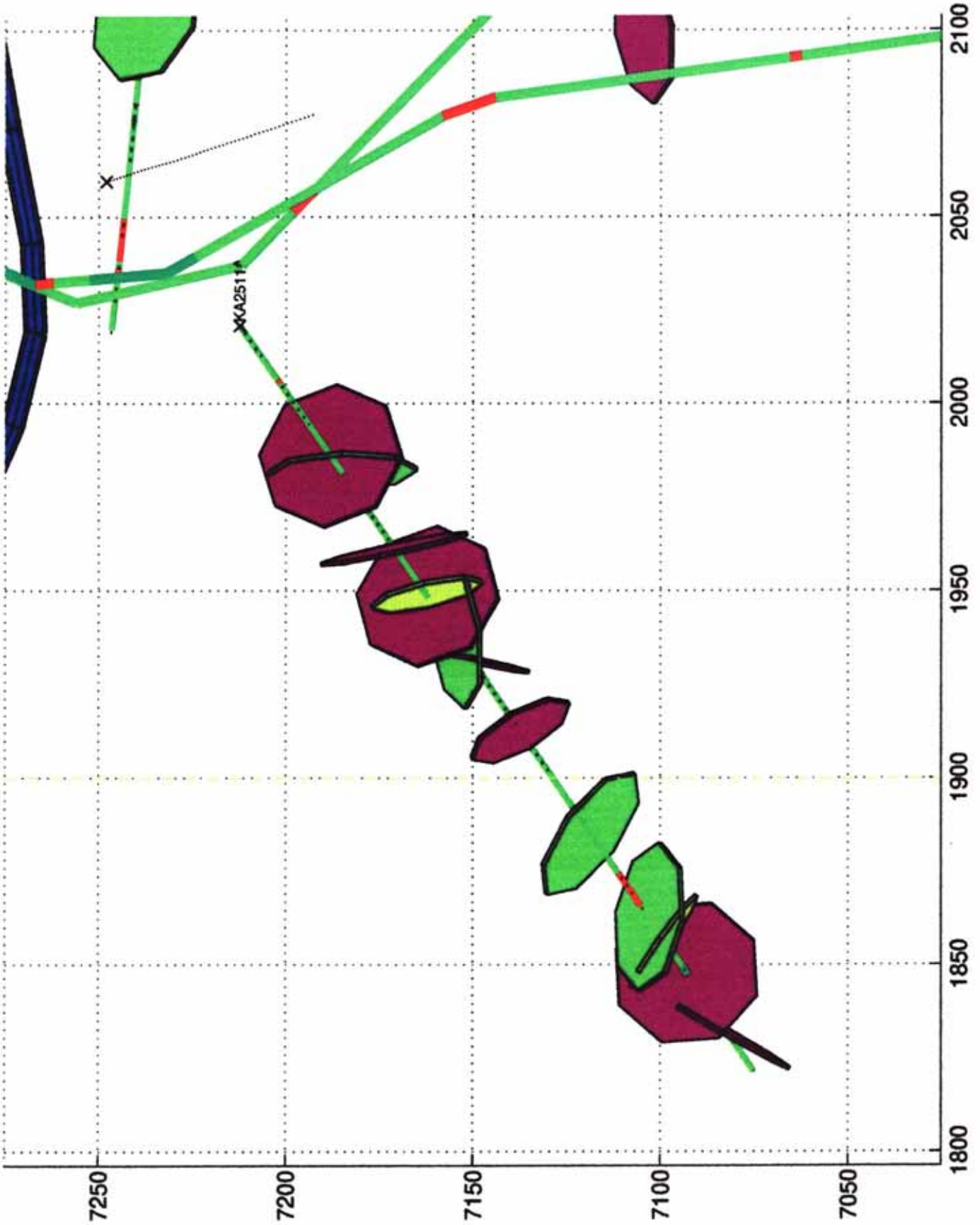

Figure 2-2 Radar (green) and seismic (purple) reflectors observed in borehole KA2511A (after Olsson et al., 1994)

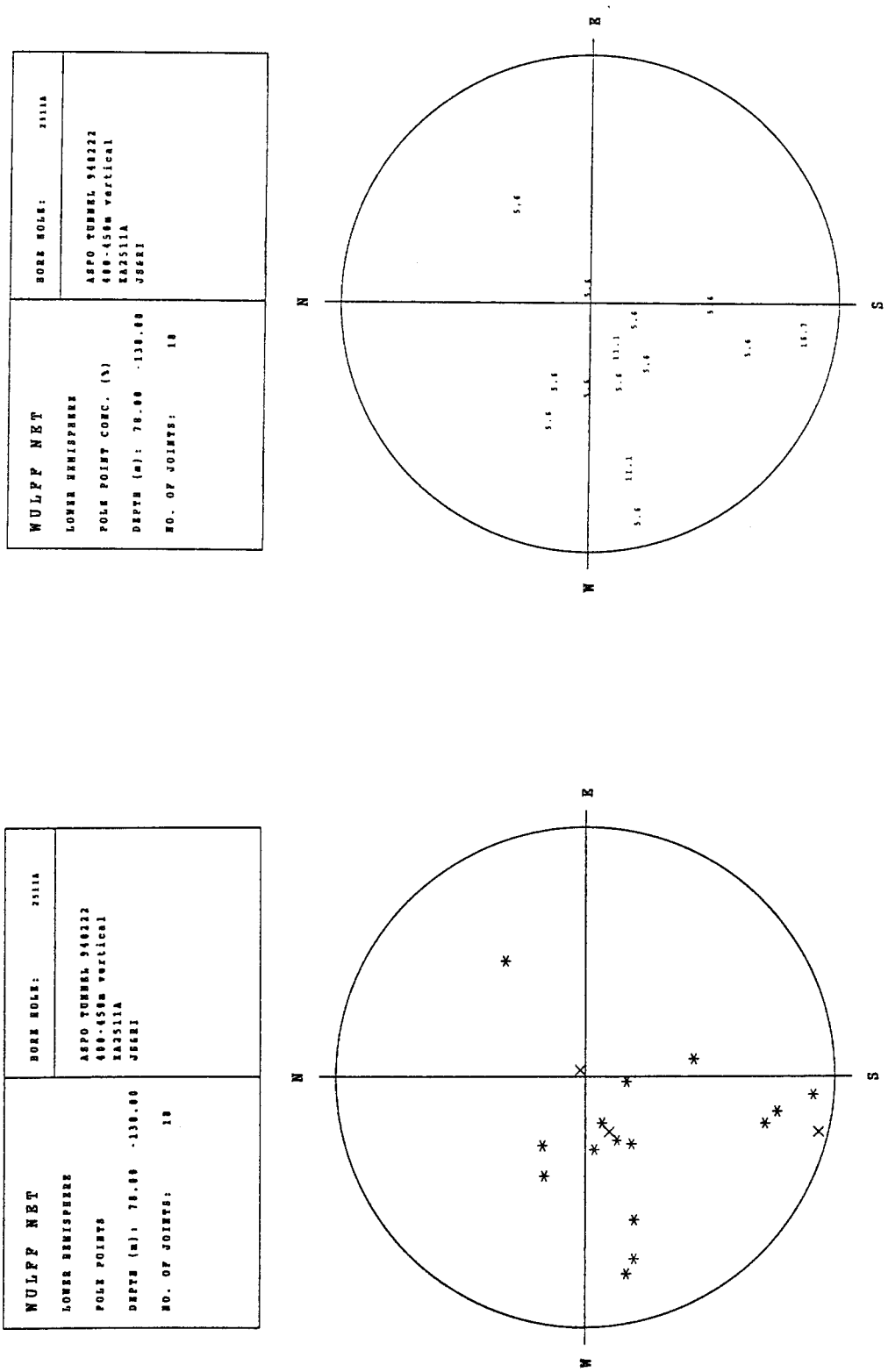

Figure 2-4 Fracture orientations in KA2511A, vertical depth 400-450m (after Olsson et al., 1994)

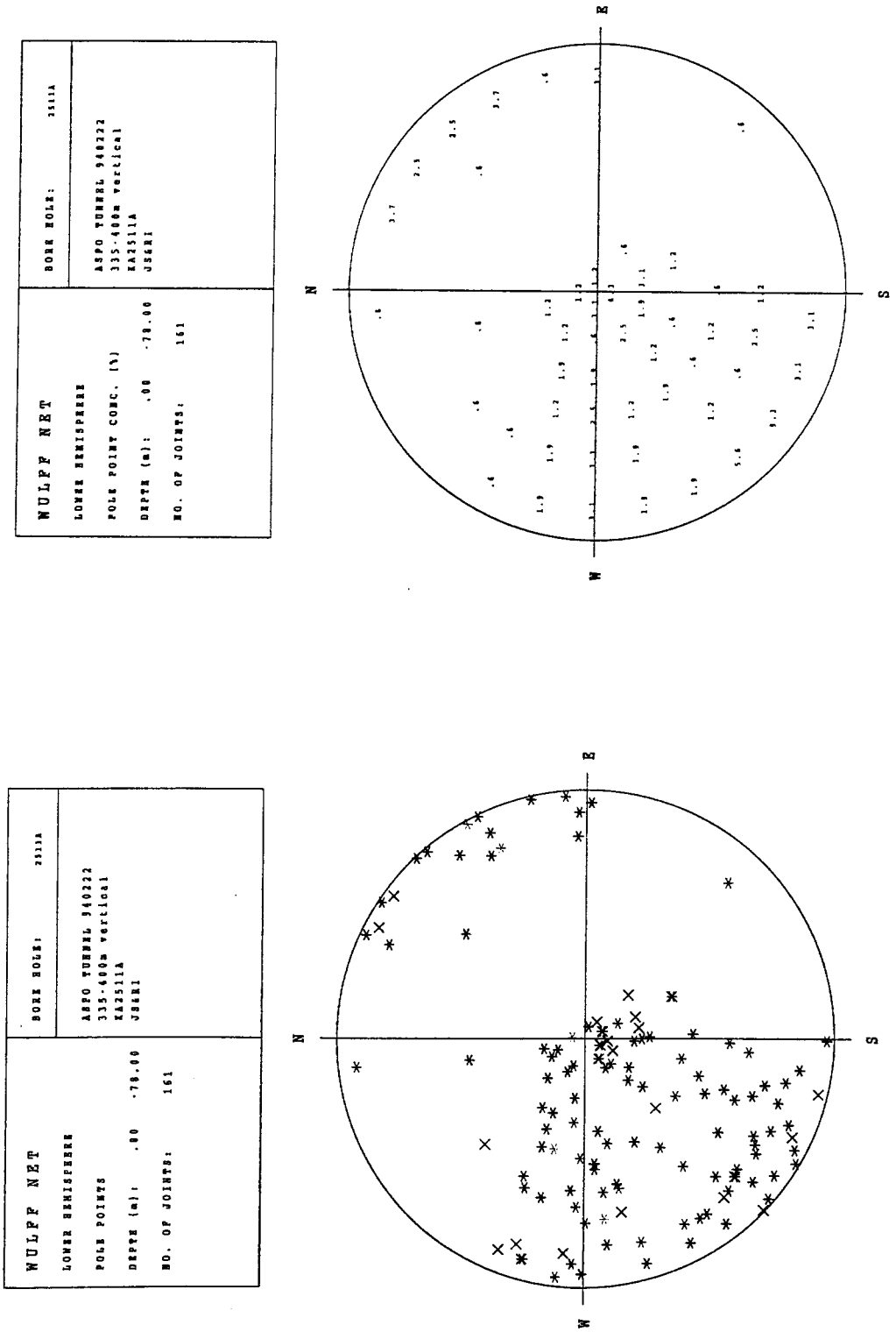

Figure 2-3 Fracture orientations in KA2511A, vertical depth 335-400m (after Olsson et al., 1994)

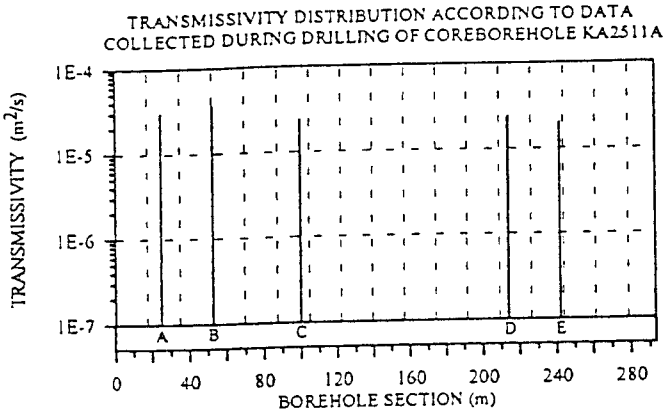

Figure 2-5 Transmissivity distribution in KA2511A from inflow measurements during drilling (after Olsson et al., 1994)

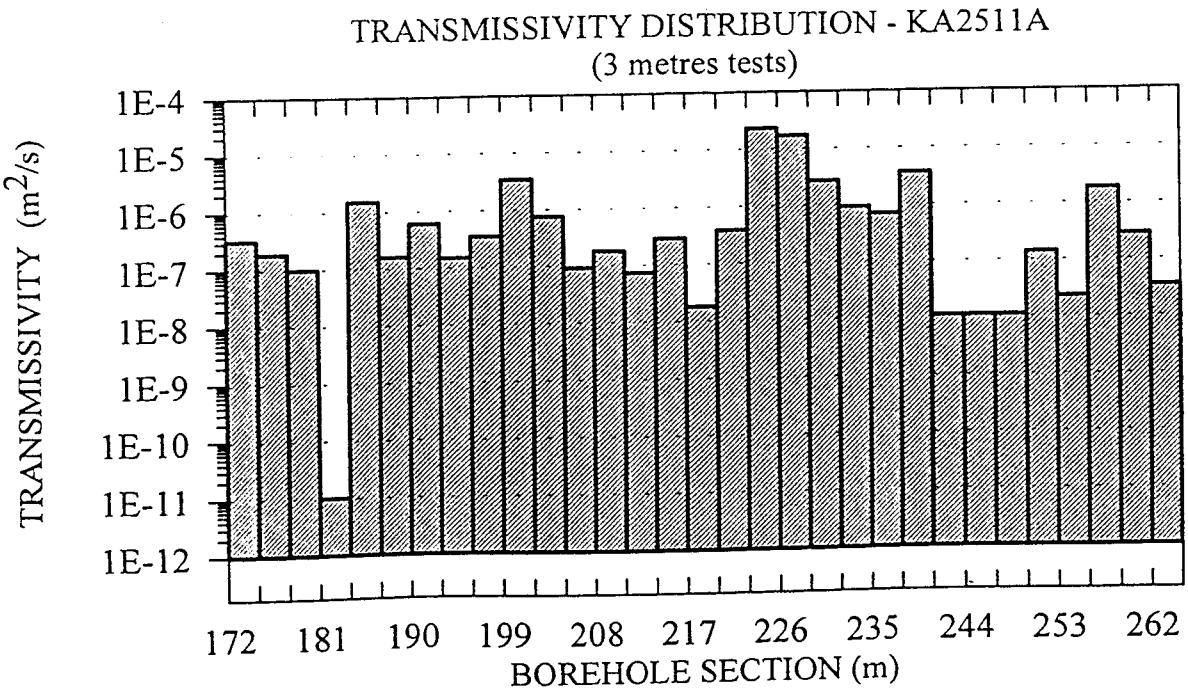

Figure 2-6 Transmissivity distribution in KA2511A from 3m packer tests, section L=172-265m (after Olsson et al., 1994)

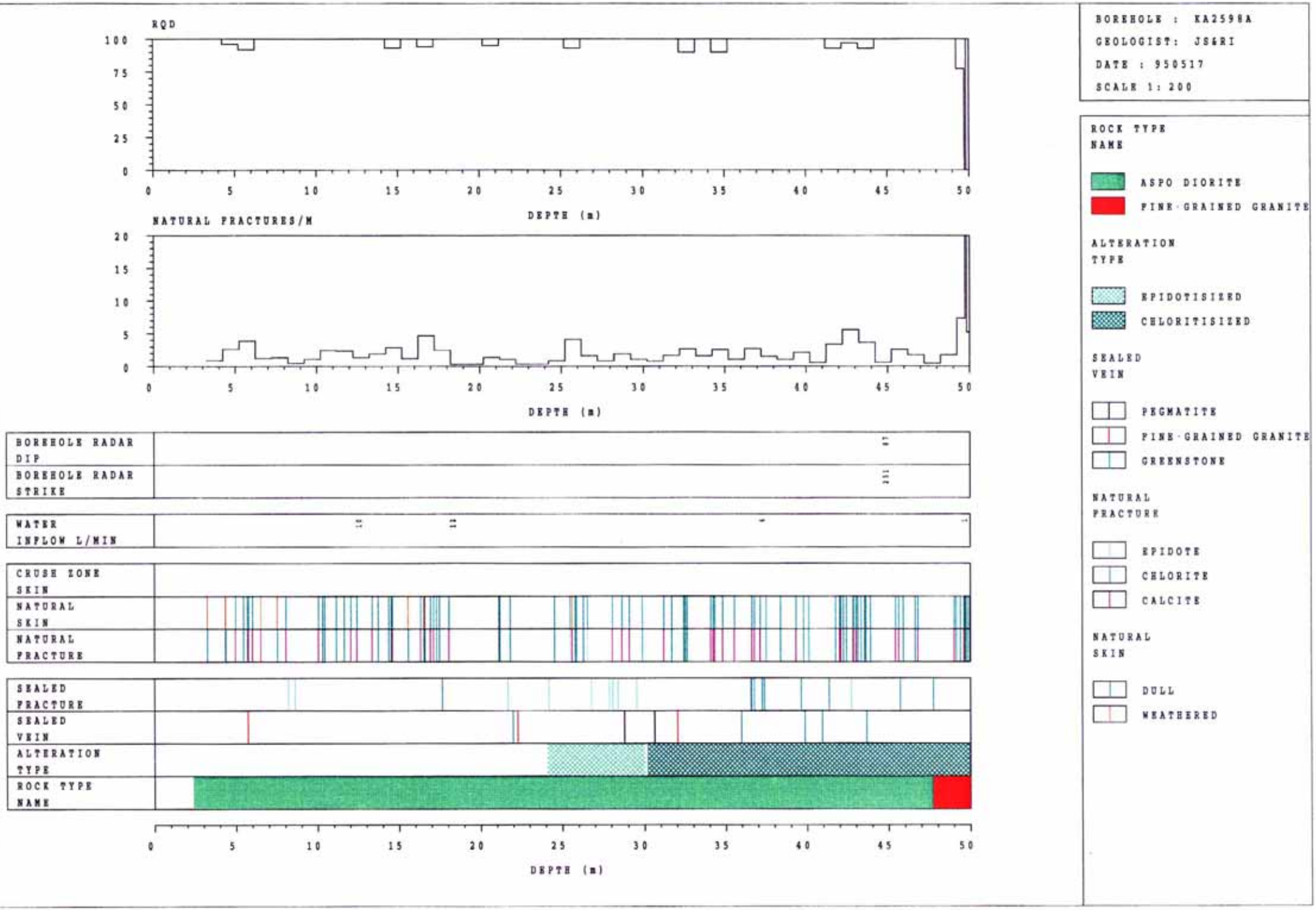

Figure 2-7a Petrocore log of core from borehole KA2598A

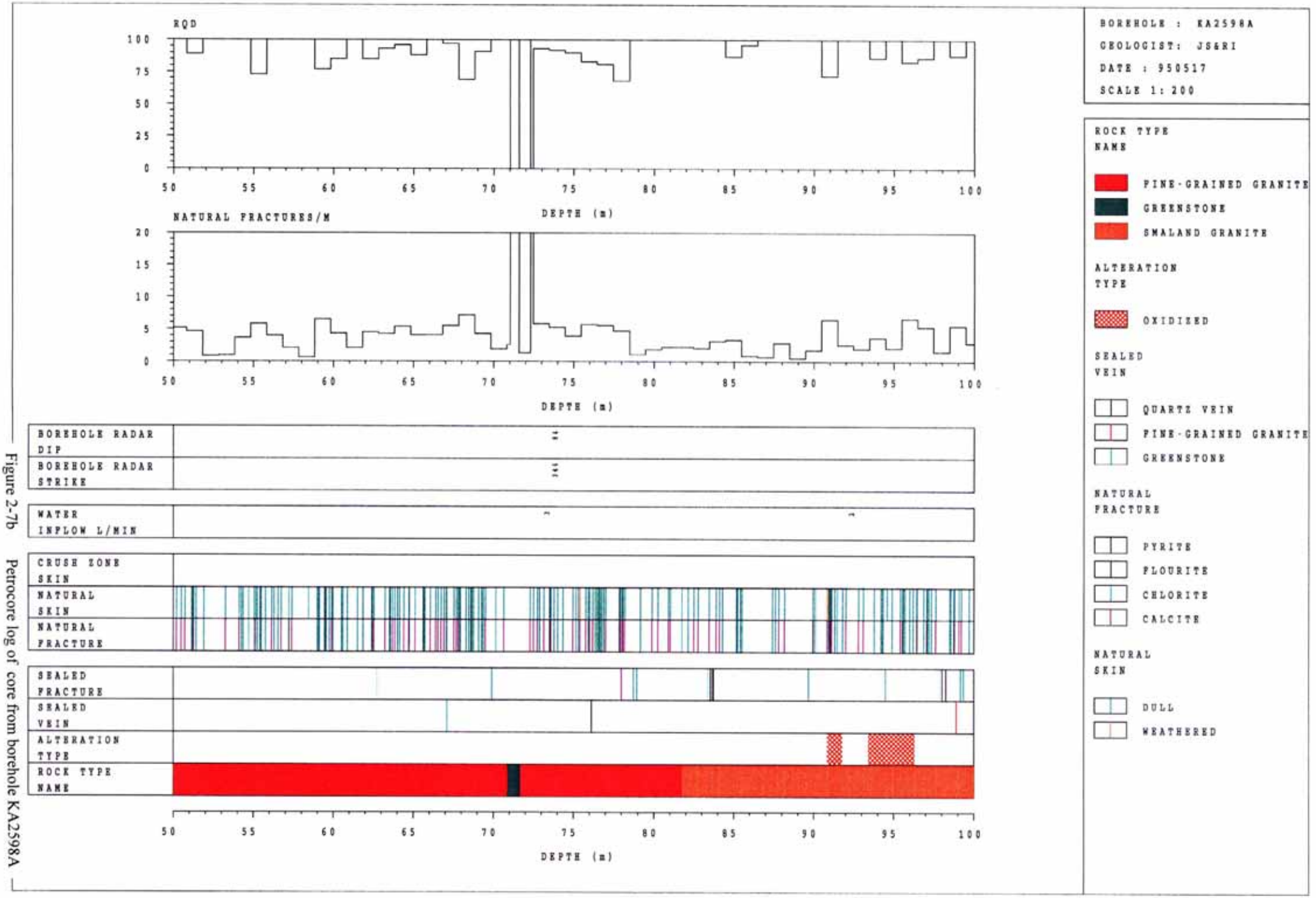

Figure 2-7b Petrocore log of core from borehole KA2598A

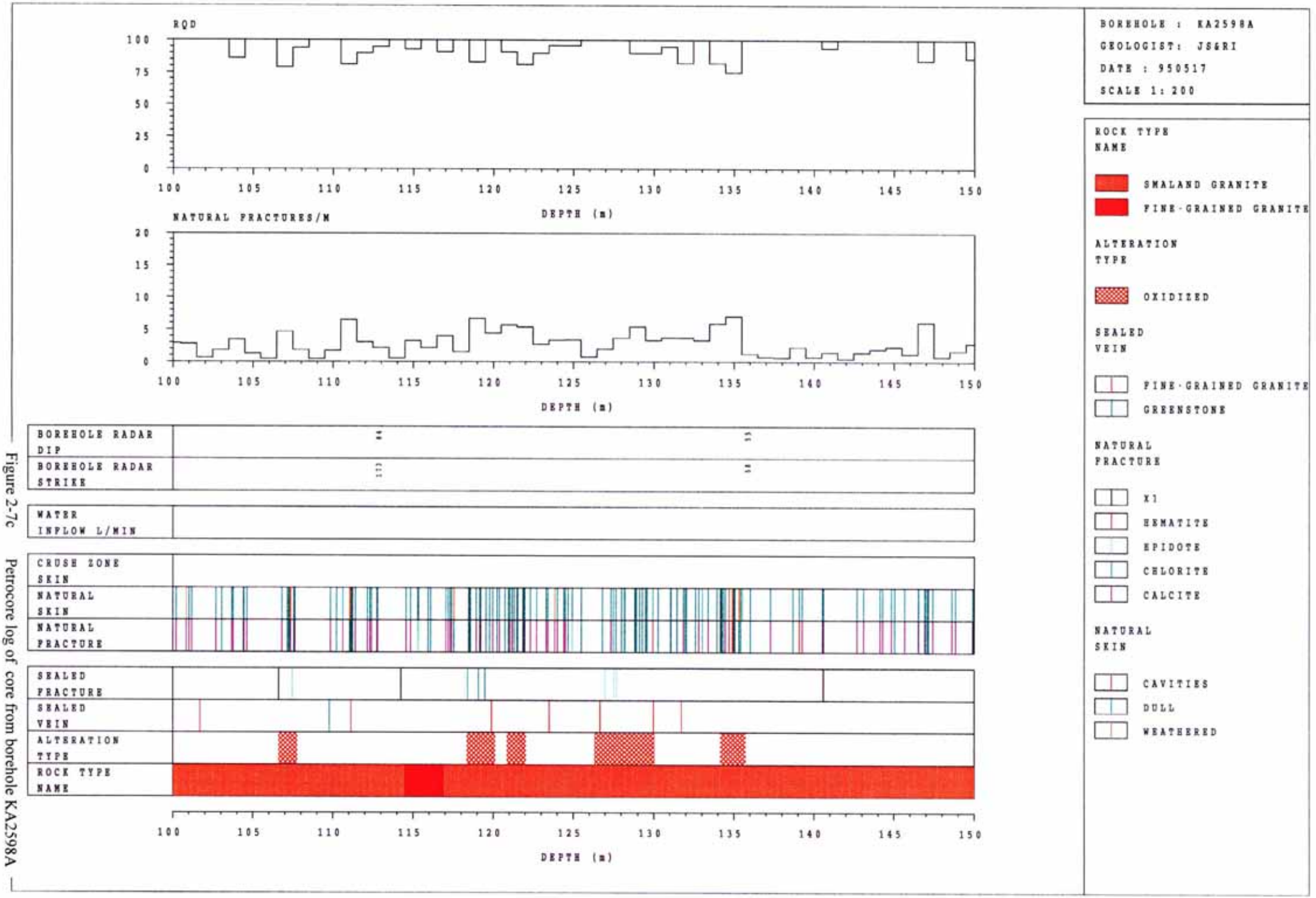

Figure 2-7c Petrocore log of core from borehole KA2598A

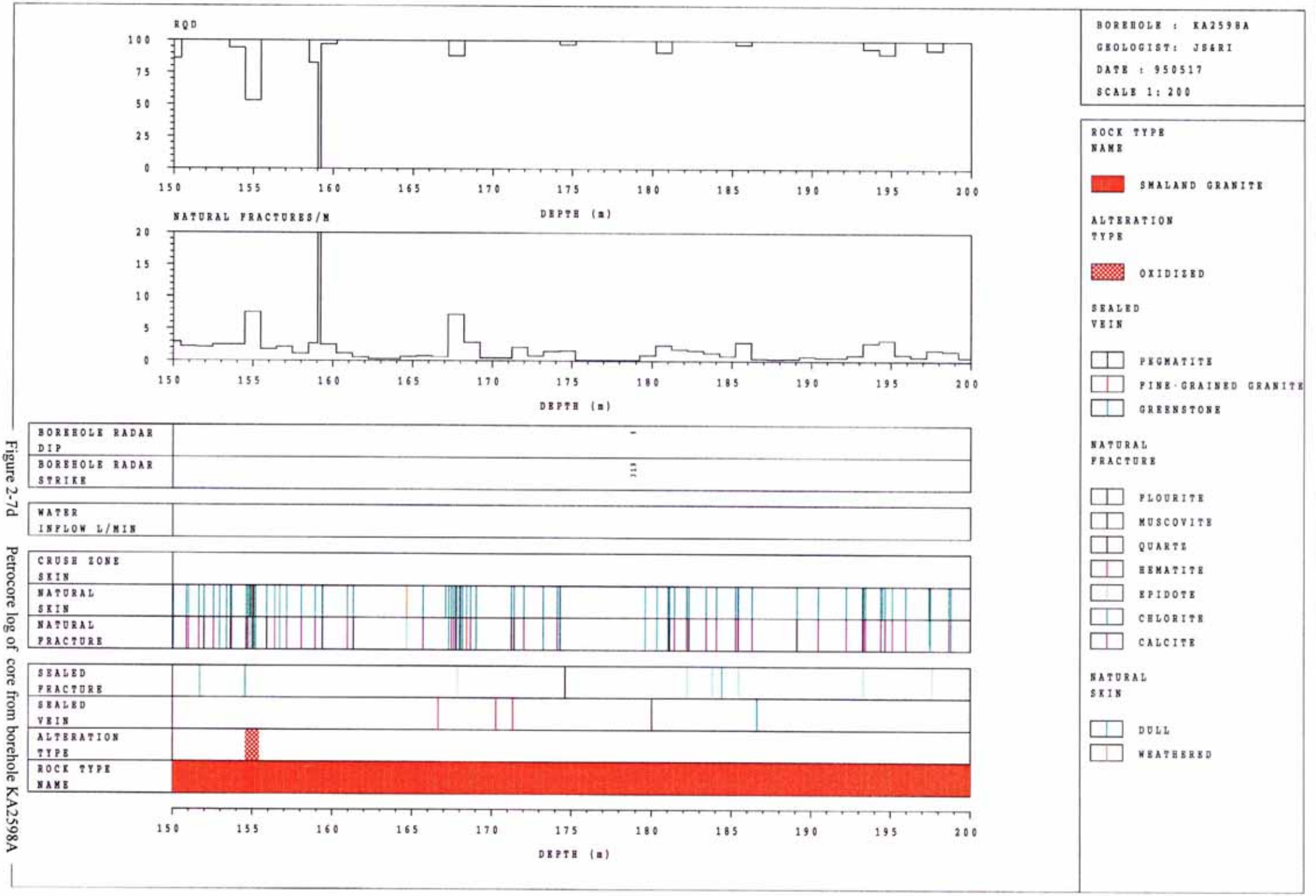

Figure 2-7d Petrocore log of core from borehole KA2598A

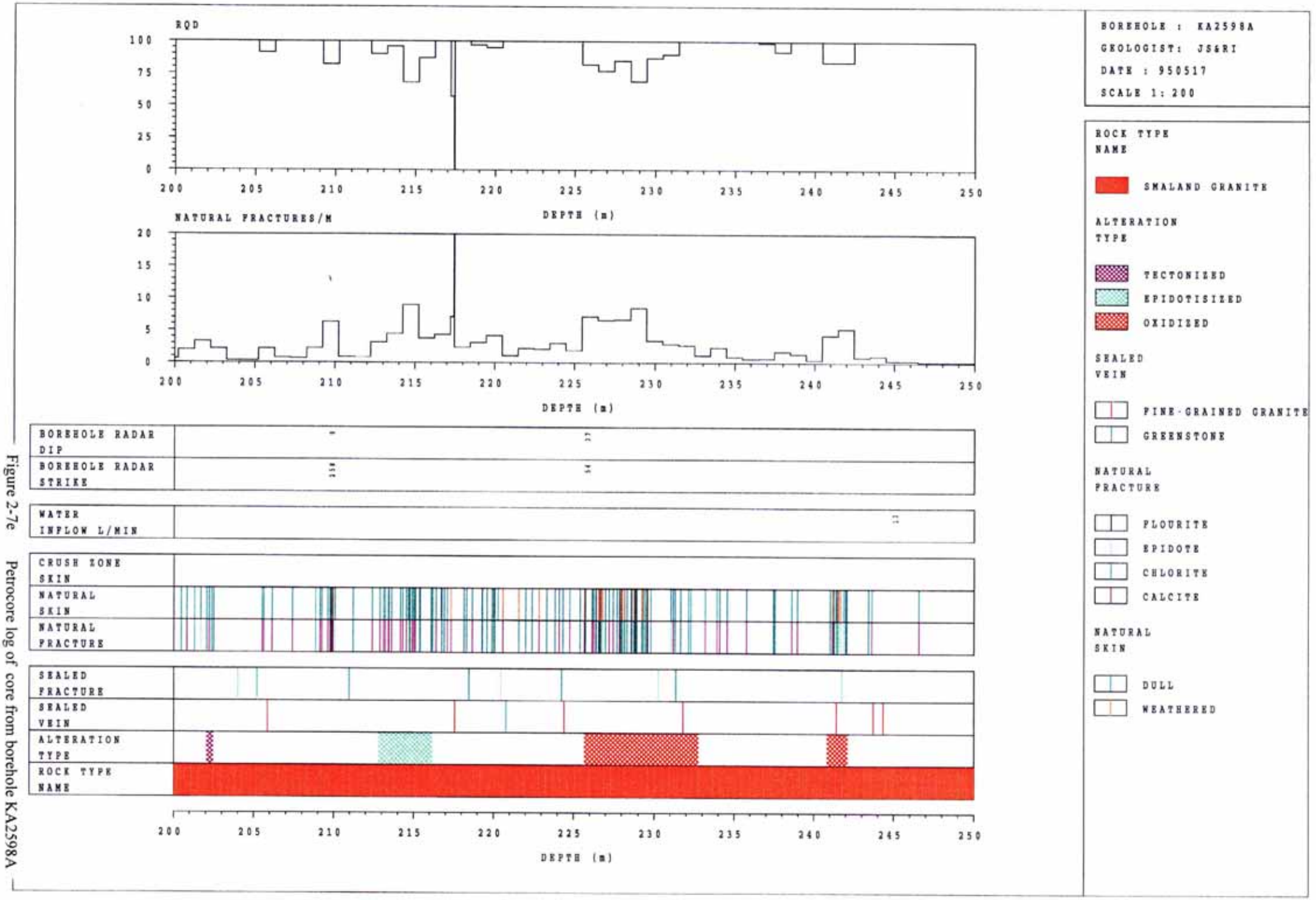

Figure 2-7e Petrocore log of core from borehole KA2598A

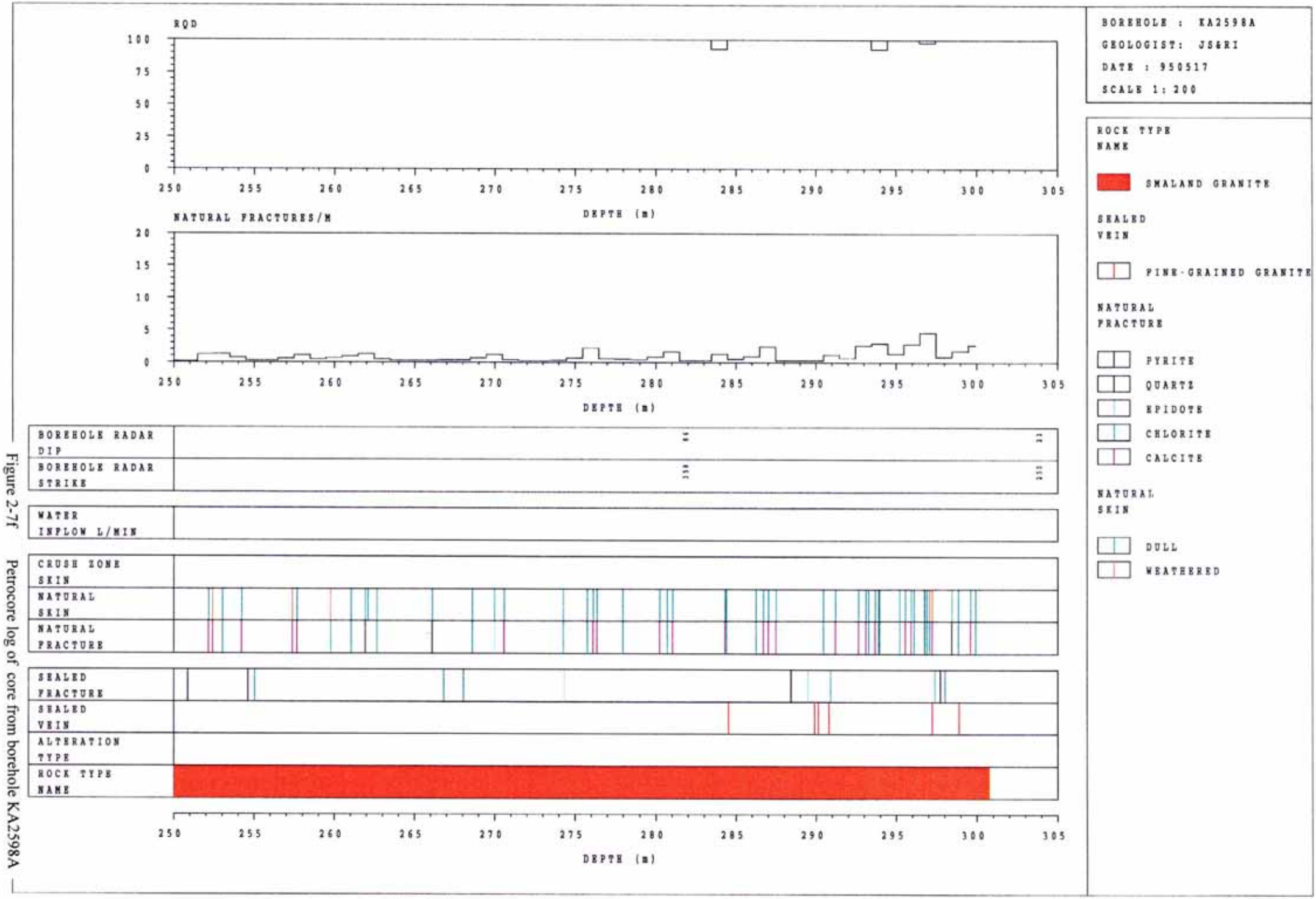

Figure 2-7f Petrocore log of core from borehole KA2598A

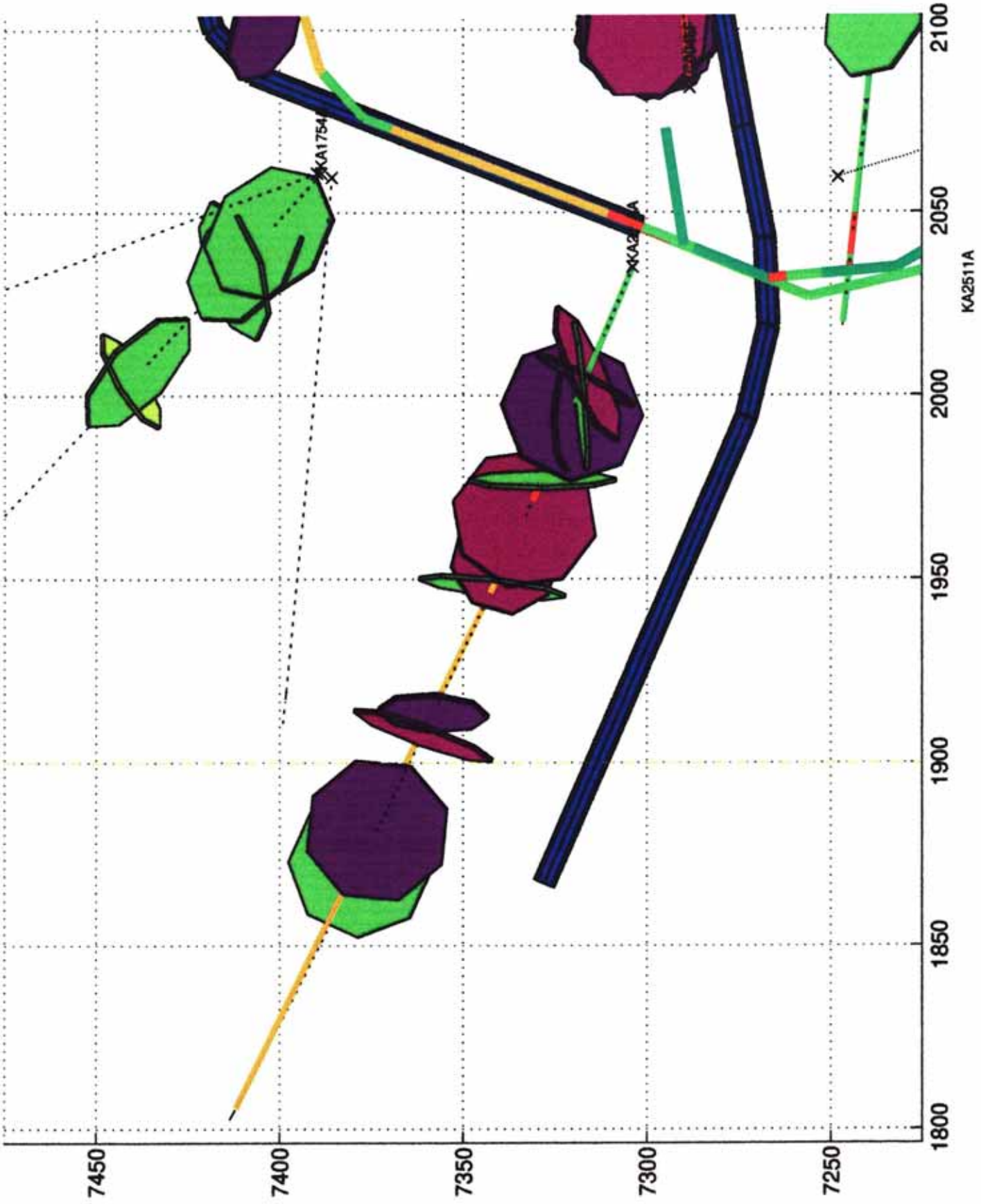

Figure 2-8 Radar (green) and seismic (purple) reflectors observed in borehole KA2598A (after Olsson et al., 1994)

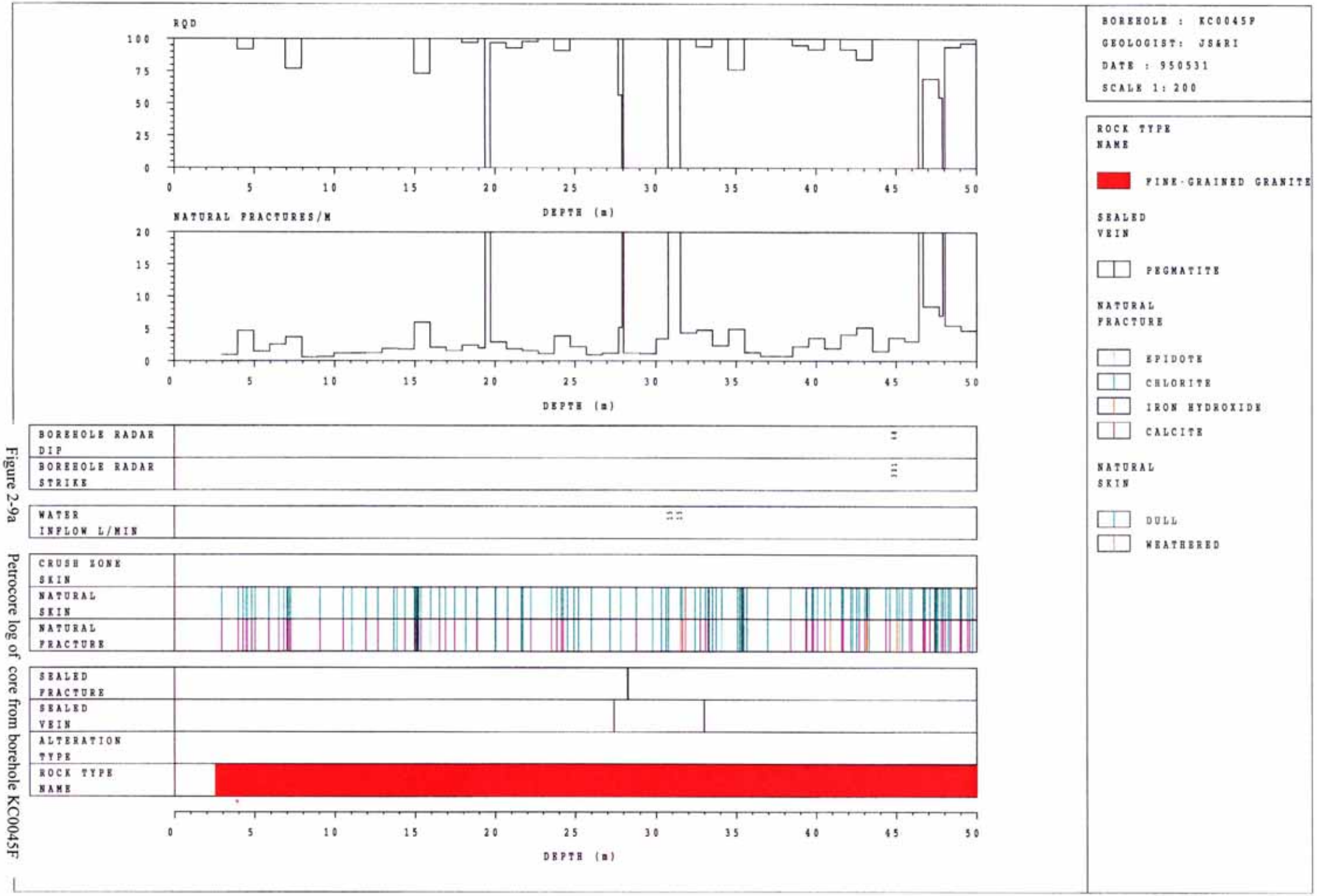

Figure 2-9a Petrocore log of core from borehole KC0045F

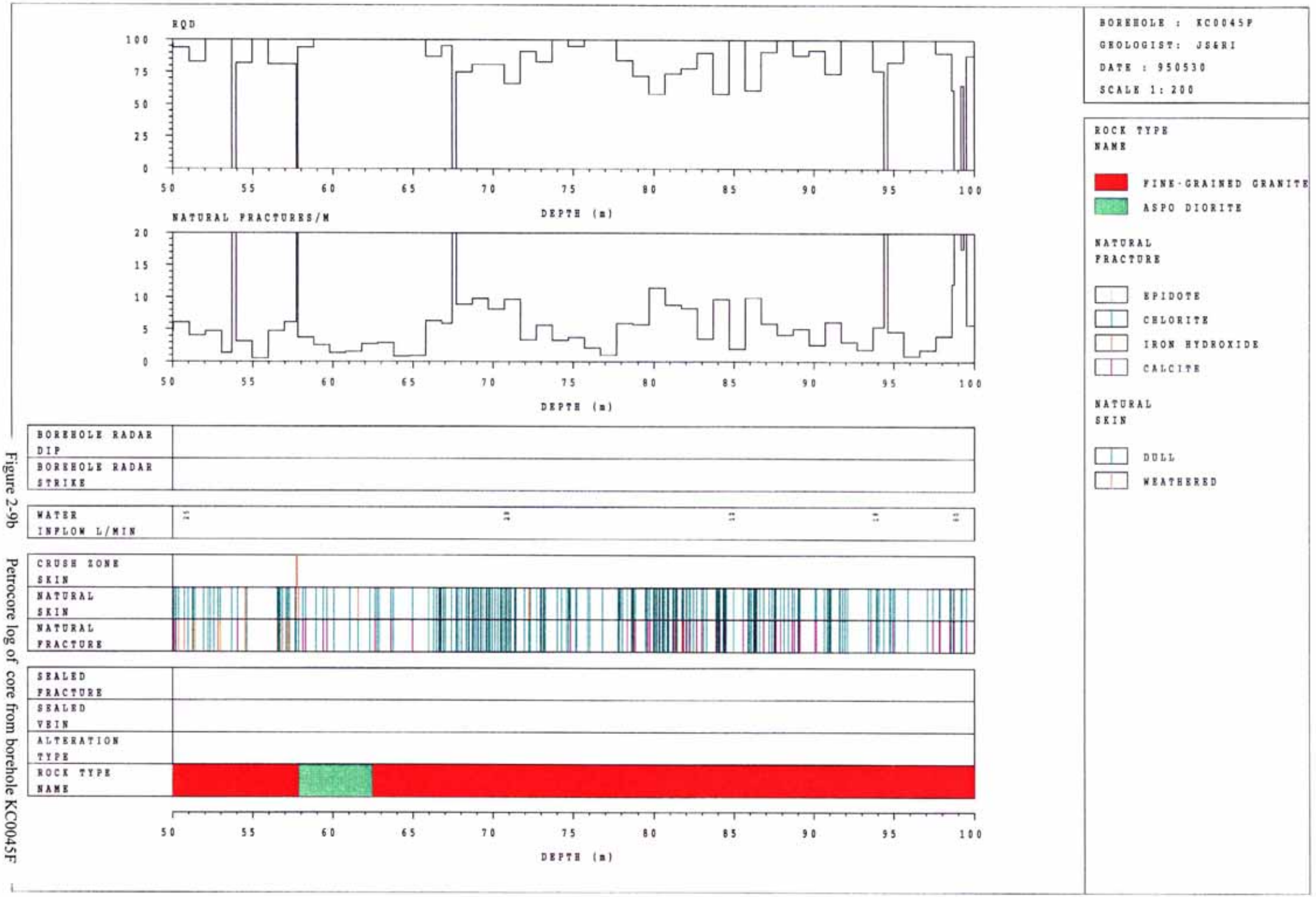

Figure 2-9b Petrocore log of core from borehole KC0045F

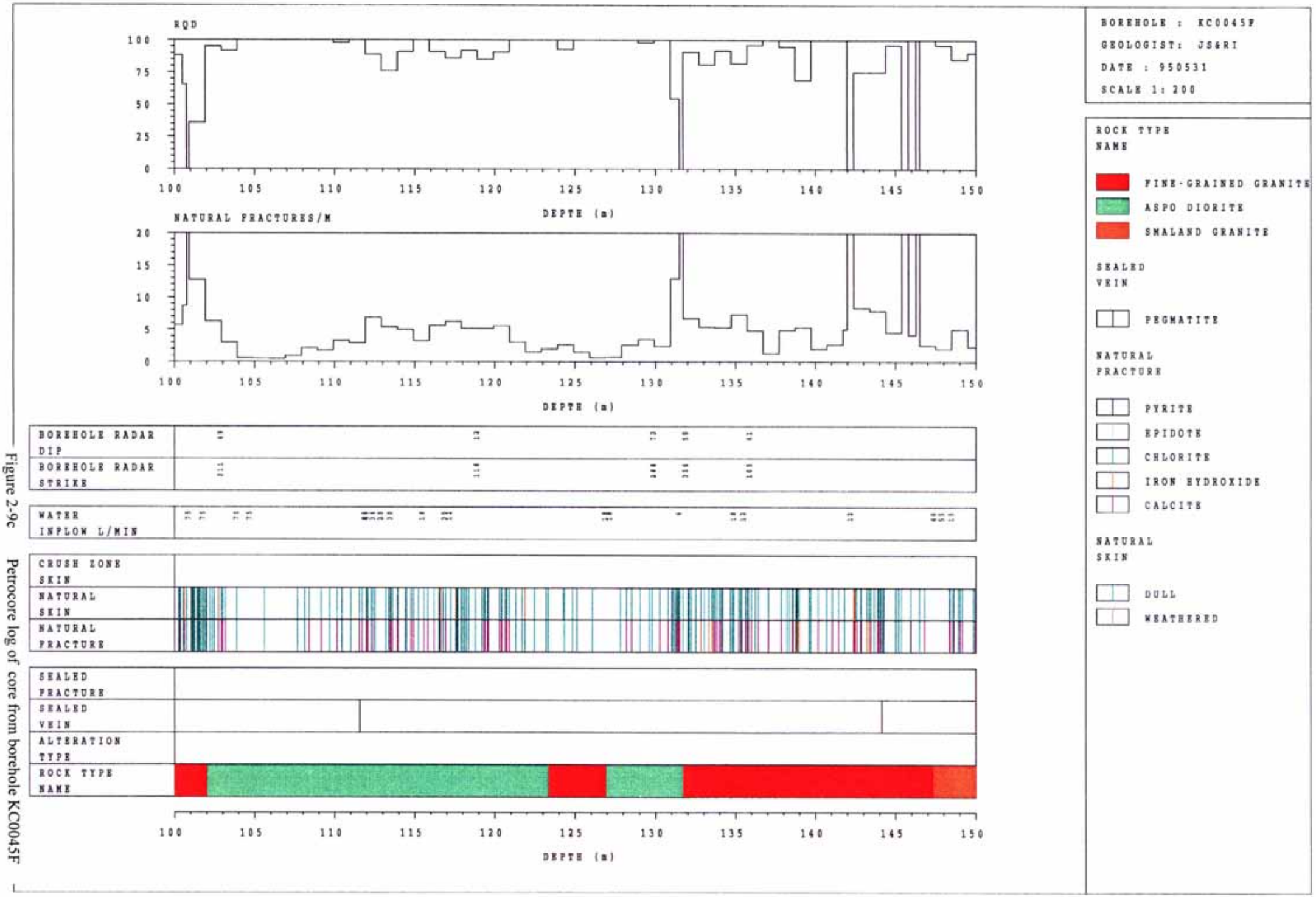

Figure 2-9c Petrocore log of core from borehole KC0045F

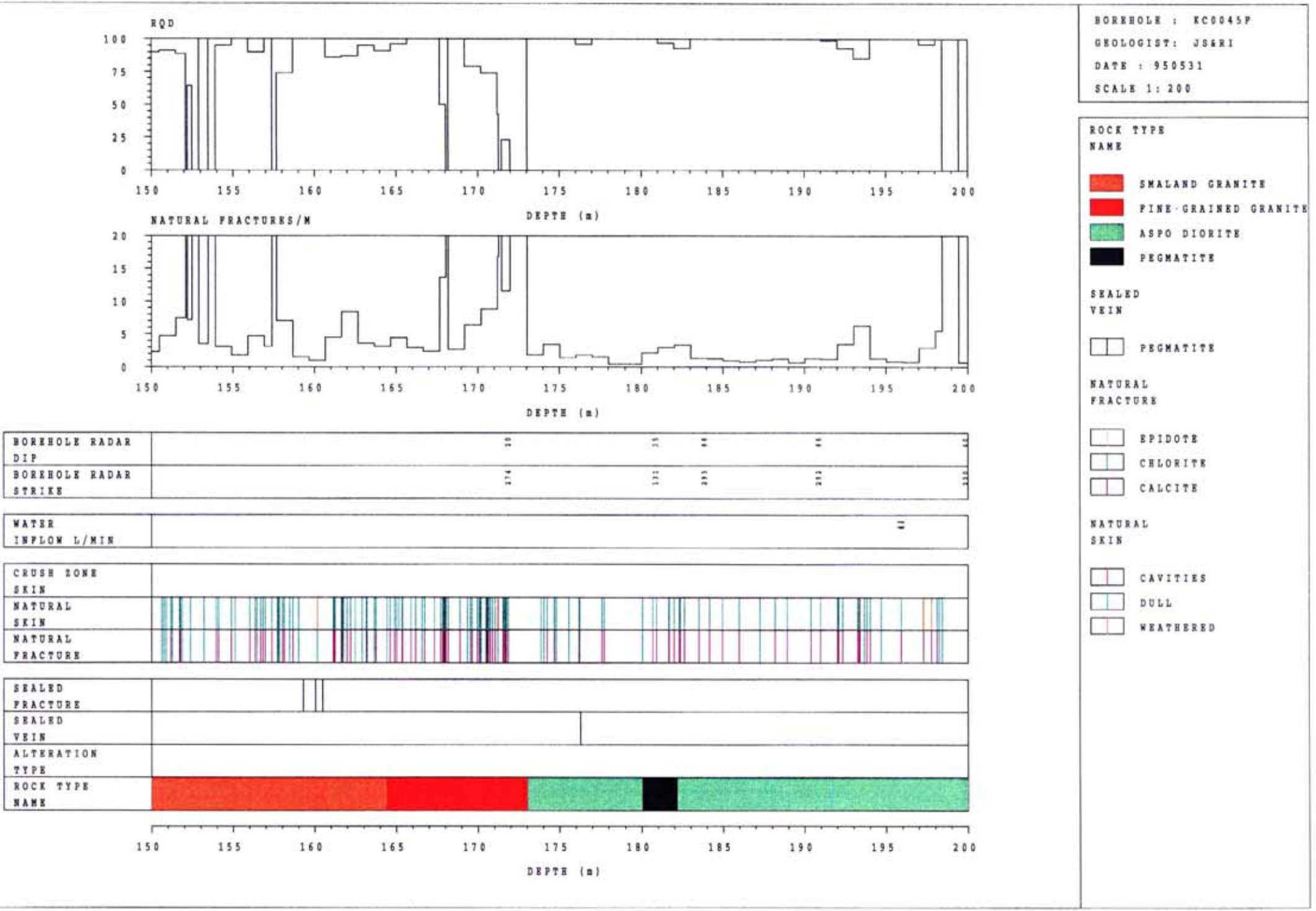

Figure 2-9d Petrocore log of core from borehole KC0045F

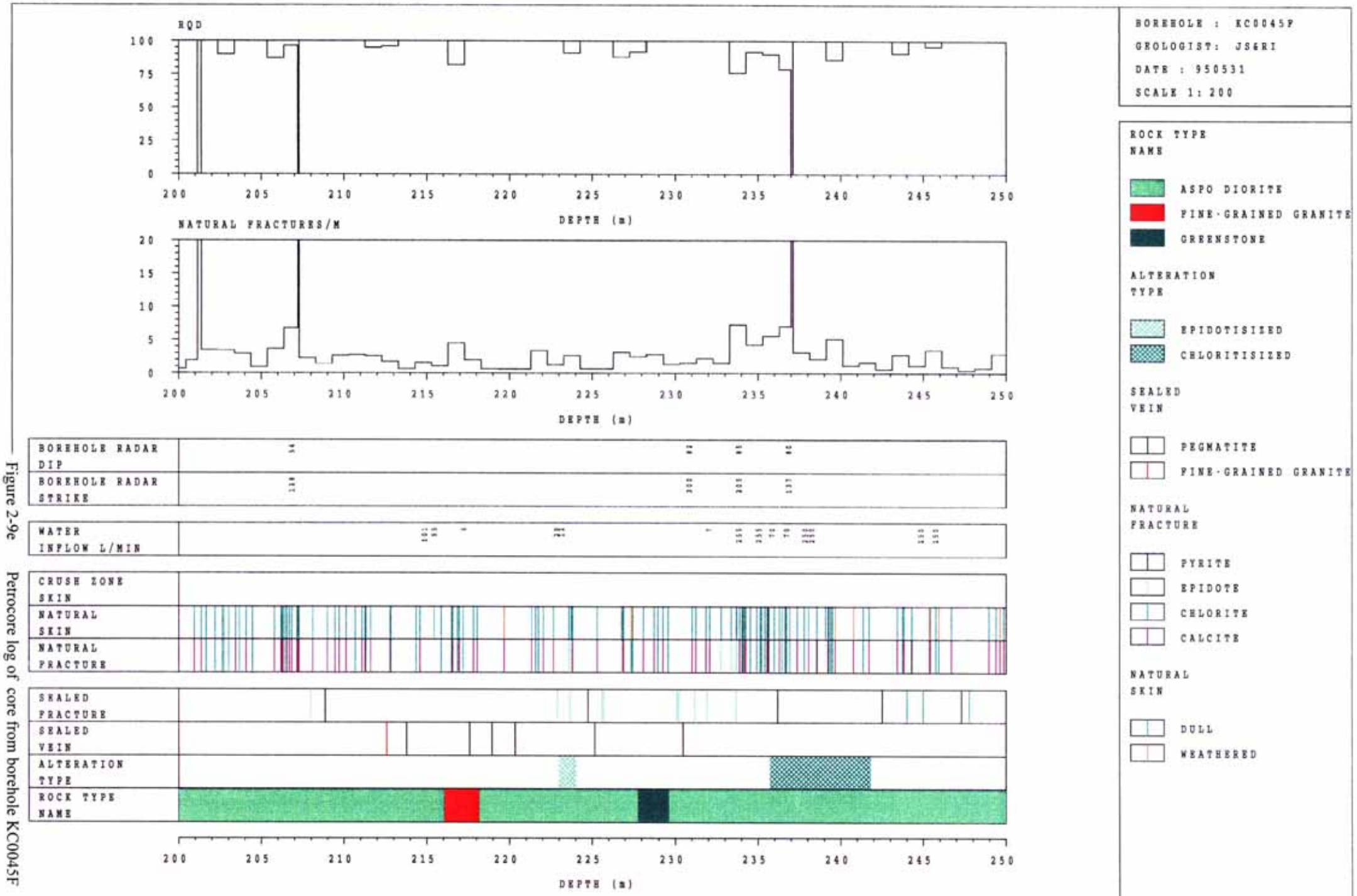

Figure 2-9e Petrocore log of core from borehole KC0045F

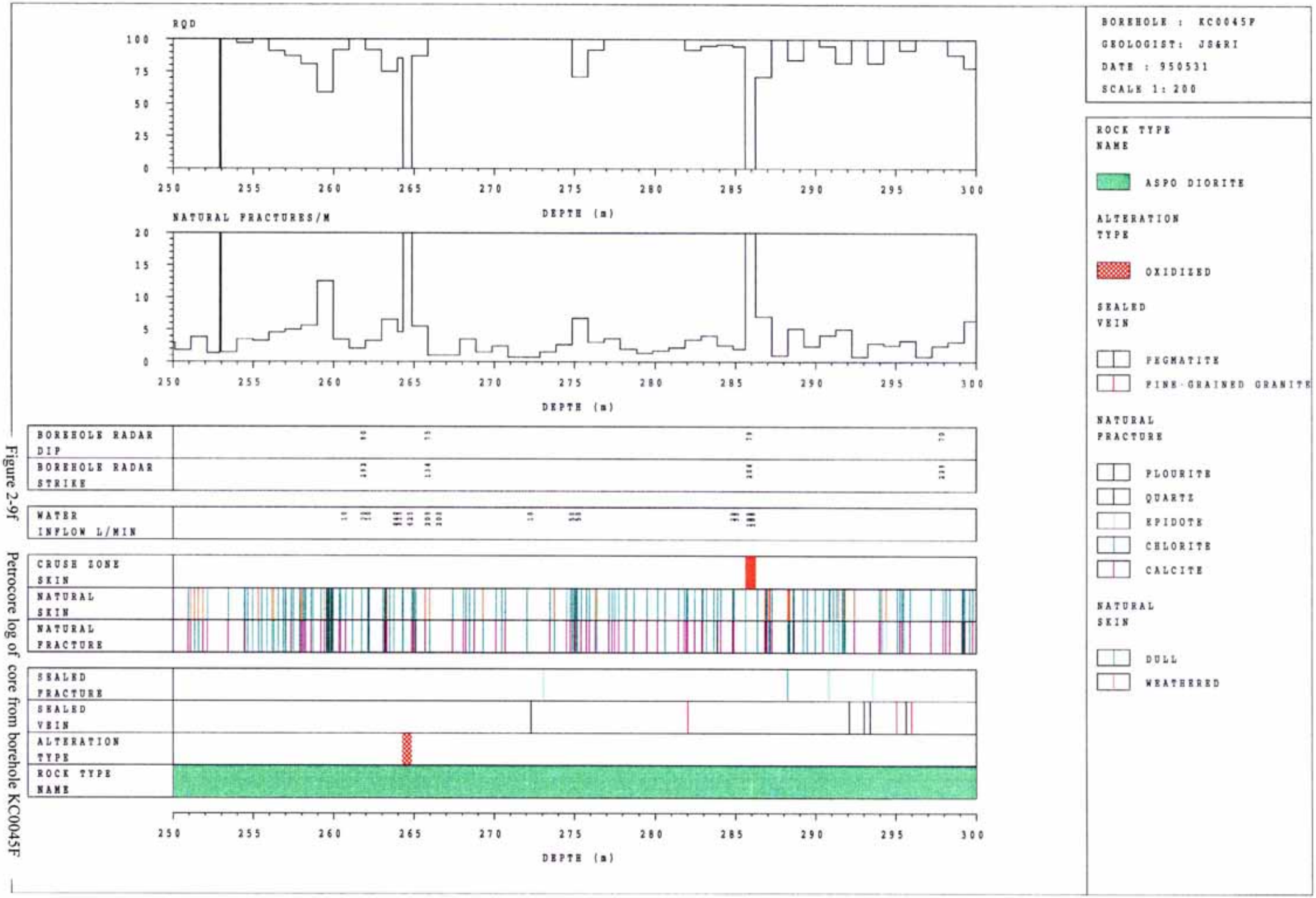

Figure 2-9f Petrocore log of core from borehole KC0045F

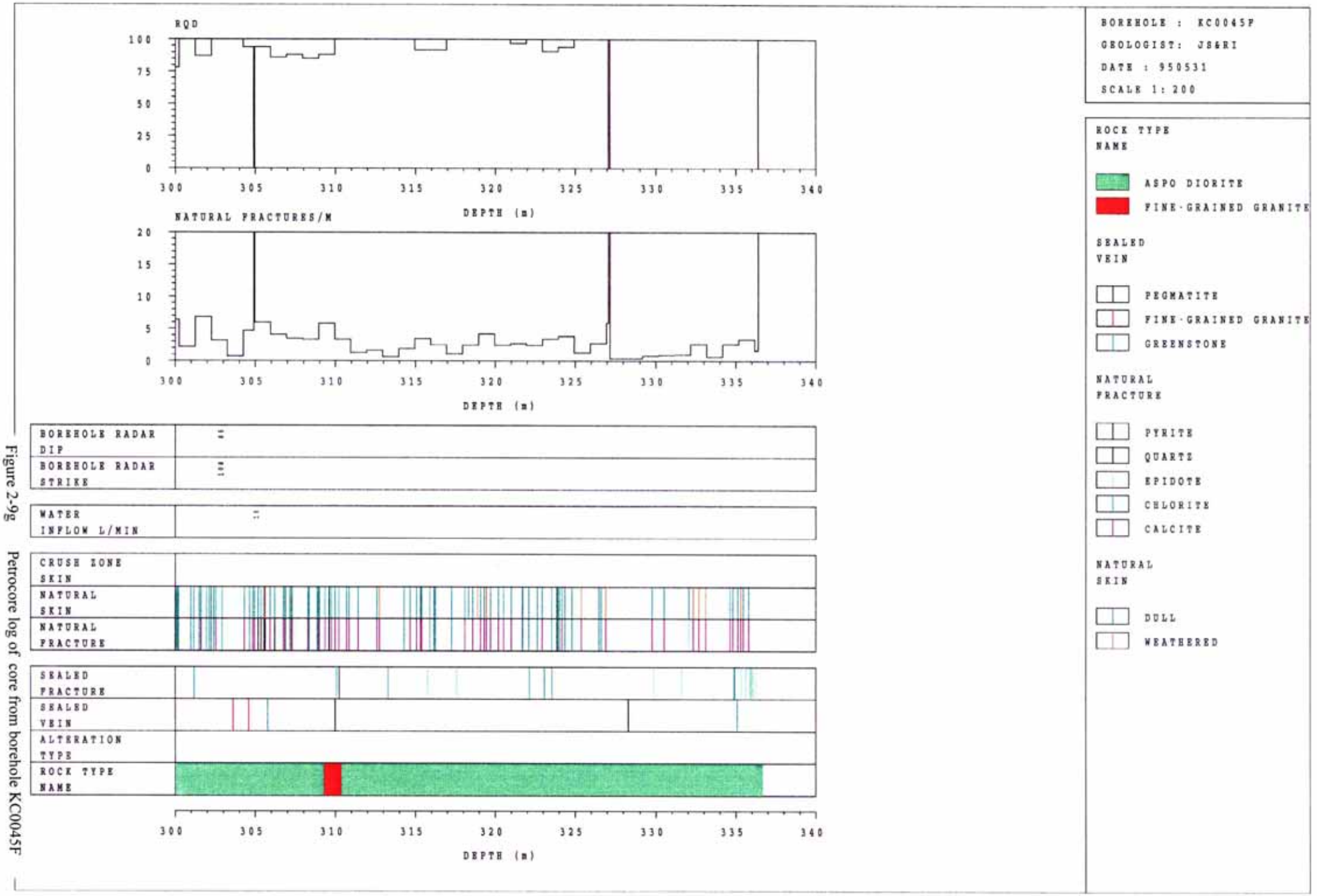

Figure 2-9g Petrocore log of core from borehole KC0045F

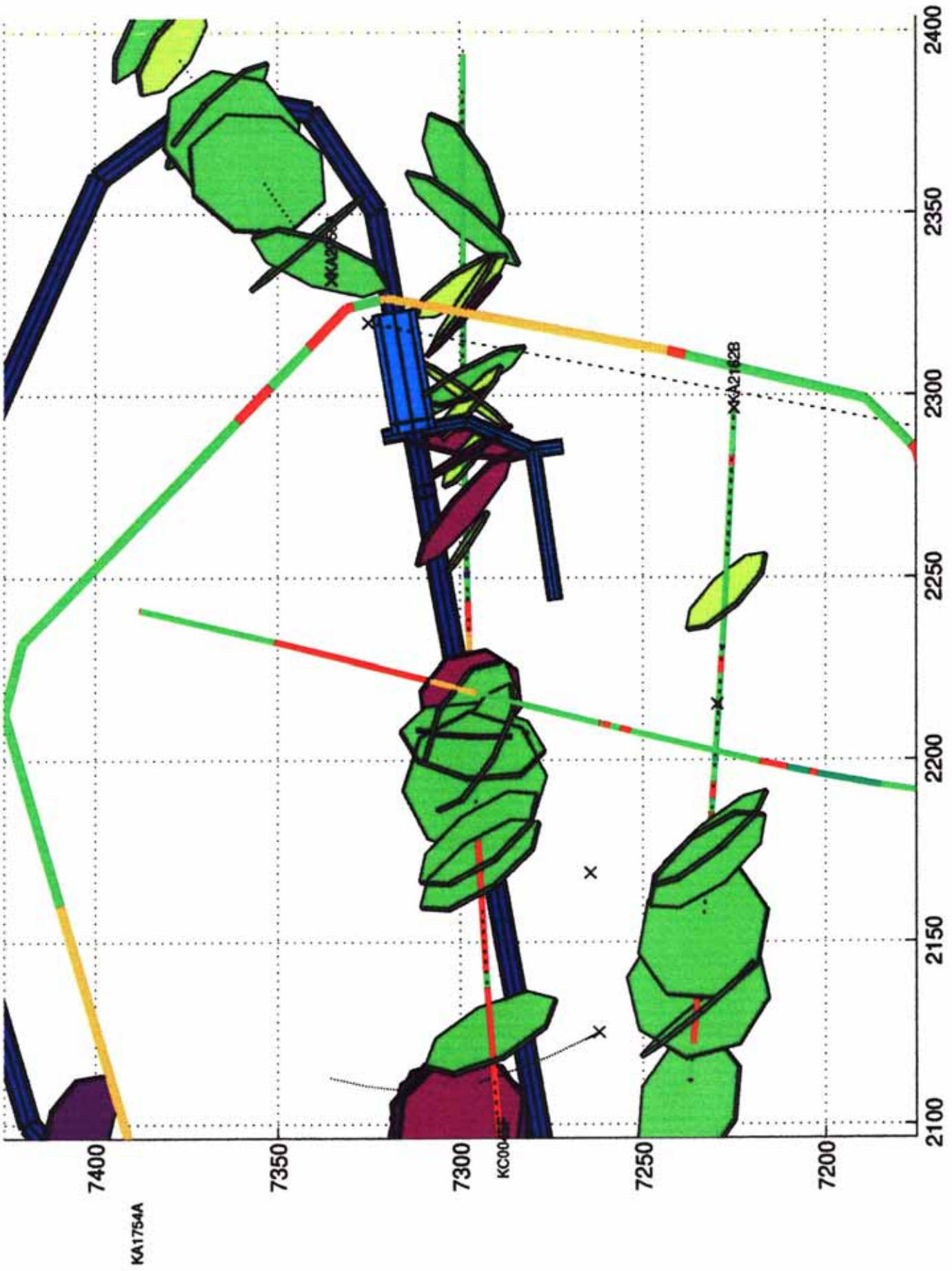

Figure 2-10 Radar (green) and seismic (purple) reflectors observed in borehole KC0045FA (after Olsson et al., 1994)

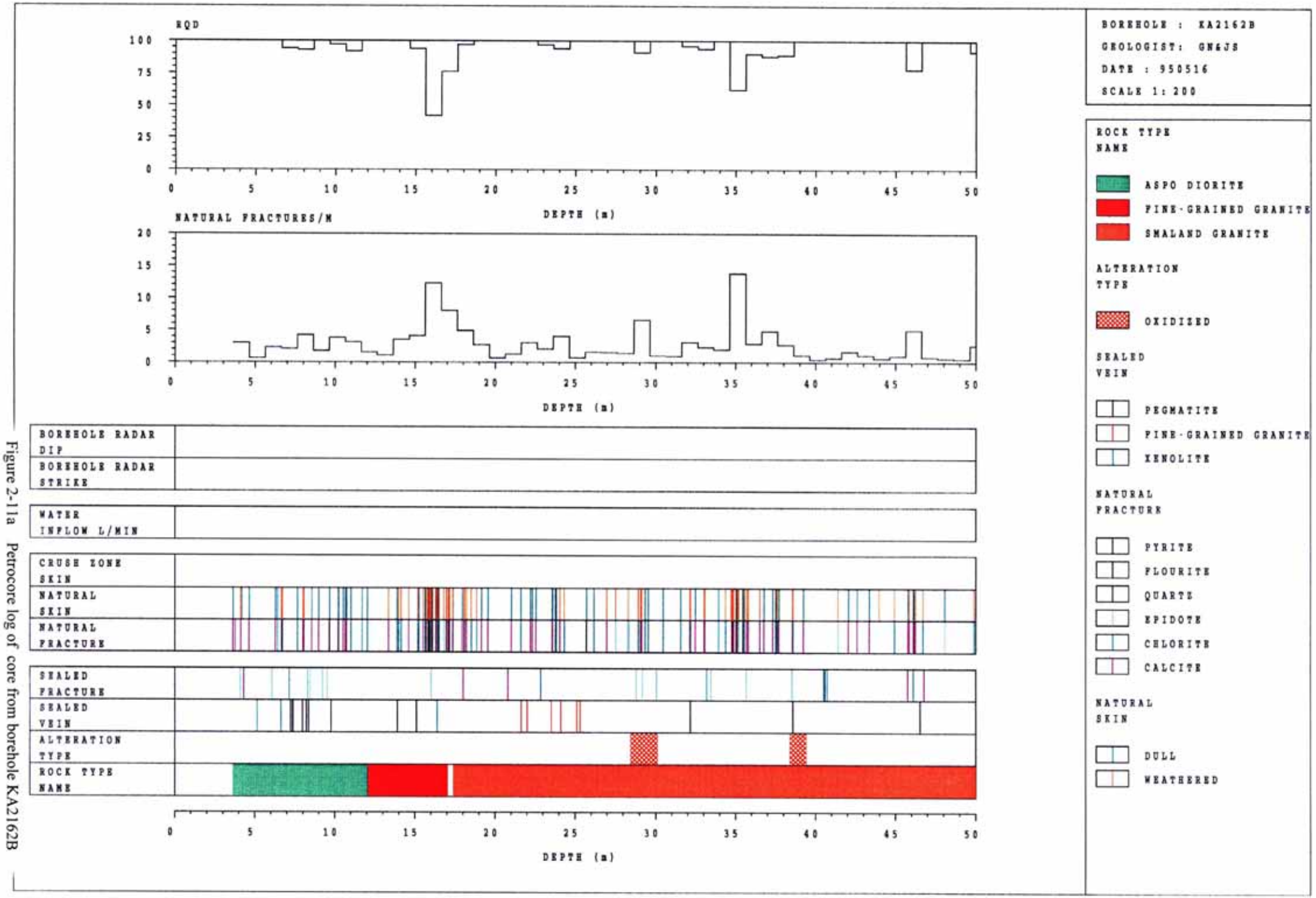

Figure 2-11a Petrocore log of core from borehole KA2162B

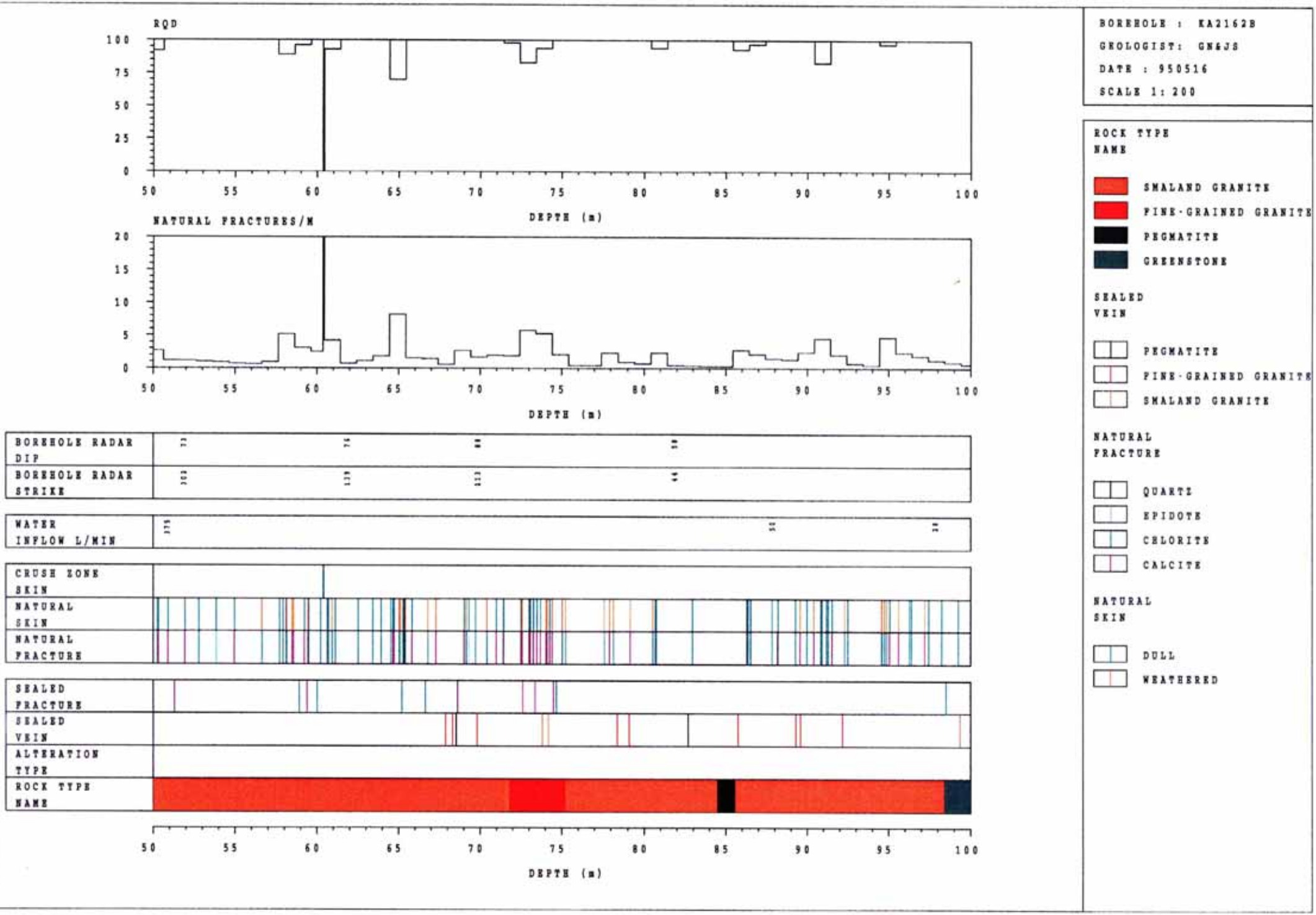

Figure 2-11b Petrocore log of core from borehole KA2162B

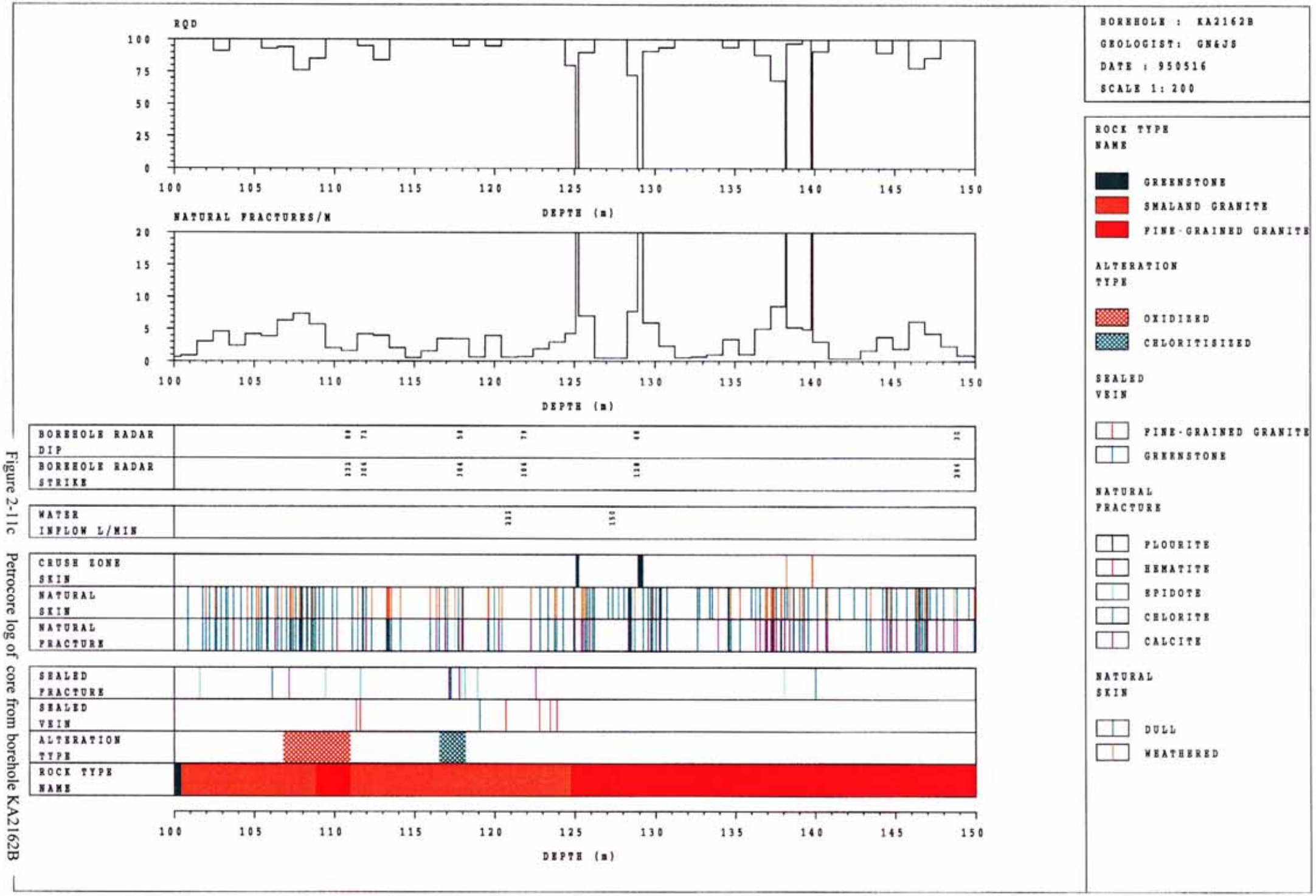

Figure 2-11c Petrocore log of core from borehole KA2162B

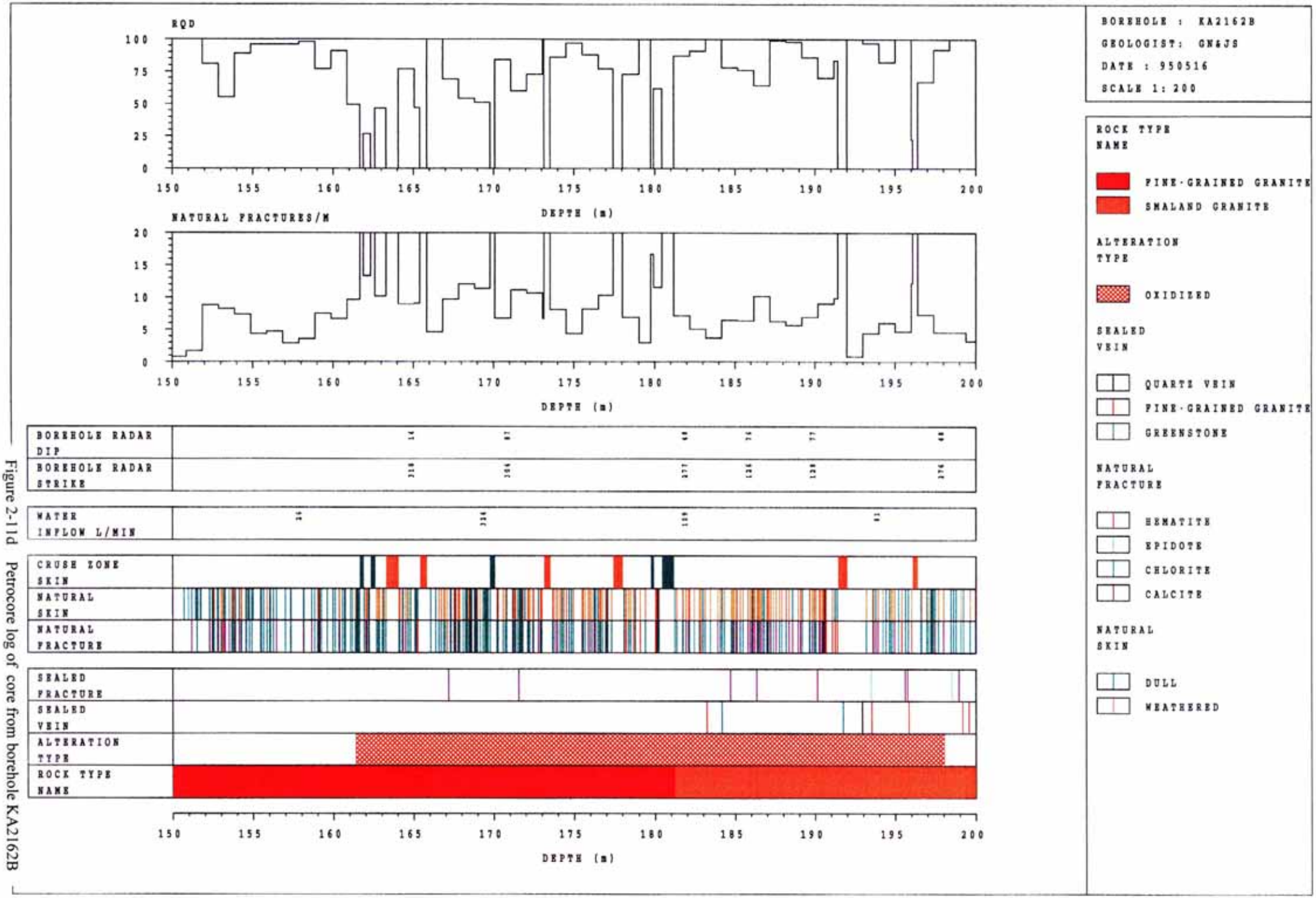

Figure 2-11d Petrocore log of core from borehole KA2162B

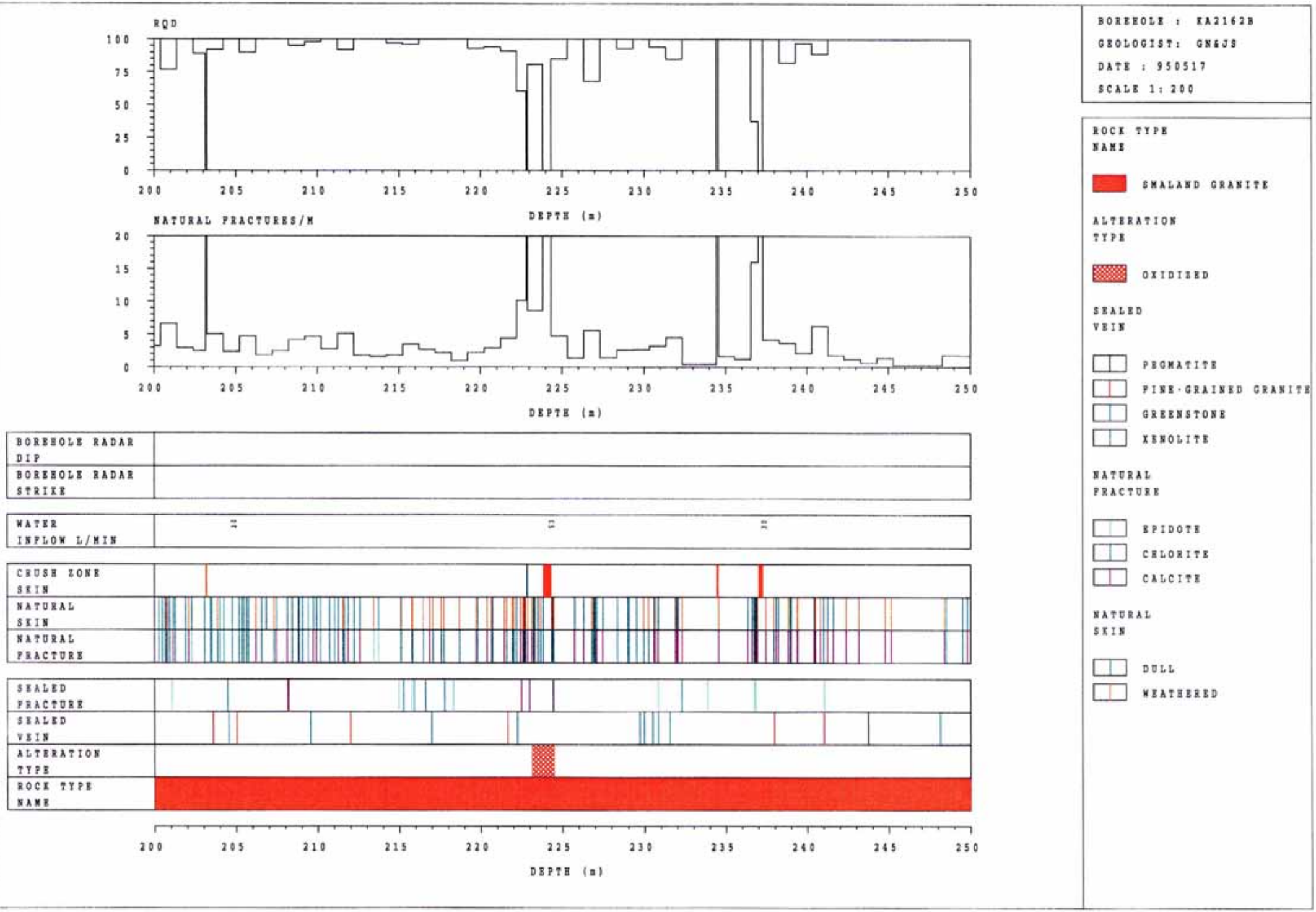

Figure 2-11e Petrocore log of core from borehole KA2162B

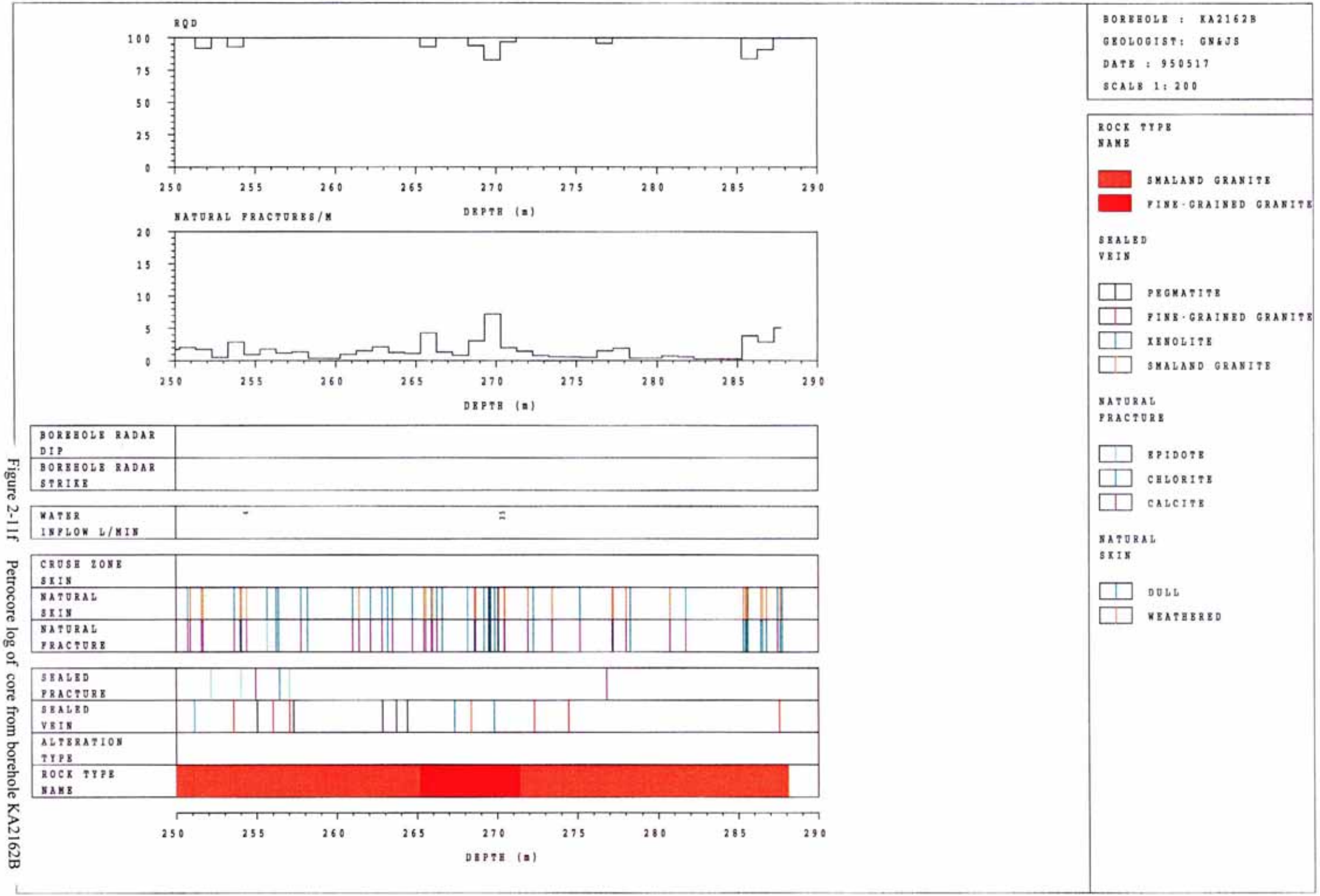

Figure 2-11f Petrocore log of core from borehole KA2162B

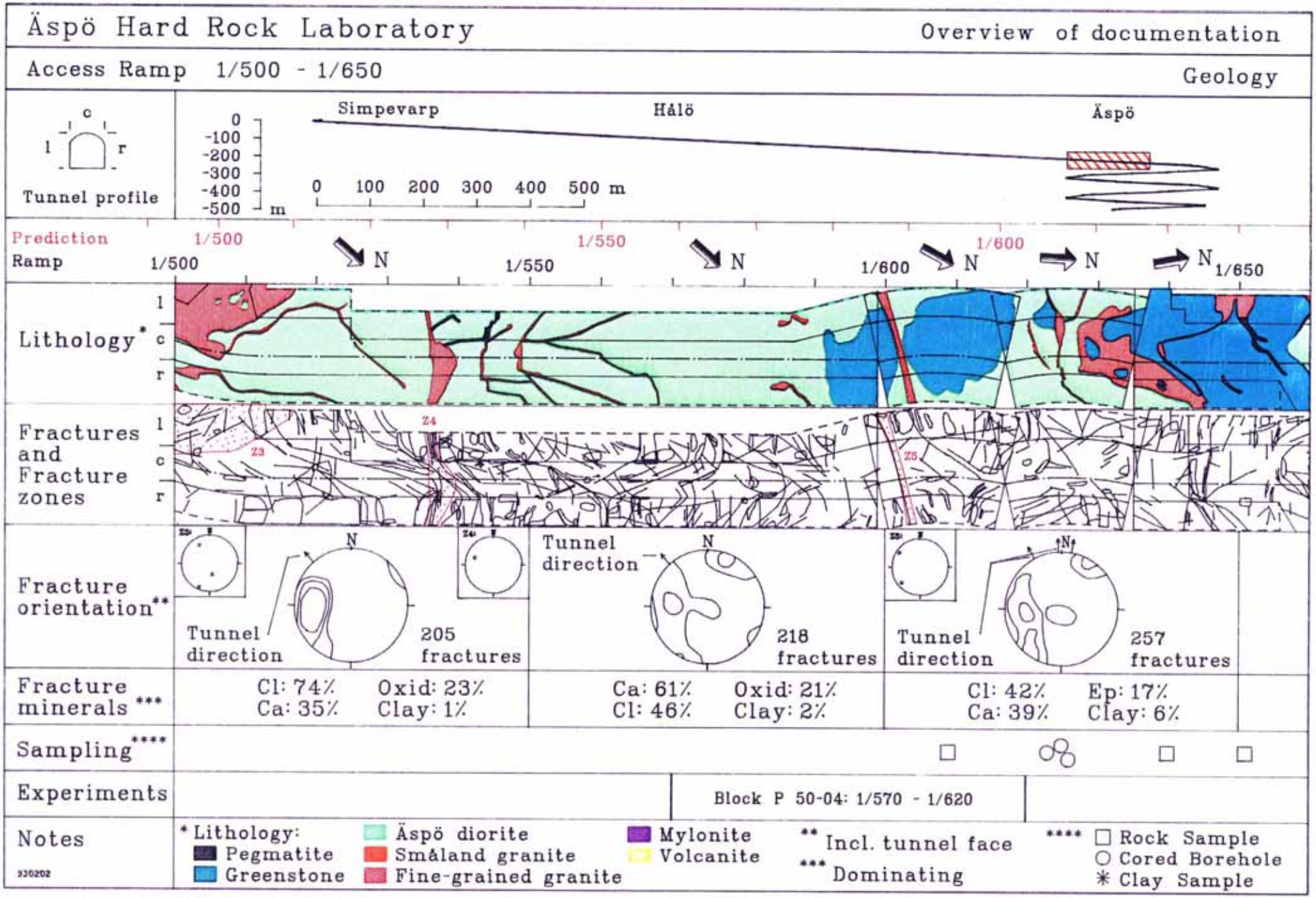

Figure 2-12 Overview of geological documentation, L=1500-1650m

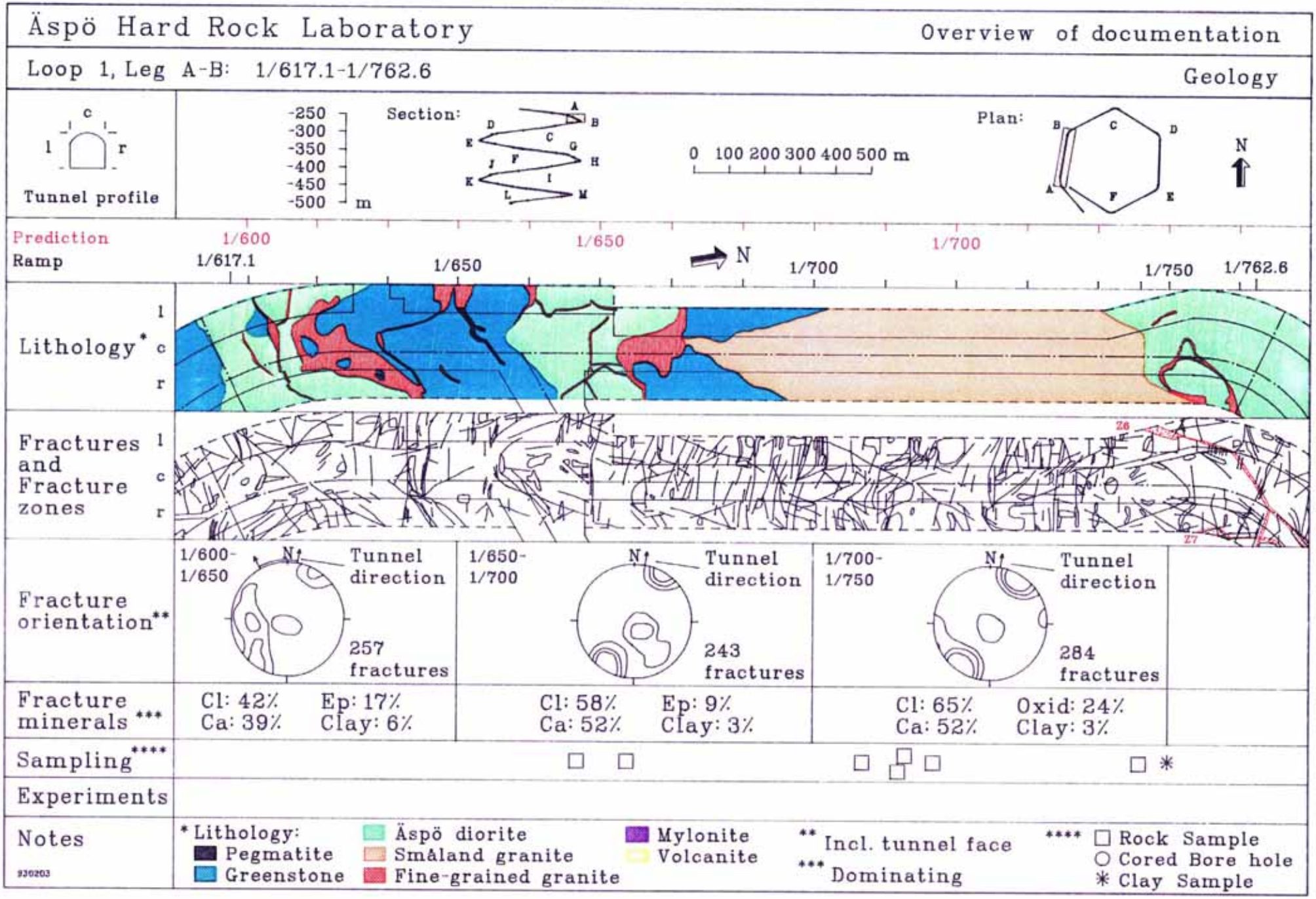

Figure 2-13 Overview of geological documentation, L=1617.1-1762.6m

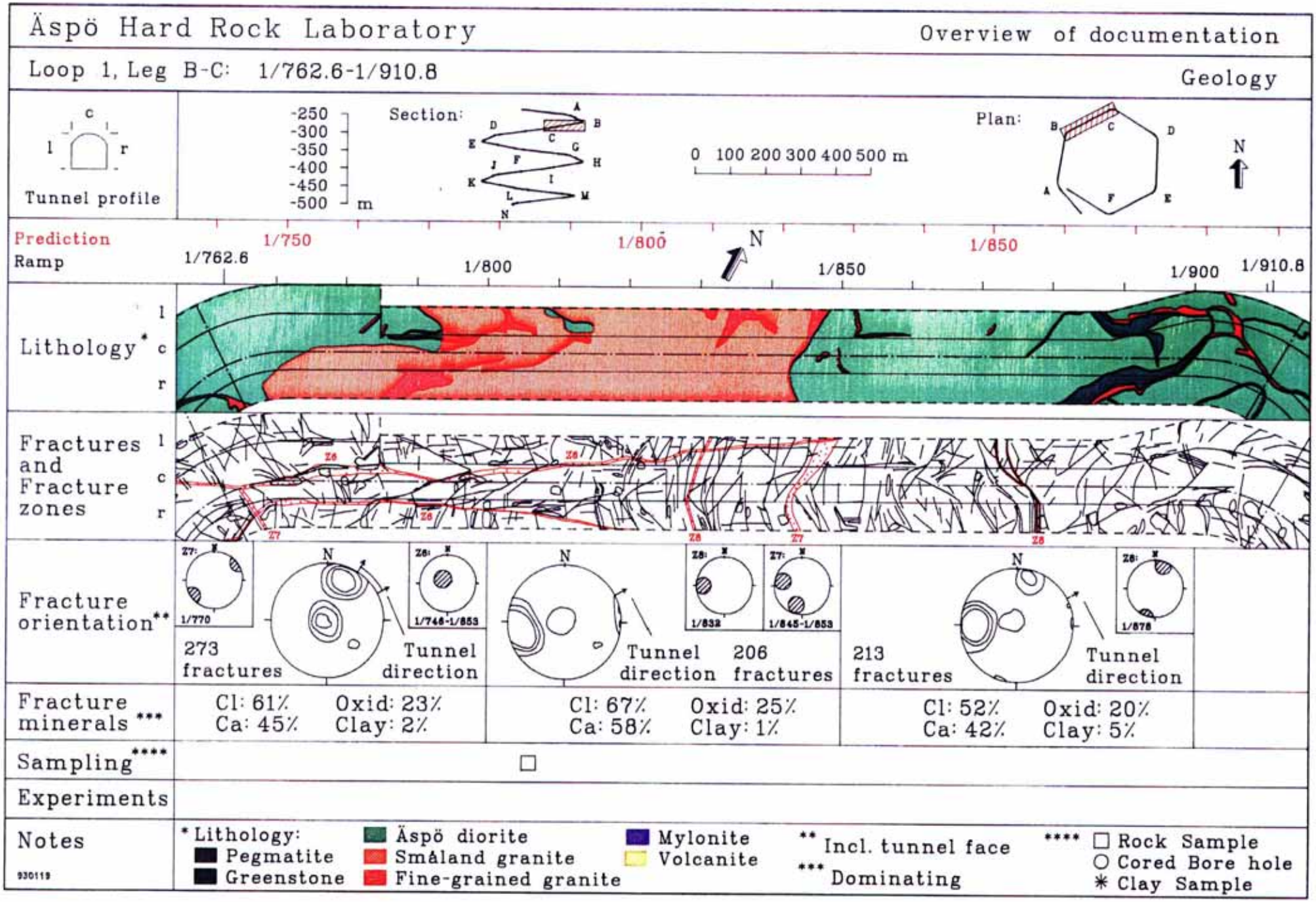

Figure 2-14 Overview of geological documentation. L=1762.1-1910.8m

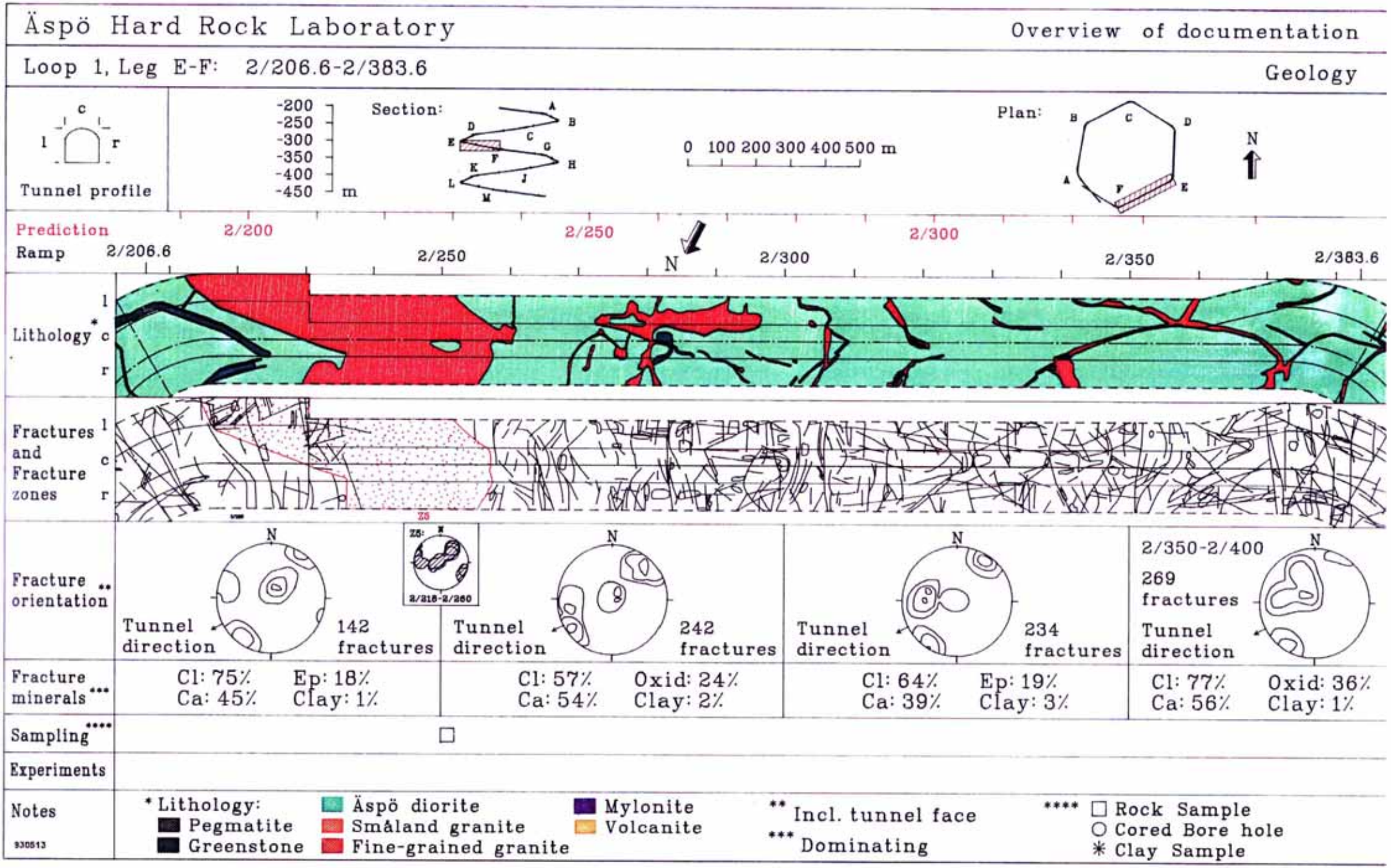

Figure 2-15 Overview of geological documentation, L=2206.6-2383.6m

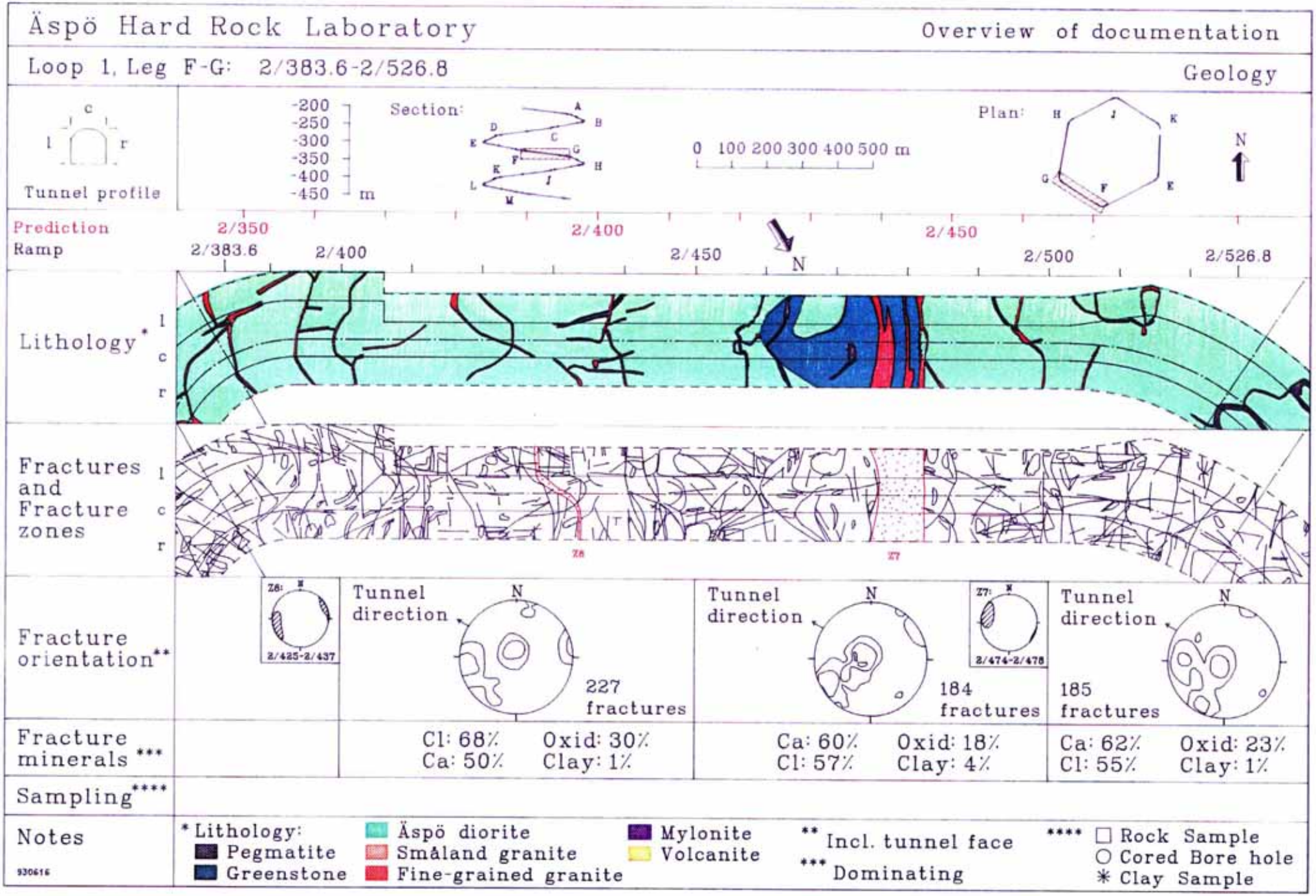

Figure 2-16 Overview of geological documentation, L=2383.6-2526.8m

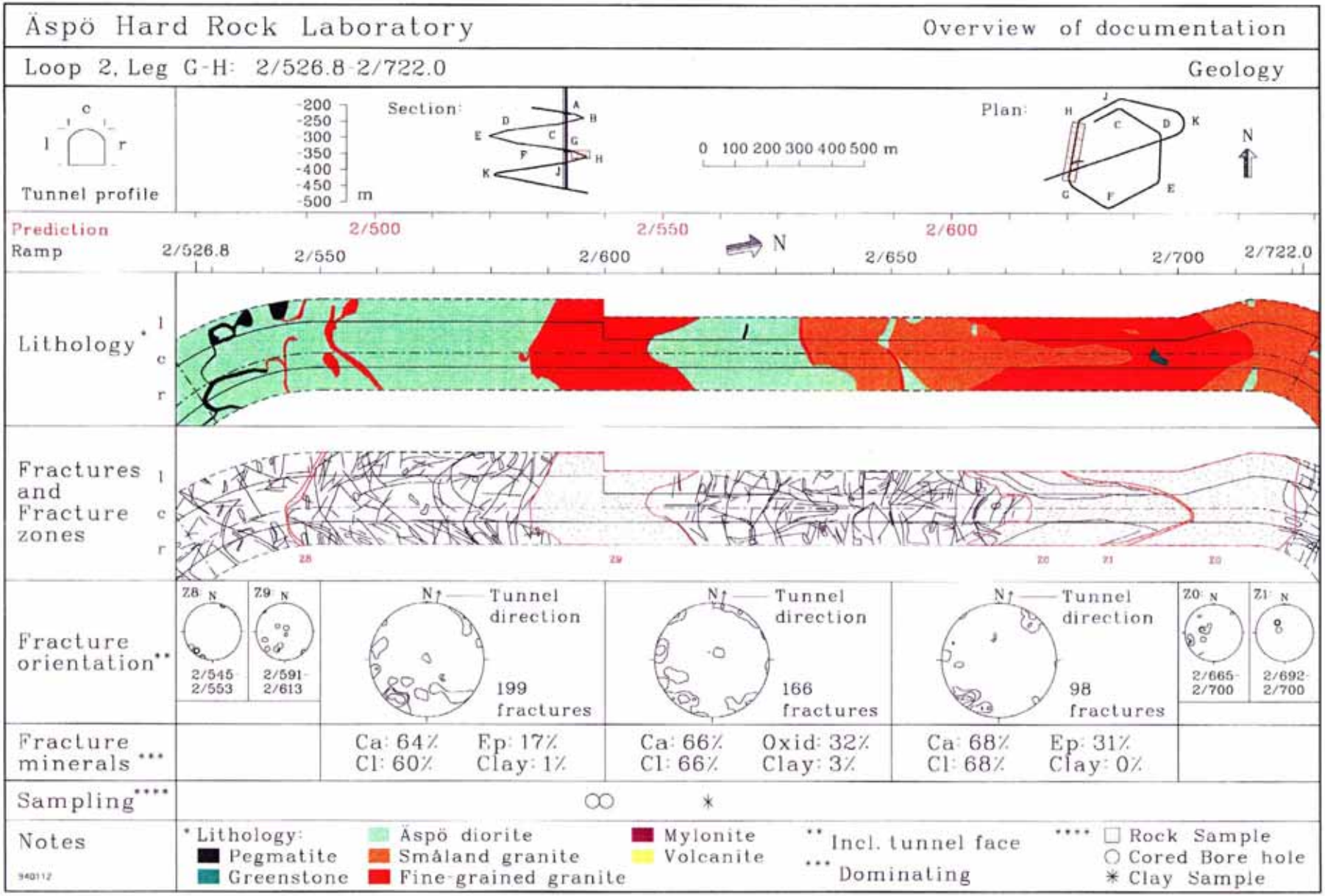

Figure 2-17 Overview of geological documentation, L=2526.8-2722.0m

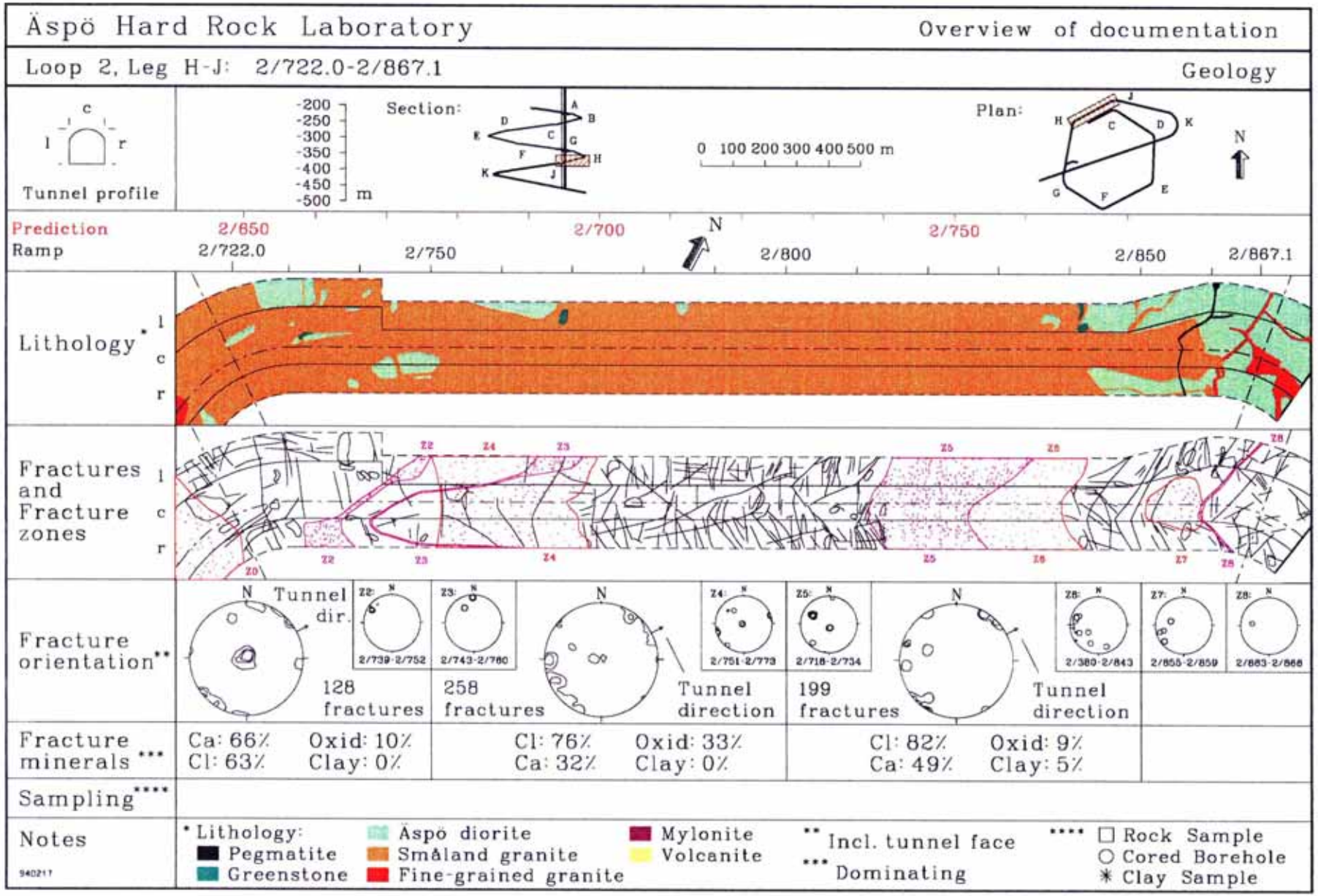

Figure 2-18 Overview of geological documentation. L=2722.0-2867.1m

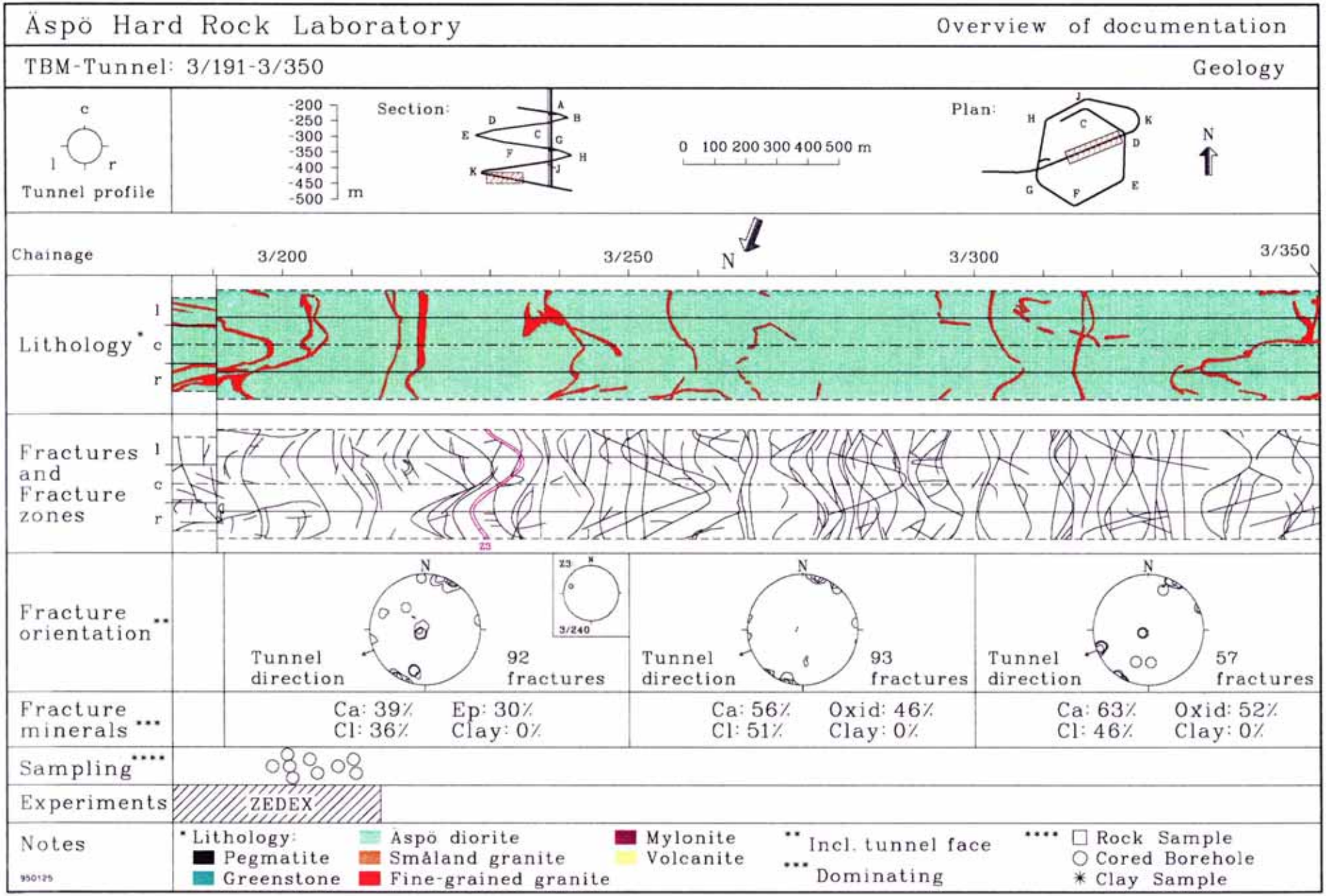

Figure 2-19 Overview of geological documentation, L=3191-3350m

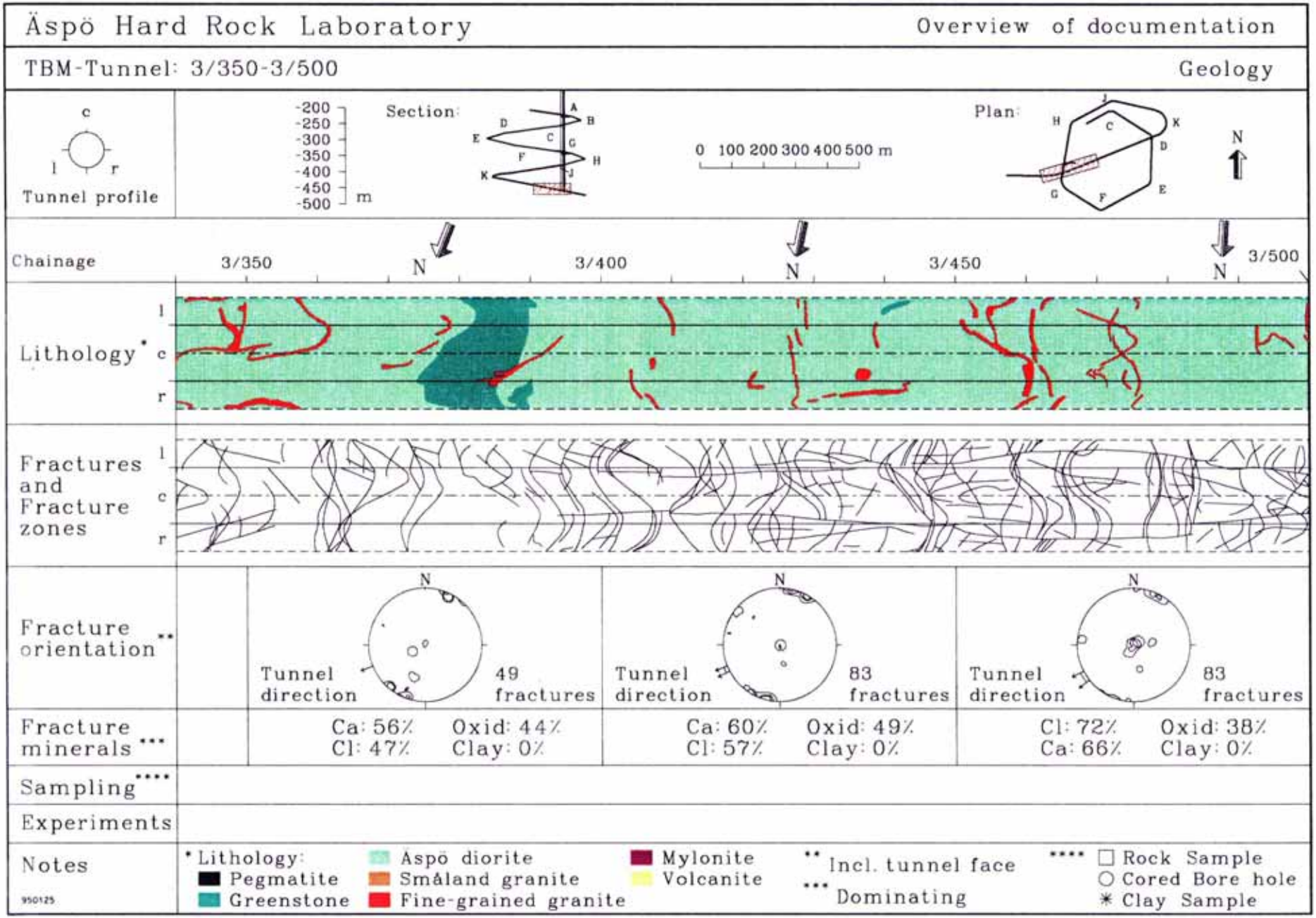

Figure 2-20 Overview of geological documentation, L=3350-3500m

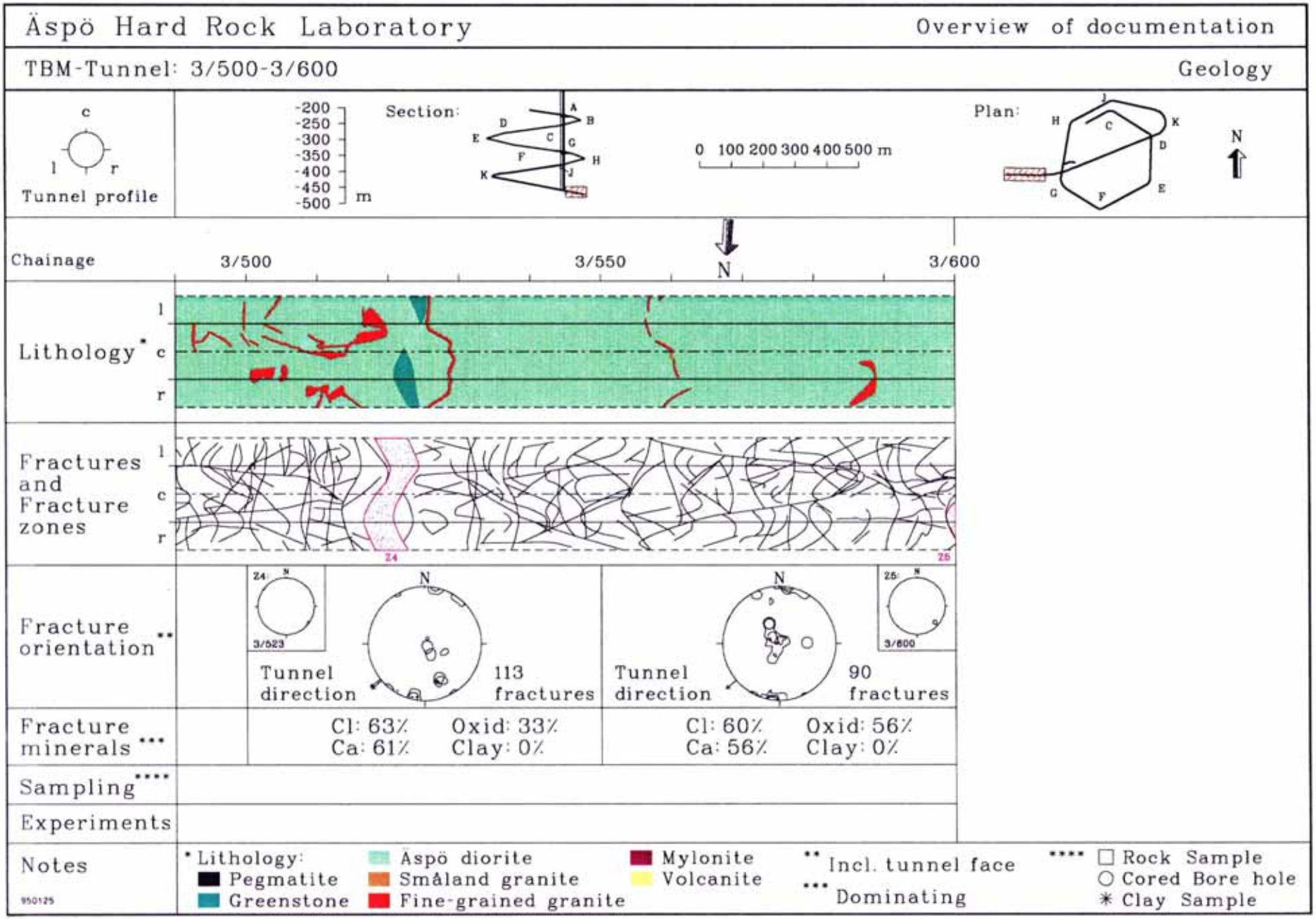

Figure 2-21 Overview of geological documentation, L=3500-3600m

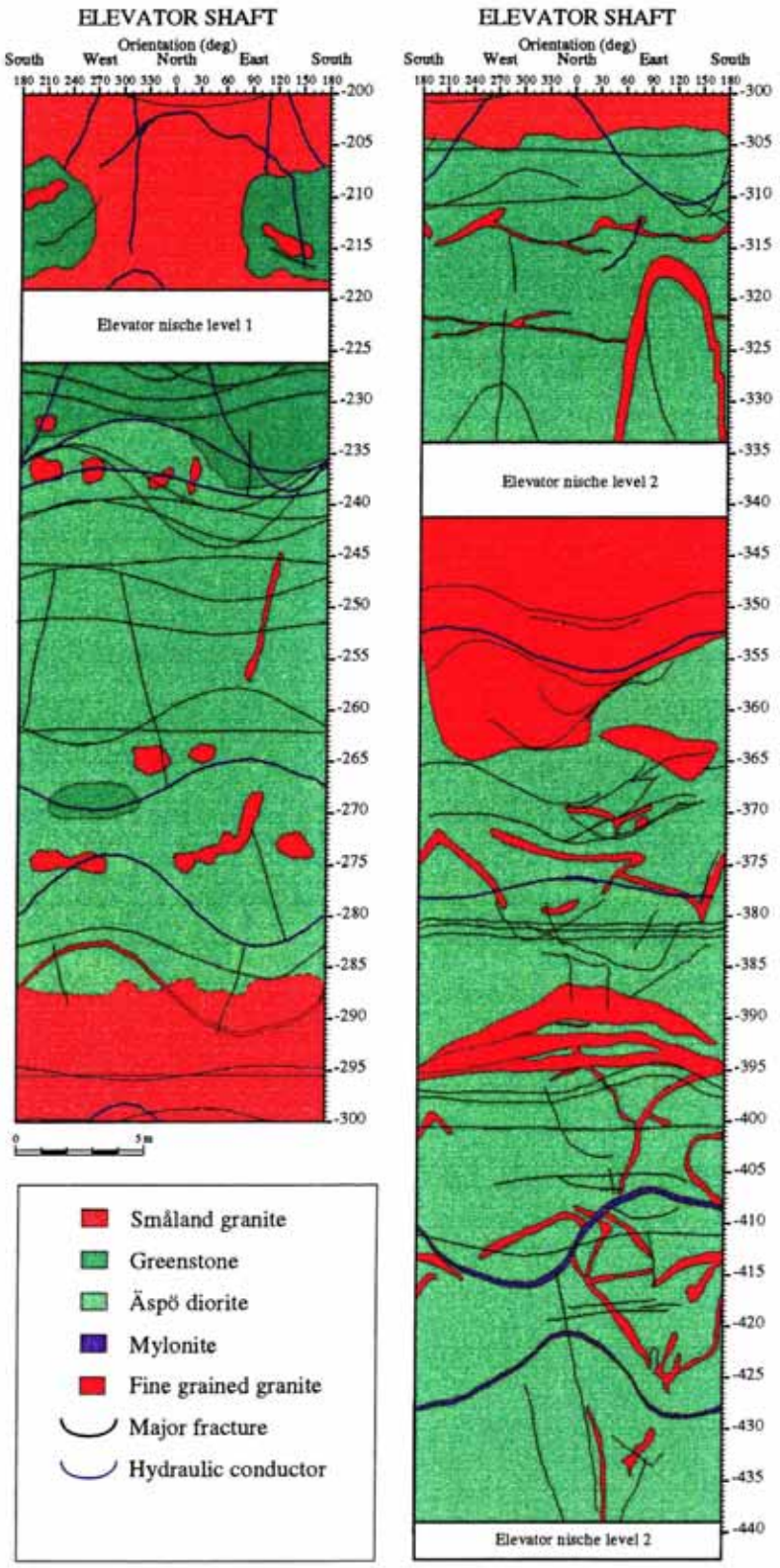

Figure 2-22 Geological mapping of elevator shaft, Z=-200 to -440m (from Munier 1995)

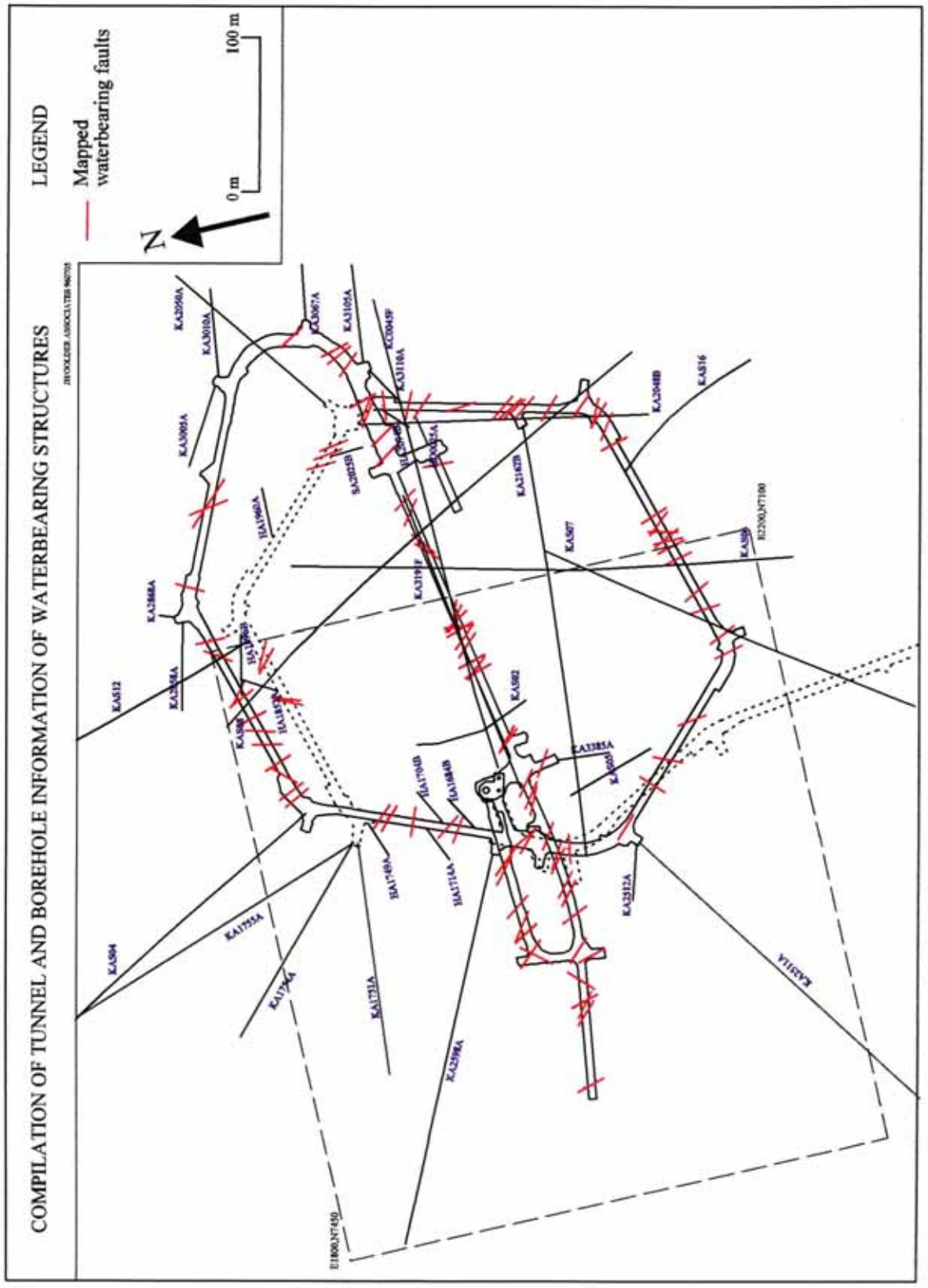

Figure 2-23 Location of water-bearing structures in the Äspö HRL tunnel

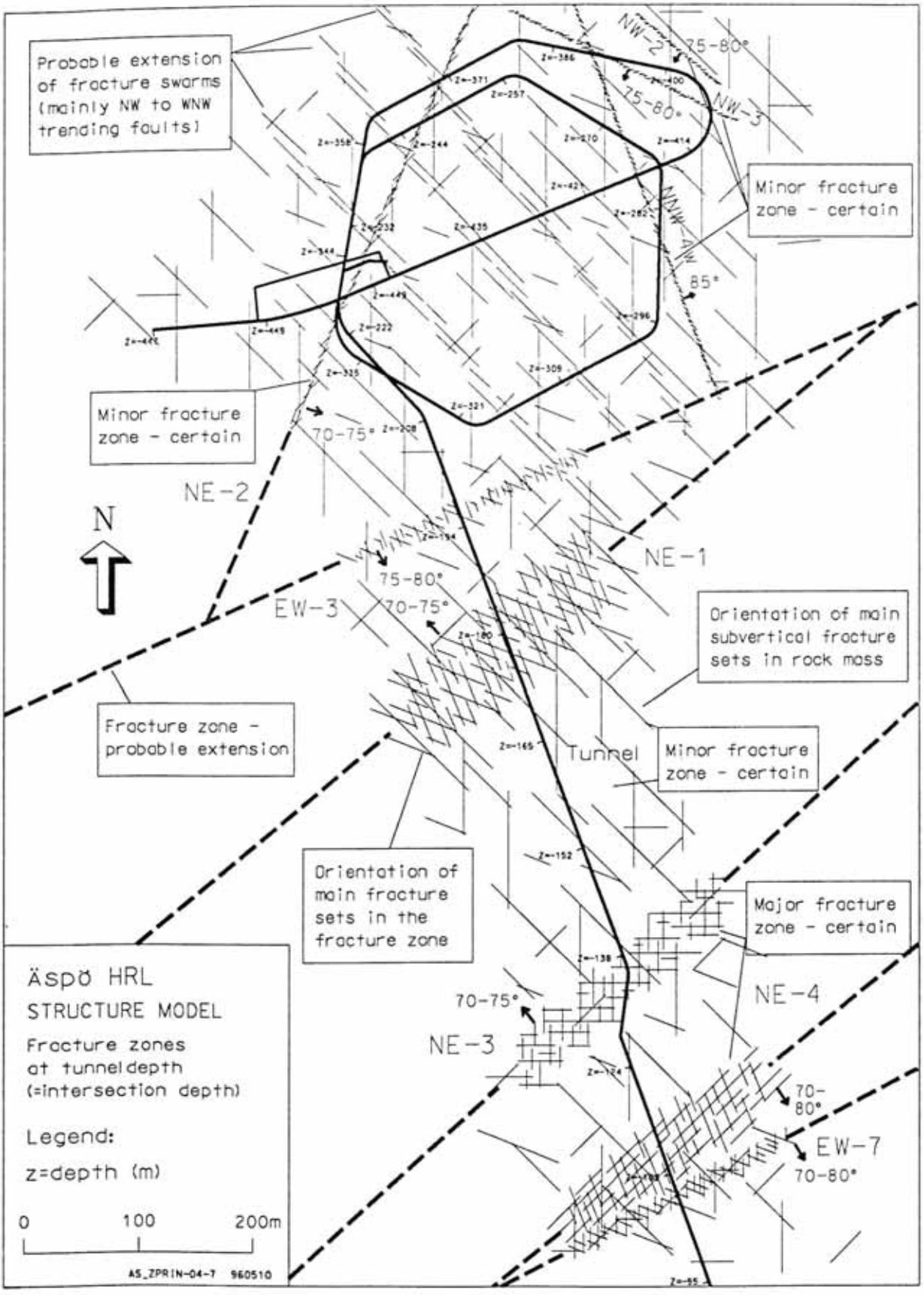

Figure 3-1 Structural model of Äspö HRL (Rhen and Stanfors , 1996)

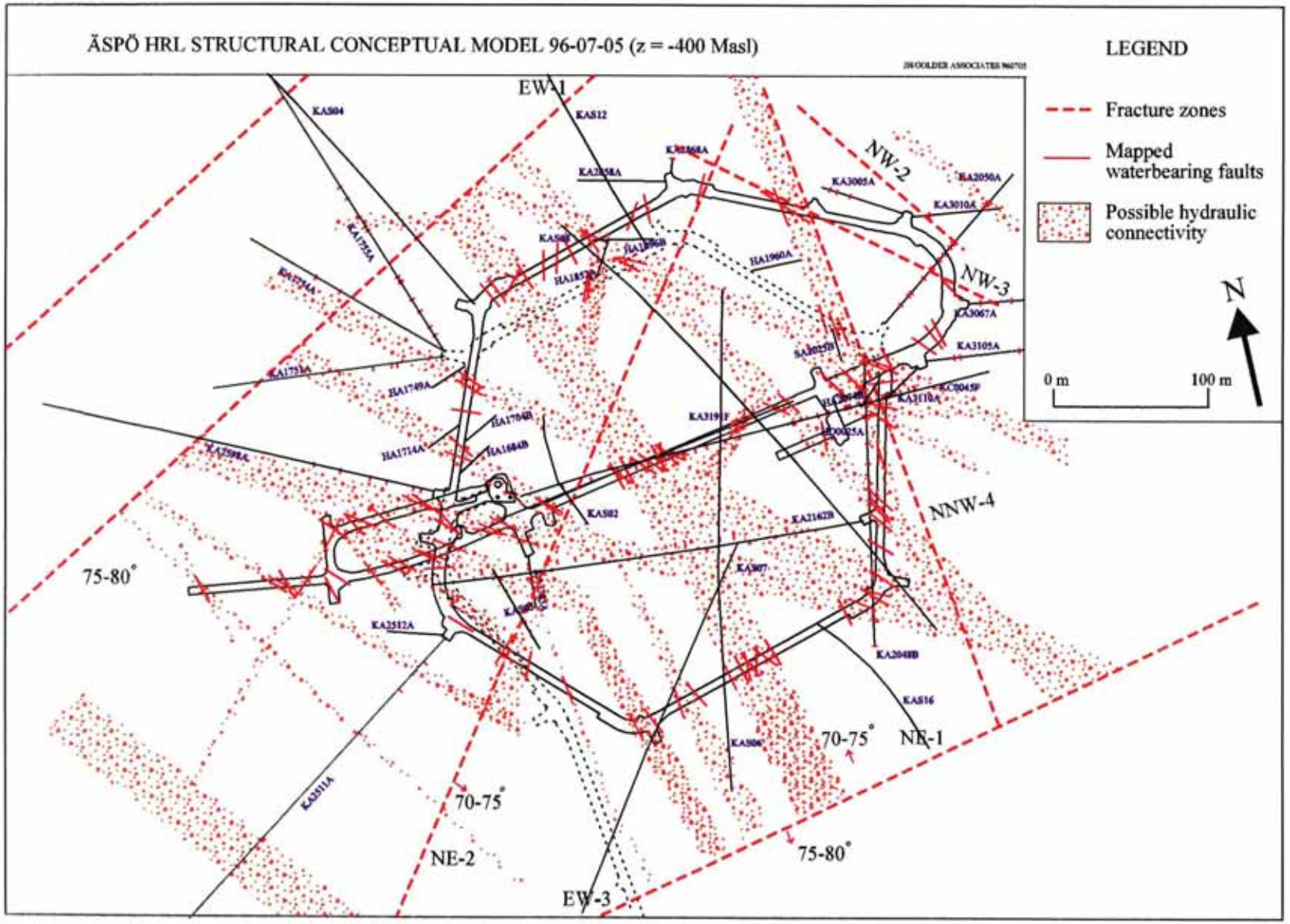

Figure 3-2 Updated structural model at Z=-400masl

Perspective View of Fracture Plane and Boreholes

Heterogeneous fracture plane. The outer region is very large and more transmissive compared to the inner region.

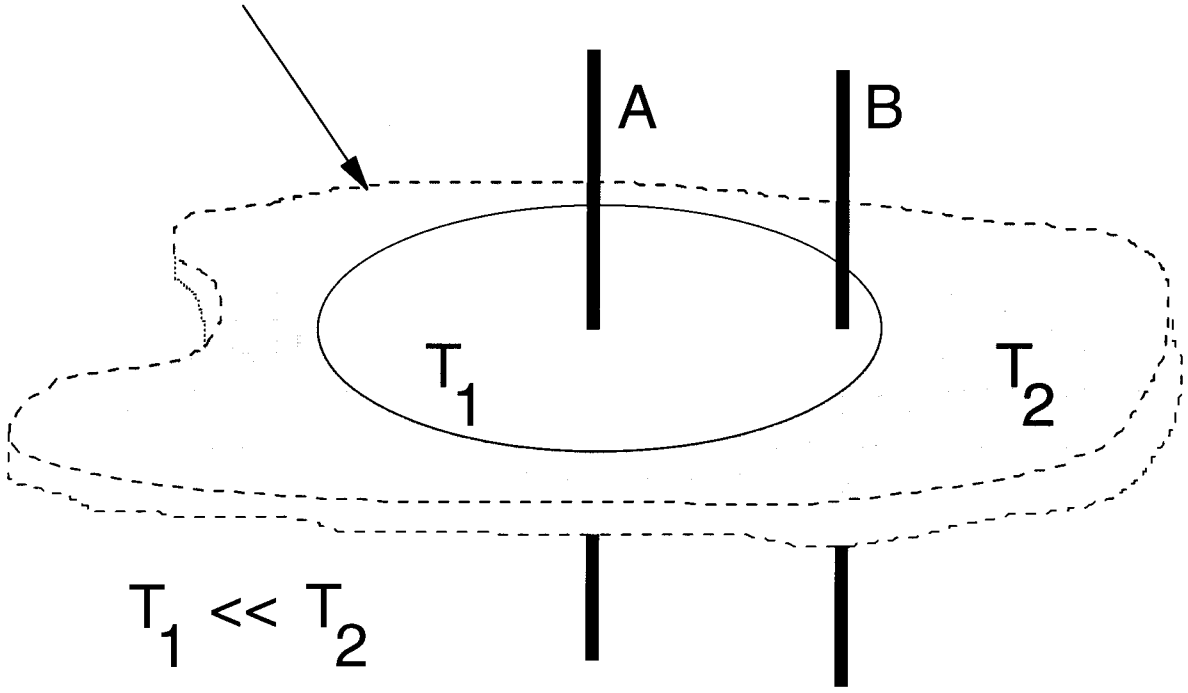

Horizontal Section of Pressure Responses

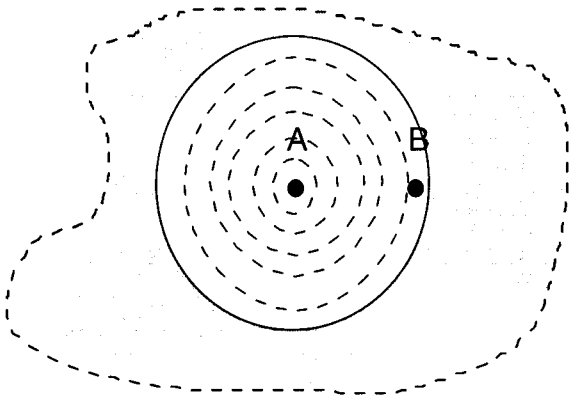

Pressure response while pumping at A

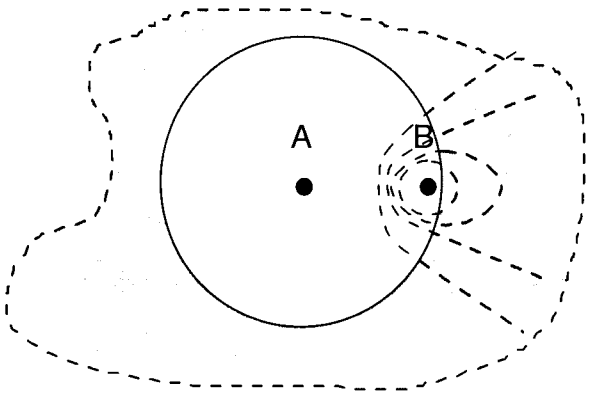

Pressure response while pumping at B

Figure 4-1 A heterogeneous fracture plane intersected by two vertical boreholes, A and B. Borehole A is located in the center of a region with low transmissivity whereas borehole B is closer to the region where the transmissivity is much higher. Hydraulic testing will yield different pressure responses in the two boreholes depending on which one that is acting as source well.

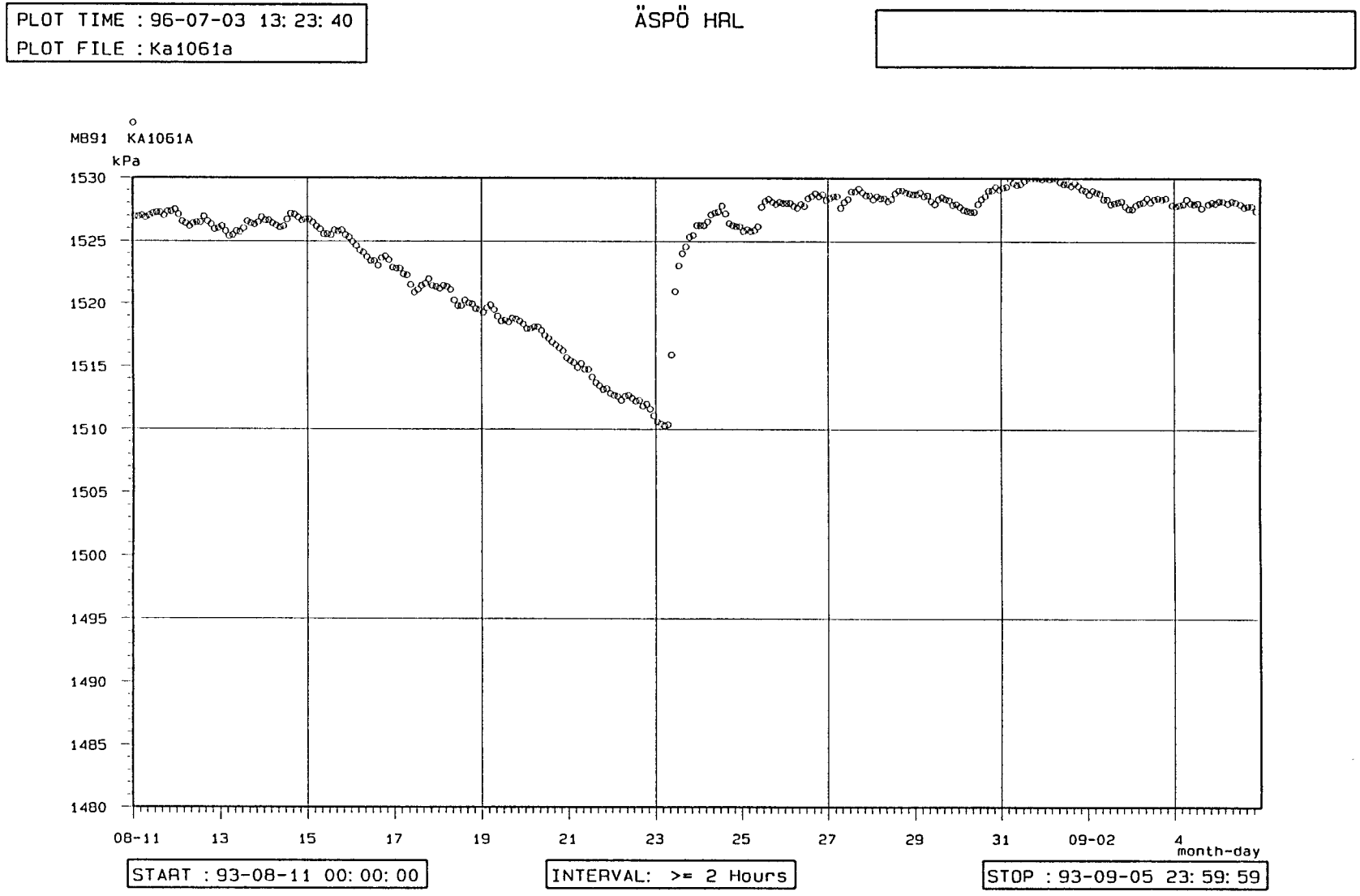

Figure 4-2 Pressure responses in borehole KA1061A during drilling of KA2511A

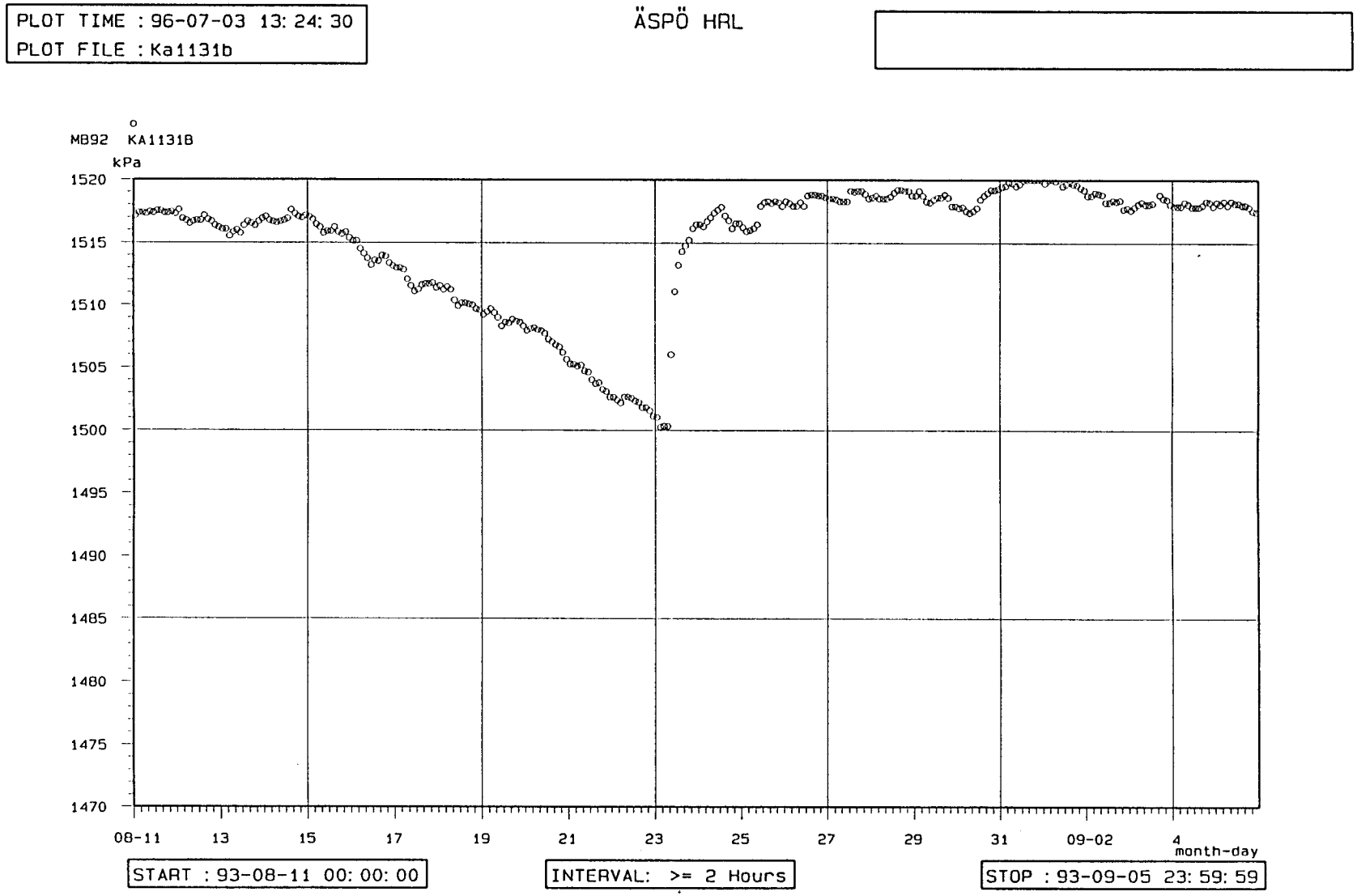

Figure 4-3 Pressure responses in borehole KA1131A during drilling of KA2511A

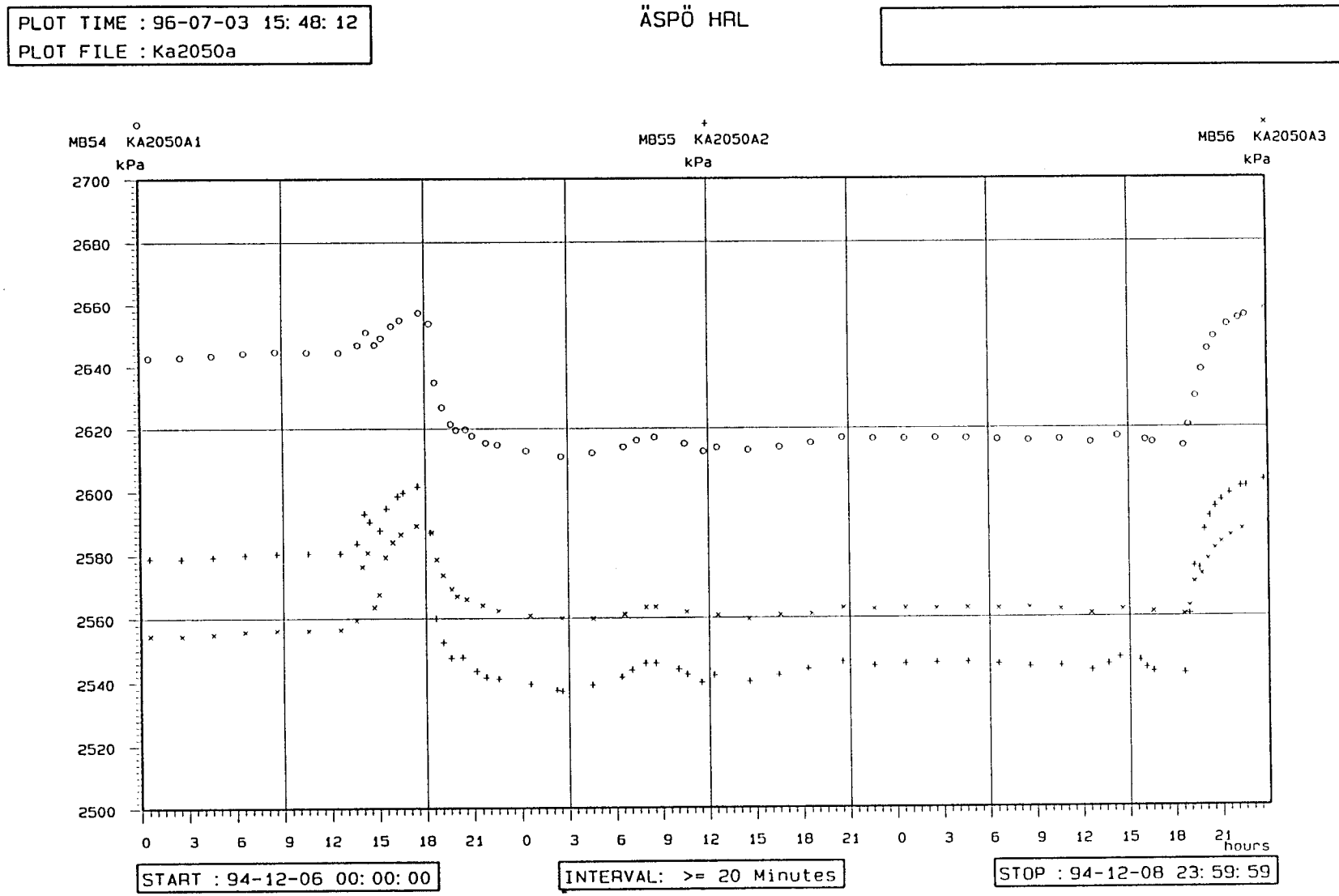

Figure 4-4 Pressure responses in borehole KA2050A during drilling of KA3010A

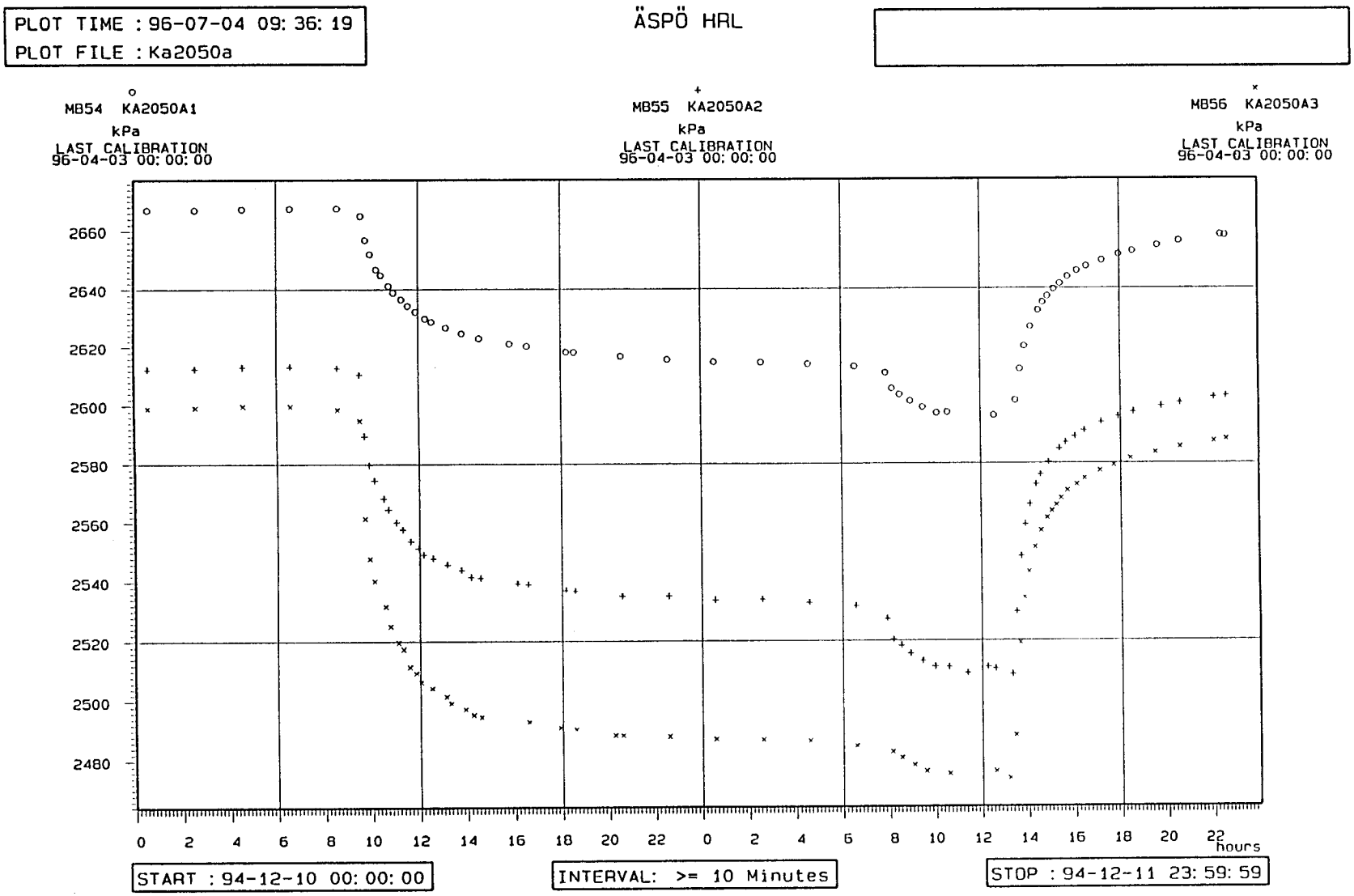

Figure 4-5 Pressure responses in borehole KA2050A during drilling of KA3067A

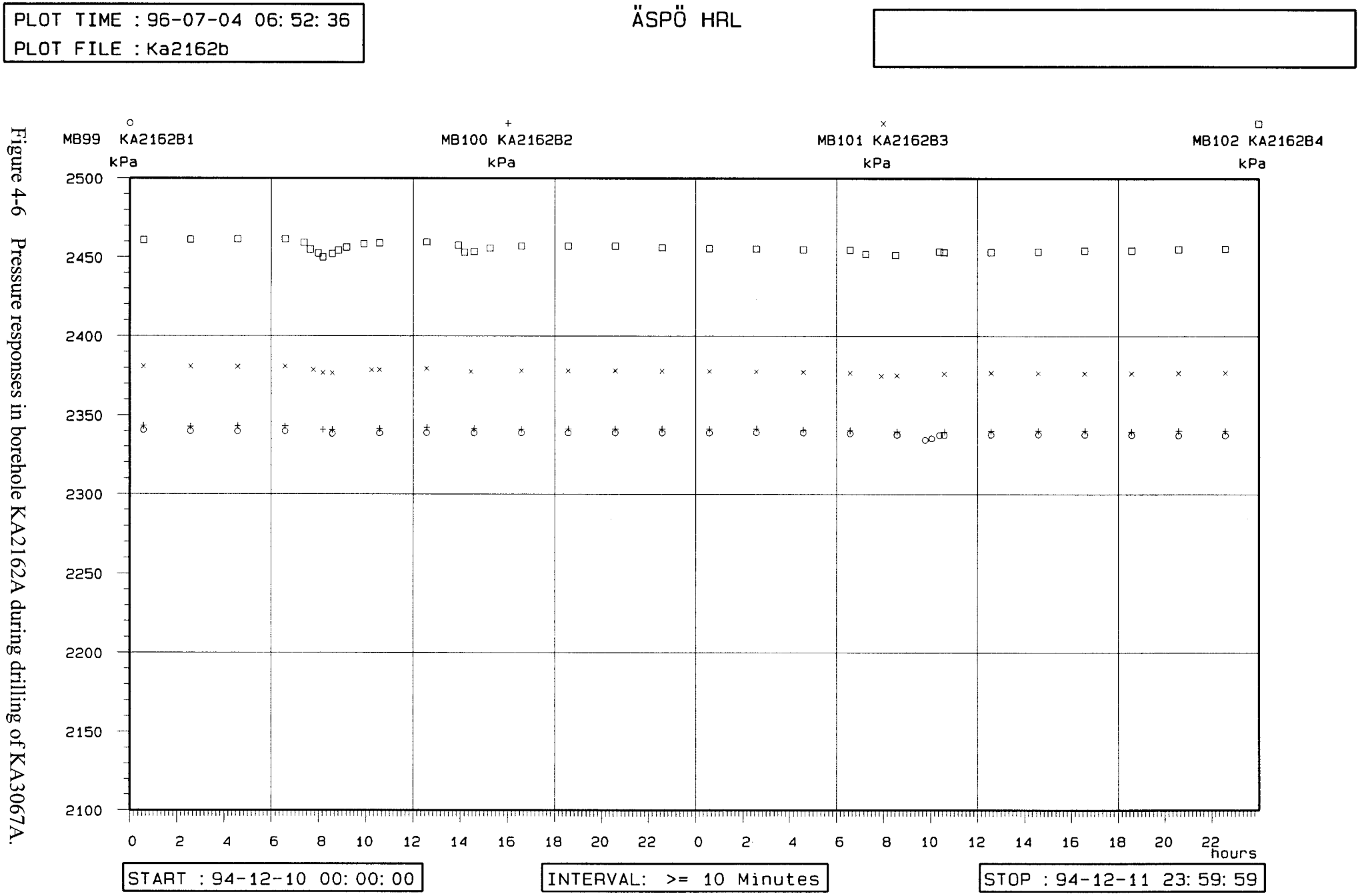

Figure 4-6 Pressure responses in borehole KA2162A during drilling of KA3067A.

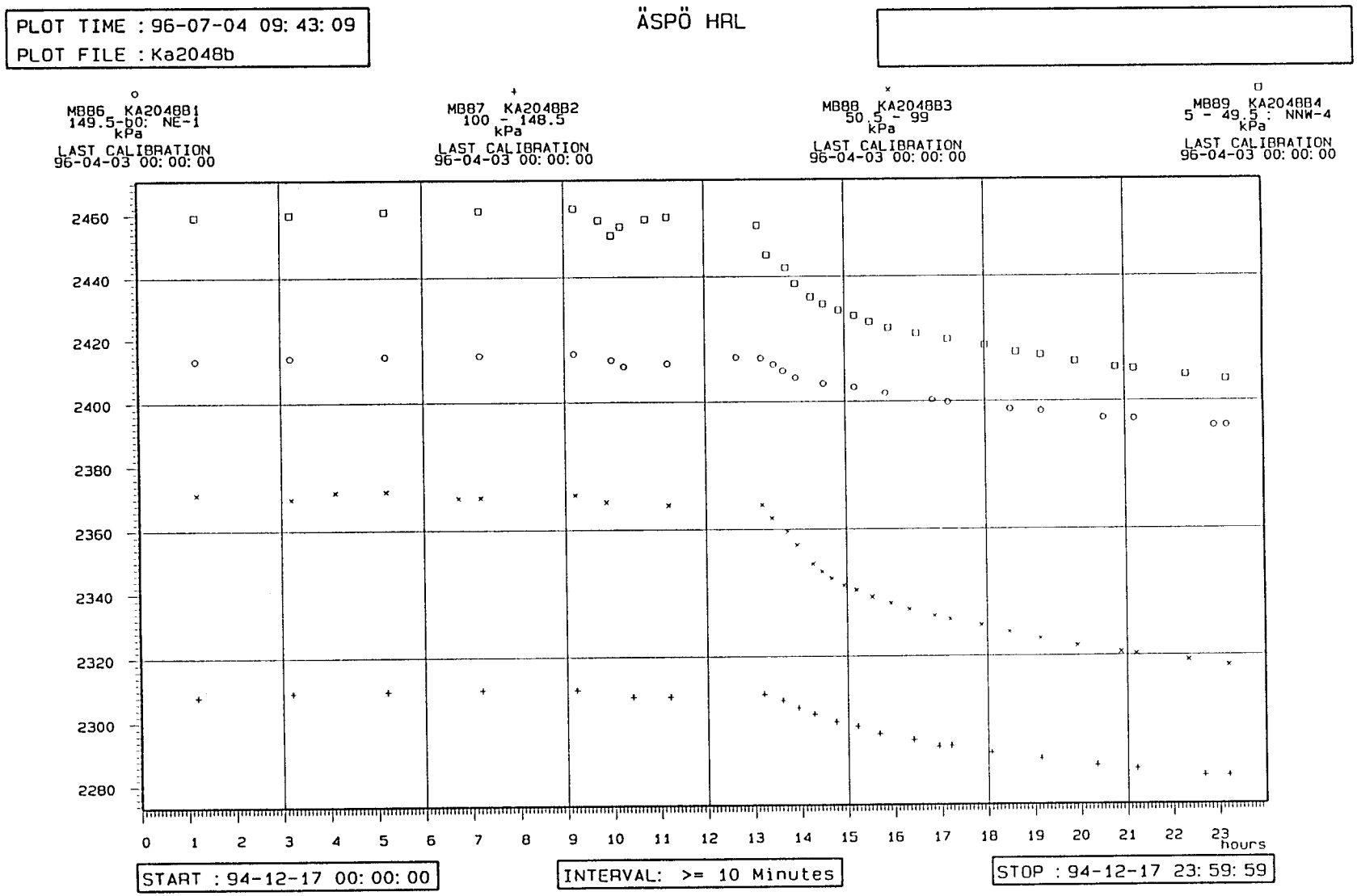

Figure 4-7 Pressure responses in borehole KA2048A during drilling of KA3110A

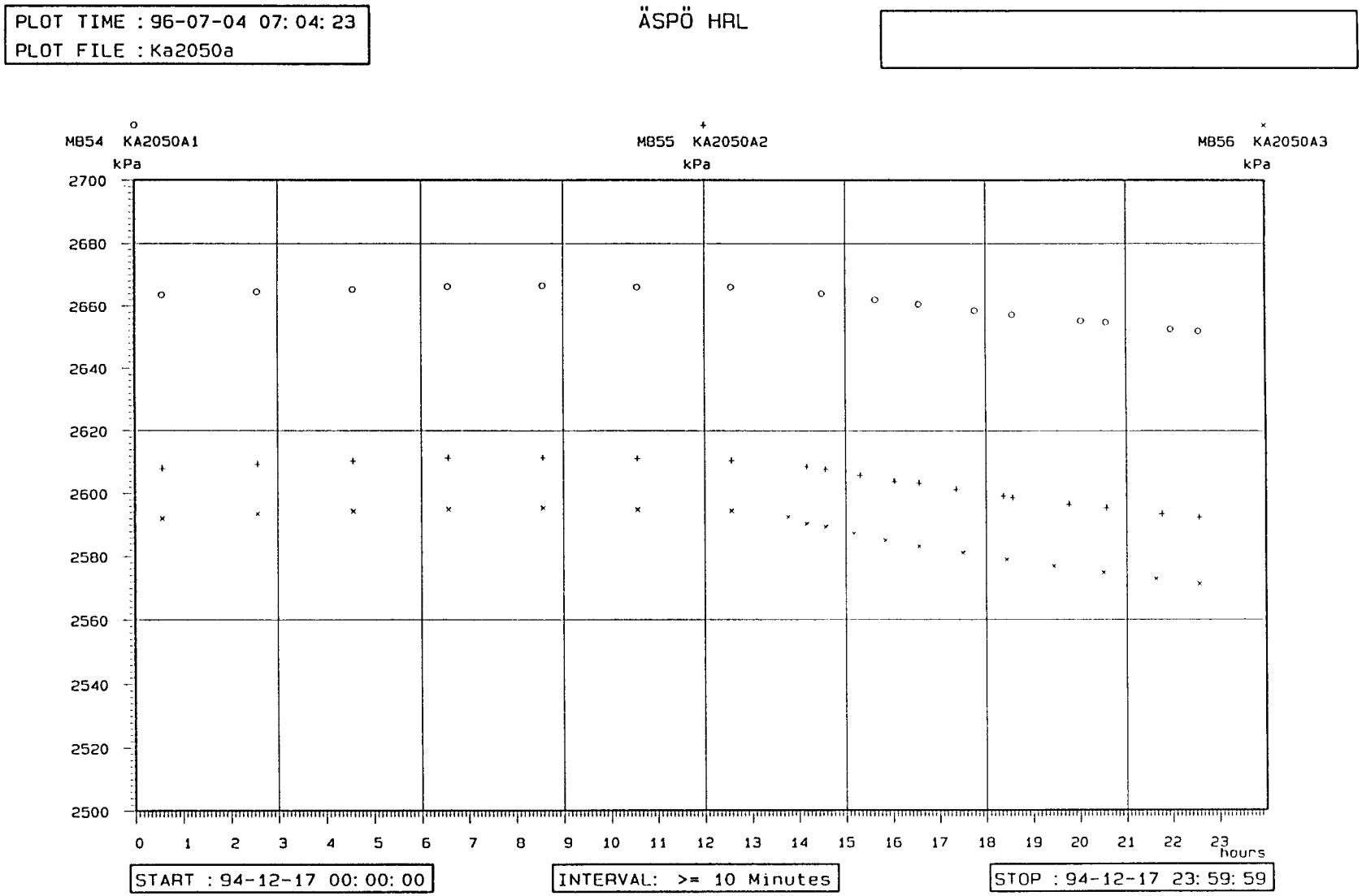

Figure 4-8 Pressure responses in borehole KA2050A during drilling of KA3110A

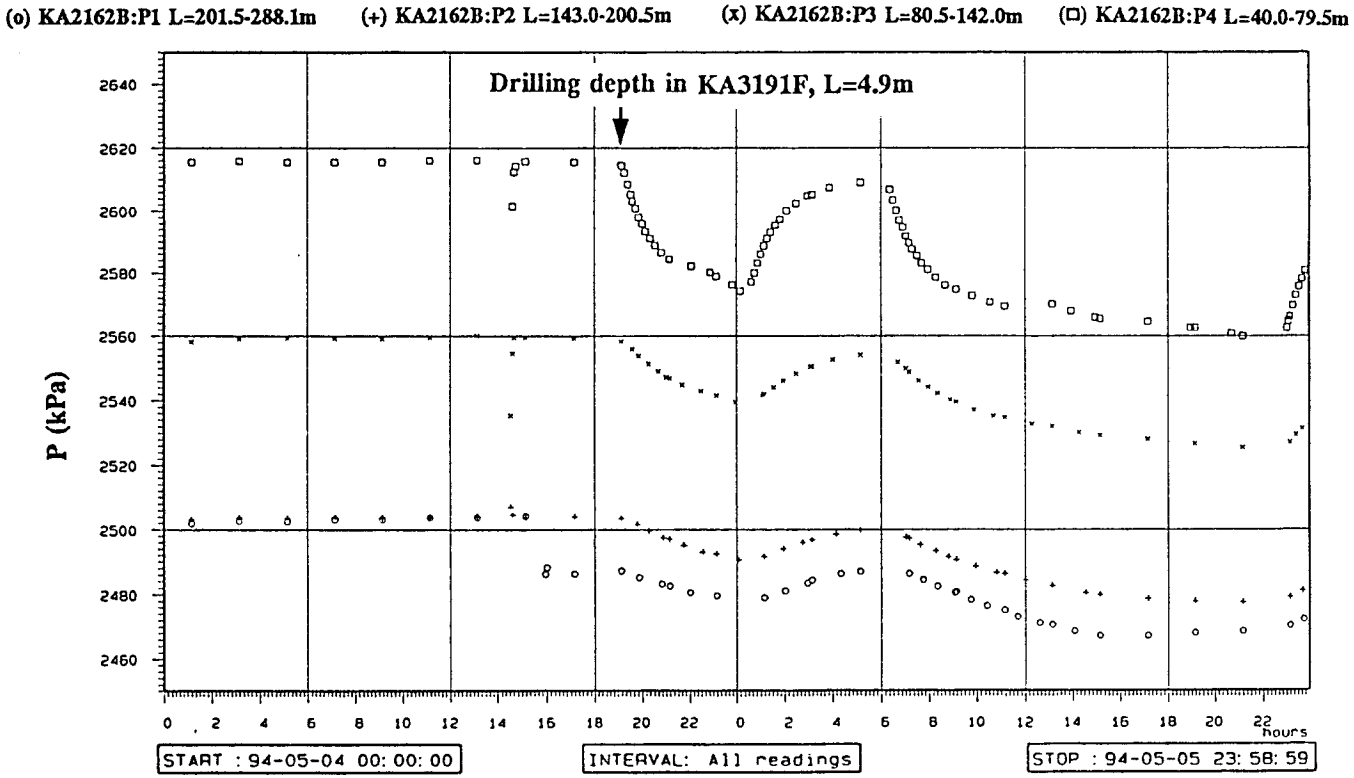

Figure 4-9 Pressure responses in borehole KA2162B during drilling of initial parts of the TBM pilot borehole KA3191F (from Winberg et al., 1996a)

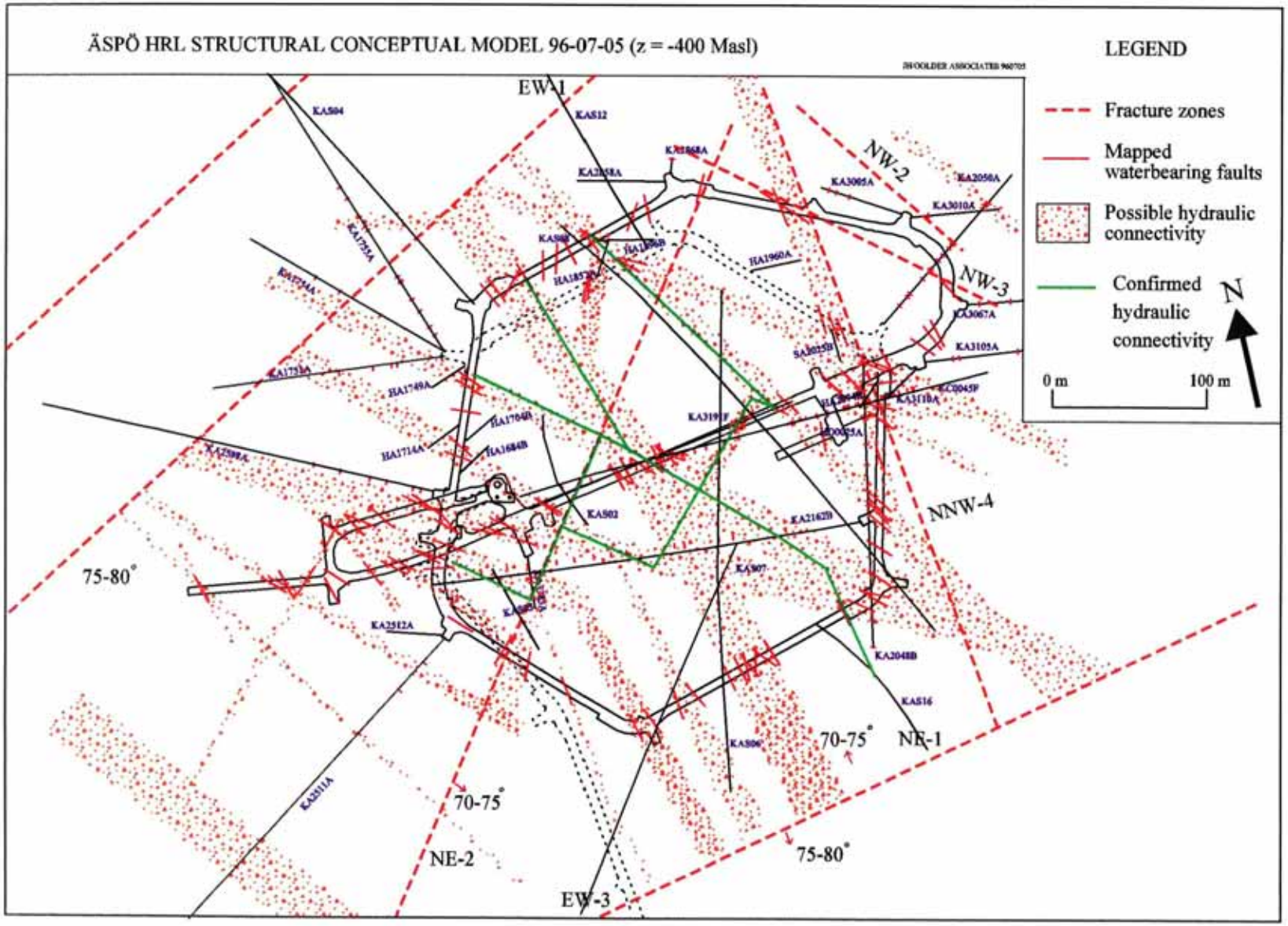

Figure 4-10 Hydraulic connectivity model interpreted from pressure responses recorded during drilling of KA3191F

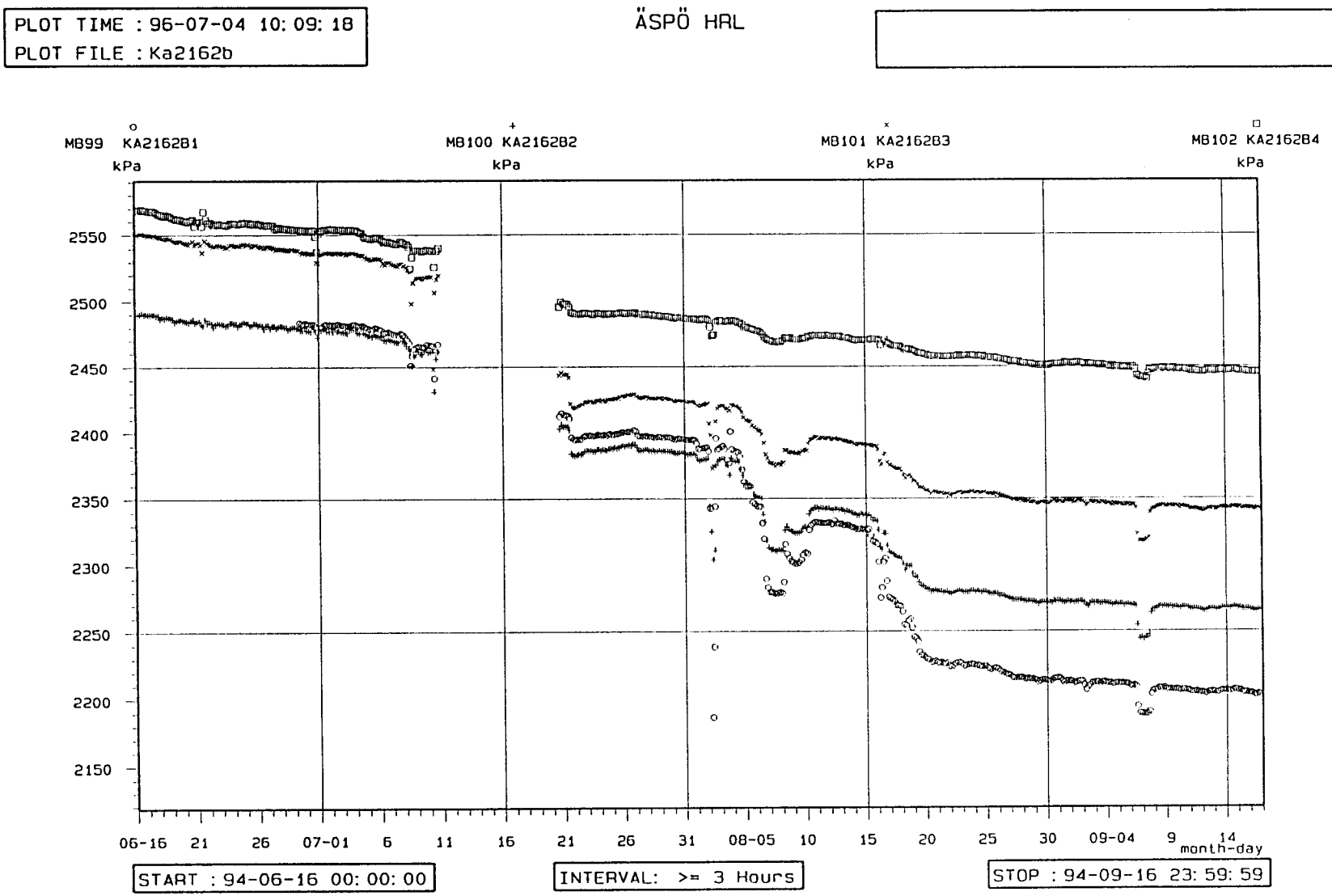

Figure 4-11 Pressure responses in borehole KA2162B during drilling of the TBM tunnel

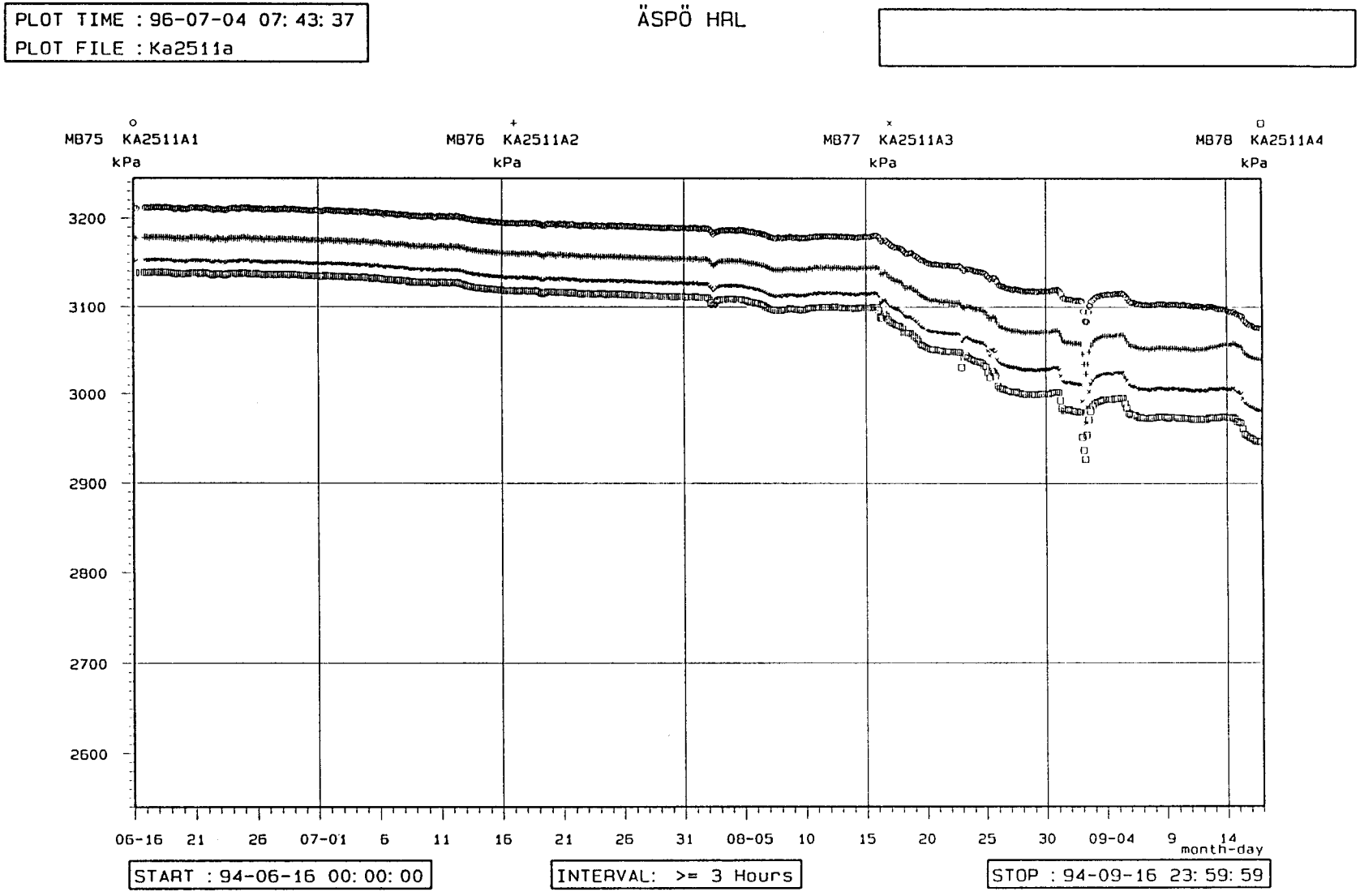

Figure 4-12 Pressure responses in borehole KA2511A during drilling of the TBM tunnel

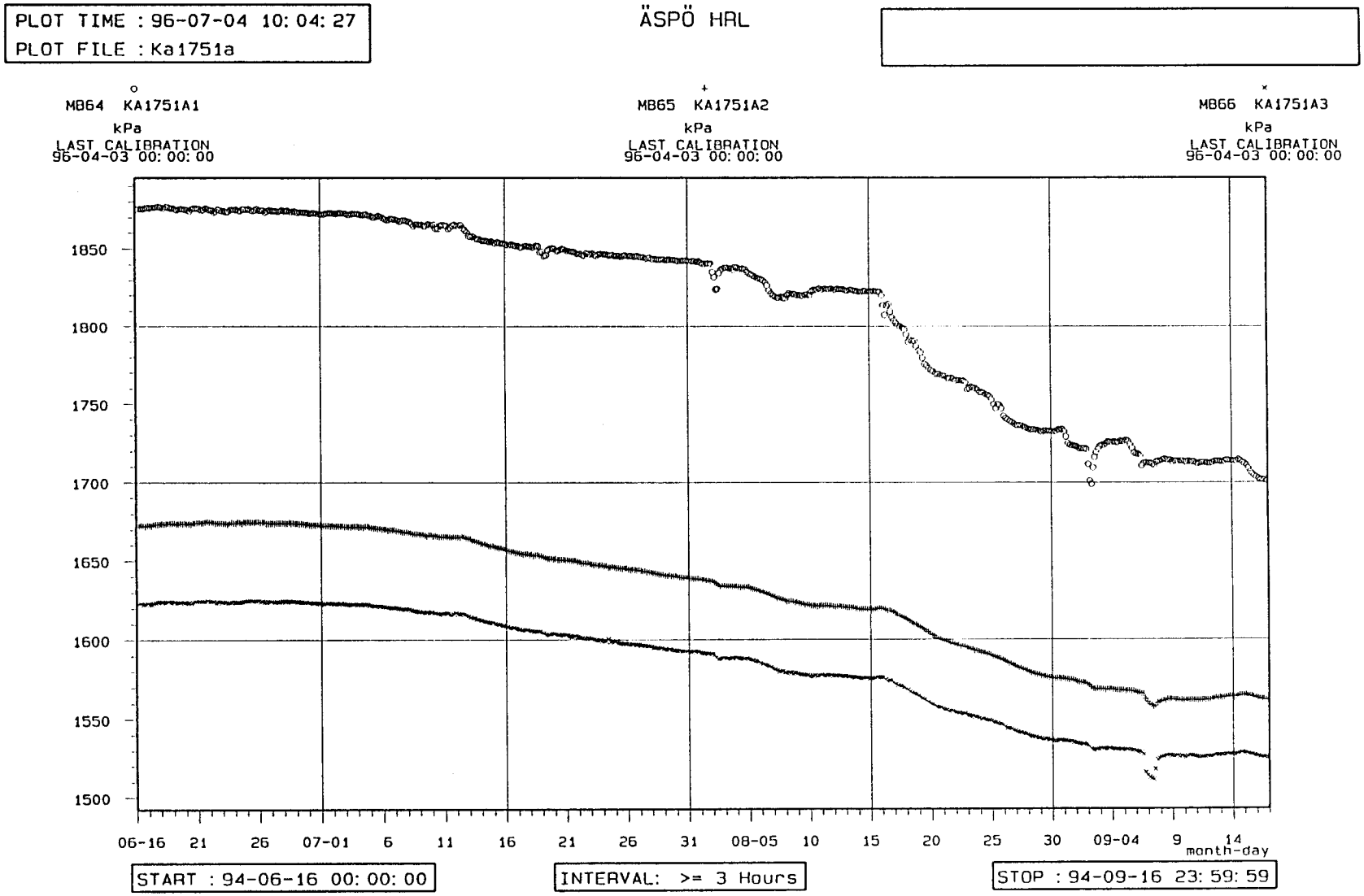

Figure 4-13 Pressure responses in borehole KA1751A during drilling of the TBM tunnel

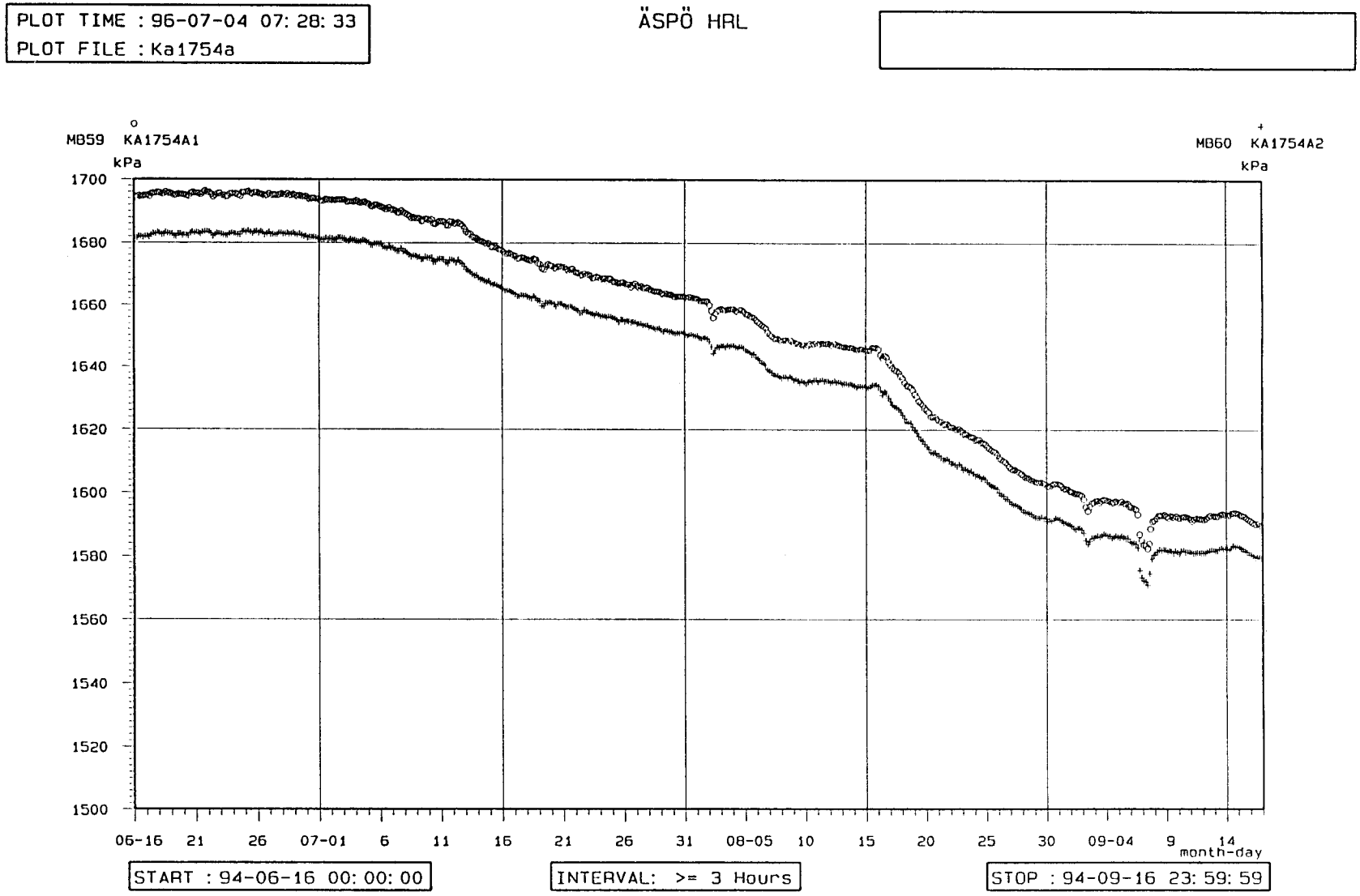

Figure 4-14 Pressure responses in borehole KA1754A during drilling of the TBM tunnel

Figure 6-1 Lithology of the Äspö HRL.

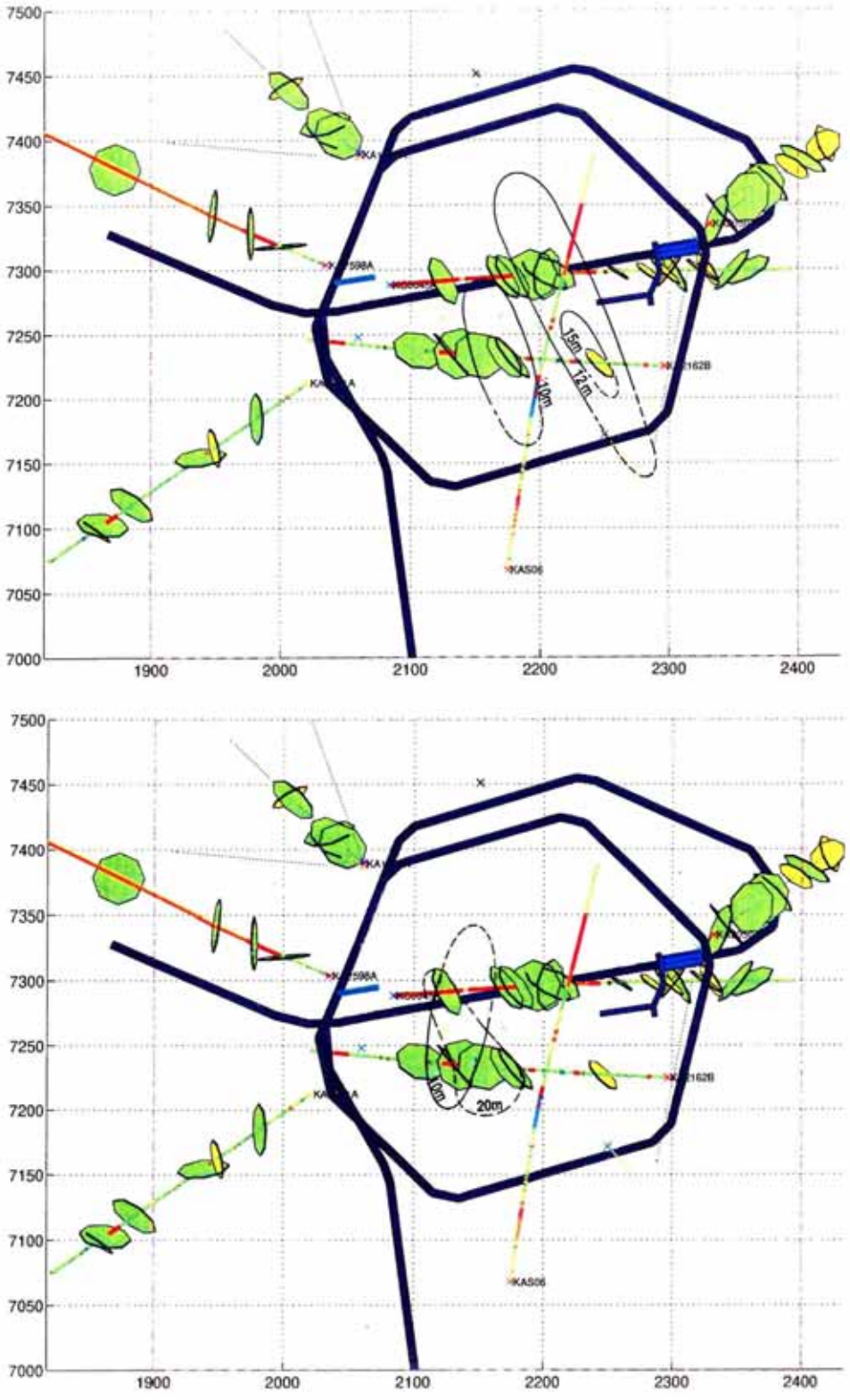

Figure 6-2 Drawdown observed during drilling of TBM pilot borehole KA3191F

Upper : Drawdown ellipse caused by drilling through a water conductor at L= 49-53m. Drawdown ellipse caused by drilling through a water conductor at L=121m.

Lower : Drawdown ellipse caused by drilling through a water conductor at L=165-174m. Recovery during pressure build-up in test section L=122.8-180m.

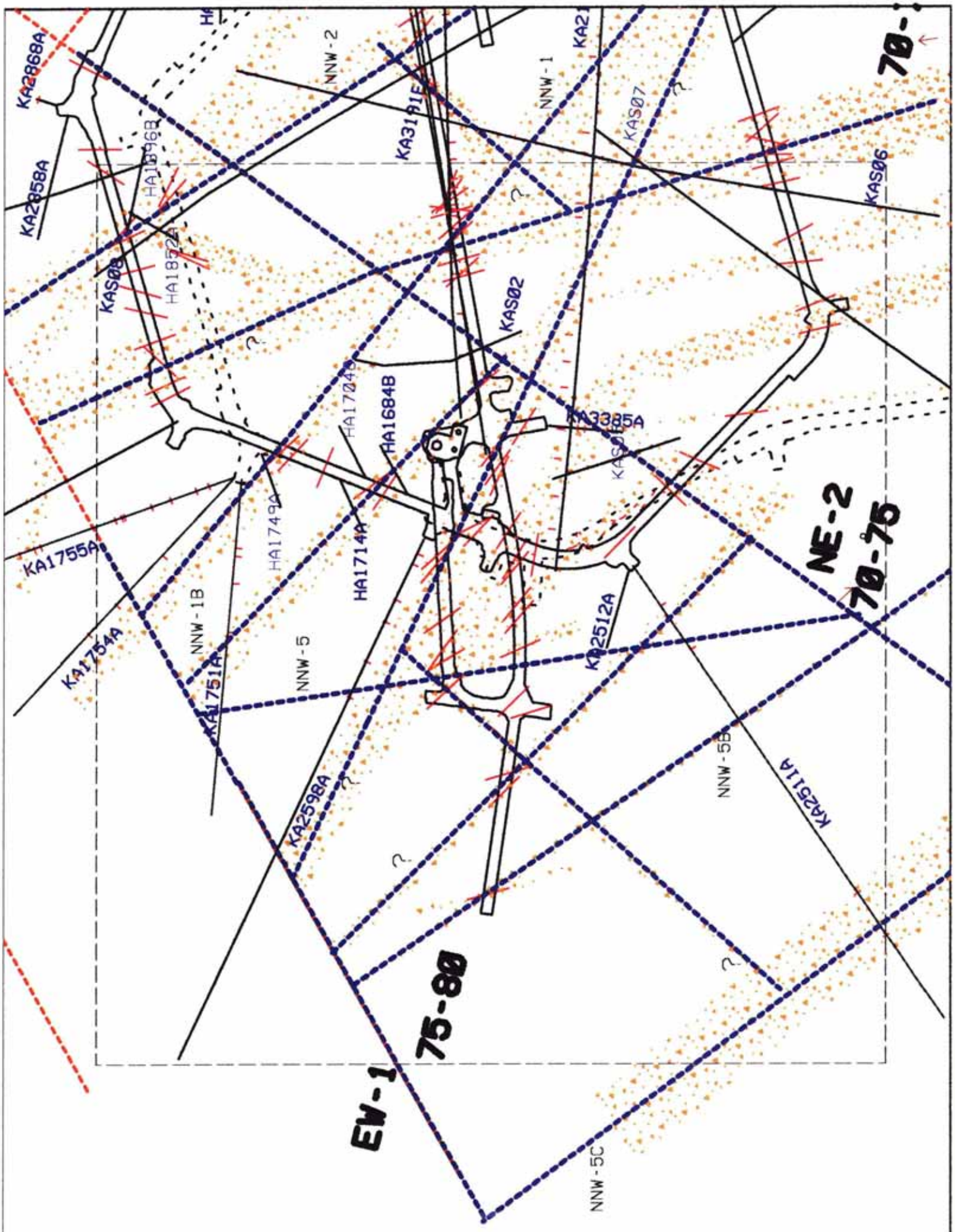

Figure 6-3 Connectivity inferred for the target volume